Data Encoding using Periodic Nano-Optical Features

by

Siamack Vosoogh-Grayli

B.Eng., Aachen University of Applied Sciences, 2007

Thesis Submitted In Partial Fulfillment of the
Requirements for the Degree of
Master of Applied Science

in the
School of Engineering Sciences
Faculty of Applied Sciences

SIMON FRASER UNIVERSITY

Fall 2012

Approval

Name: **Siamack Vosoogh-Grayli**

Degree: **Master of Applied Sciences**

Title of Thesis: **Data Encoding using Periodic Nano-Optical Features**

Examining Committee: **Chair: Dr. John Jones (Associate Professor)**

Dr. Bozena Kaminska
Senior Supervisor
Professor

Dr. Faisal Beg
Supervisor
Associate Professor

Dr. Parvaneh Saeedi
Associate Professor
Internal Examiner

Date Defended/Approved: November 29th 2012

Partial Copyright Licence

Abstract

Successful trials have been made through a designed algorithm to quantize, compress and optically encode unsigned 8 bit integer values in the form of images using Nano optical features. The periodicity of the Nano-scale features (Nano-gratings) have been designed and investigated both theoretically and experimentally to create distinct states of variation (three on states and one off state). The use of easy to manufacture and machine readable encoded data in secured authentication media has been employed previously in bar-codes for bi-state (binary) models and in color barcodes for multiple state models. This work has focused on implementing 4 states of variation for unit information through periodic Nano-optical structures that separate an incident wavelength into distinct colors (variation states) in order to create an encoding system. Compared to barcodes and magnetic stripes in secured finite length storage media the proposed system encodes and stores more data. The benefits of multiple states of variation in an encoding unit are 1) increased numerically representable range 2) increased storage density and 3) decreased number of typical set elements for any ergodic or semi-ergodic source that emits these encoding units. A thorough investigation has targeted the effects of the use of multi-varied state Nano-optical features on data storage density and consequent data transmission rates. The results show that use of Nano-optical features for encoding data yields a data storage density of circa 800 Kbits/in^2 via the implementation of commercially available high resolution flatbed scanner systems for readout. Such storage density is far greater than commercial finite length secured storage media such as Barcode family with maximum practical density of 1kbits/in^2 and highest density magnetic stripe cards with maximum density circa 3 Kbits/in^2. The numerically representable range of the proposed encoding unit for 4 states of variation is [0 255]. The number of typical set elements for an ergodic source emitting the optical encoding units compared to a bi-state encoding unit (bit) shows a 36 orders of magnitude decrease for the error probability interval of [0 0.01]. The algorithms for the proposed encoding system have been implemented in MATLAB and the Nano-optical structures have been fabricated using Electron Beam Lithography on optical medium.

Keywords: Nano optics; Surface plasmon polariton; Diffraction; Nano Fabrication; Data processing; Source Entropy

Dedication

To my Family and my kins of blood at first, where every man and woman’s foremost source of comfort comes from wherever his and her blood first forms. To my teachers and instructors at second, why the path with no guidance may never be recognized as a path to endeavour, and to myself as an entity at third, whom I must satisfy through the years of my learning to come, to know how near my goal I reside and how far off my purpose I stand.

Acknowledgements

To my senior supervisor Dr. Bozena Kaminska for accommodating an opportunity for advanced education through the course of this degree

To my long-run friend and companion, my brother Sasan, for initiation of a novel idea upon which my work of thesis is written and completed

To my knowledgeable friend and mentor of two years, Dr. Badr Omrane from whom this work has highly benefitted and resembled

To my friend and colleague Dr. Kouhyar Tavakolian for many reasons out of which a sheer guidance towards the path I have chosen outstands

To an elite professor, Dr. Faisal Beg whose course and teaching became the foundation of this work of thesis

To Dr. Donna Hohertz with whom a significant part of this study has been performed

To all of the engineers, researchers and post doctorate fellows at Ciber Lab for a period of constant learning and academic acquaintance

A notice of utter gratitude towards Dr. John Dewey Jones, Director of The school of Engineering Sciences at Simon Fraser University

Table of Contents

List of Tables

List of Figures

**Note: Appendix figures are not listed in the list of figures

List of Acronyms

LoT	List of Tables
LoF	List of Figures
ToC	Table of Contents
NOF	Nano-Optical Feature
RLE	Run-Length Encoder
State	True/False Bi-State Random Variable
SP	Surface Plasmon
SPP	Surface Plasmon Polariton
SPR	Surface Plasmon Resonance
PSK	Phase Shift Keying
QPSK	Quadrature Phase Differential Keying
QAM	Quadrature Amplitude Modulation
DPSK	Differential Phase Shift Keying
BWT	Burrows-Wheeler Transform
DCT	Discrete Cosine Transform
DWT	Discrete Wavelet Transform
GMSK	Gaussian Minimum Shift Keying
PMMA	Polymethylmethacrylate
SNR	Signal To Noise Ratio
NA	Numerical Aperture
DPA	Differential Power Analysis
DPSK	Differential Phase Shift Keying
PSNR	Peak Signal to Noise Ratio

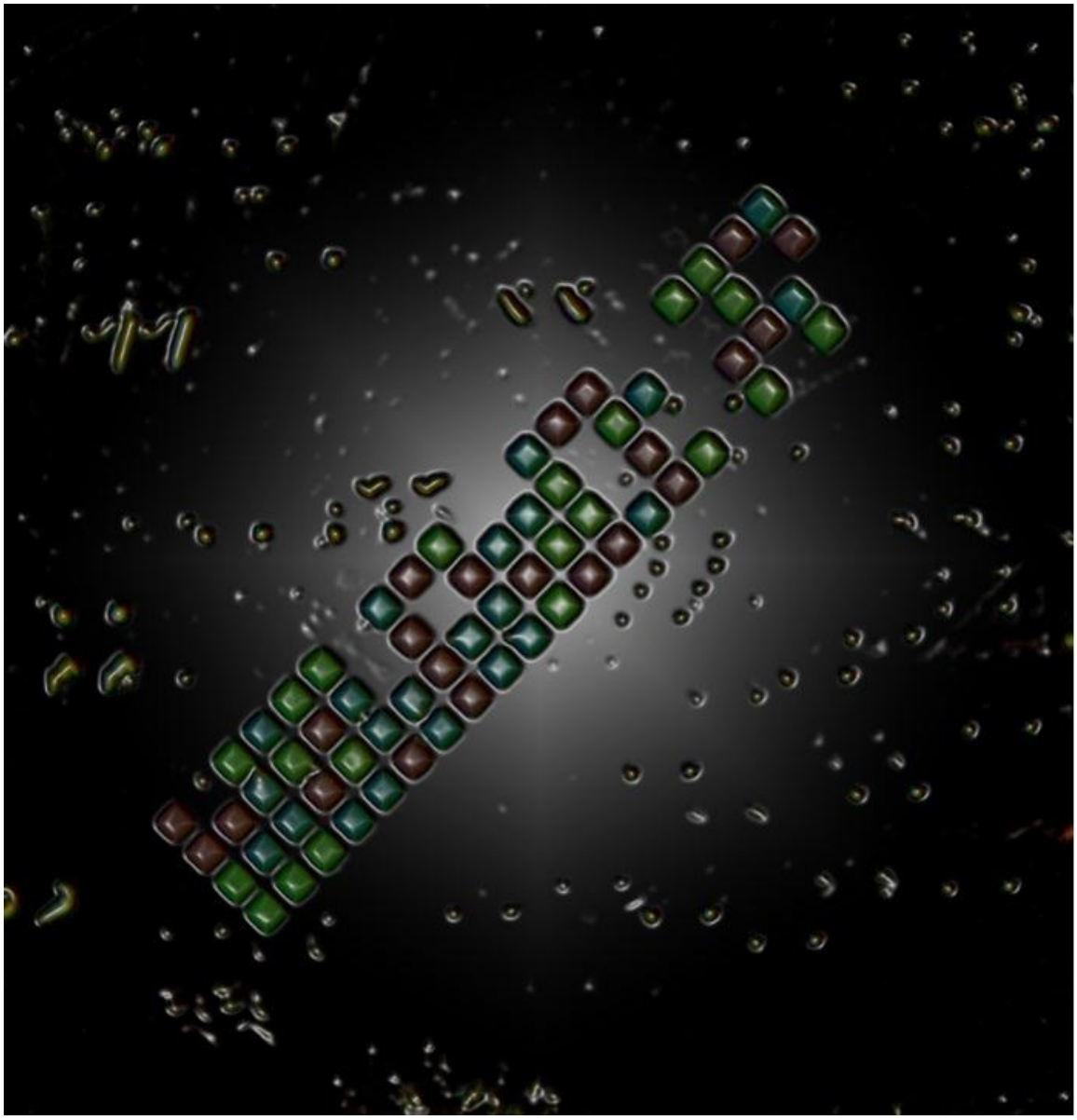

Diagram 1. Nano-optical feature's Image undergone Sobel Filtering

Chapter 1 Introduction

The use of different methods for encoding data has been researched by engineers and computer scientists over the past decades. This work focuses on the benefits of using alternative methods for encoding in order to achieve higher storage density and transmission rates. The solution to high storage density and transmission in a system is found through optimizing the data field structure and by using new physical media (Nano-Structures) that can represent the data. The properties of the data field that can be influenced by an alternate data structure are: i) the encoding scheme and ii) the source entropy measurement. The properties of the media that can be influenced by an alternate physical representation are: i) actual storage density and ii) storage dimensions. We chose light and Nano-scale optical features as our data field and medium respectively. Our research focuses on using Nano-optical features in the form of periodic Nano-hole arrays for encoding data. The need for the development of a data structure that encompasses and employs the unique properties of these features in data storage and data transmission is also investigated. The plasmonic signature and the diffracted spectrum of the Nano-hole arrays are regarded as a multidimensional field that allows more data storage.

Based on the wavelength-dependent diffractive nature of the Nano-optical features, a model is developed that allows defining a unit of information as an alternative to the classical "bit". Easy to use signal acquisition techniques and the effects of Nano-scale dimensions of the data storage media on the compression ratios are also part of this work. Our preliminary results confirm that using Nano-optics for encoding increases the accuracy for signal acquisition as a result higher signal to noise ratios for optical signals can be achieved. Our encoding scheme allows for a numerical representable range for unsigned integers of [0 255] in 4-bit (optical multi variation state bit) sequences. This is equivalent to the numerical range of 8-bit long binary sequences.

The state of art encoding techniques used in different classes of authentication media such as barcodes, radio frequency identification tags (RFIDs) and magnetic stripe cards can contribute to both security via encrypting the data and data storage density through introduction of materials and reading techniques by which the size of the stored data variable decreases. Current technologies can be targeted by standard attack protocols such as differential power analysis (DPA) and encoded media replication. Introduction of the nano-optical features (NOF) through thesis referenced as [1] has proved to be creating a secure medium for storing multi-color state optical variables as data color-bits. The potential wavelength-dependent optically secure encoding medium sets the stage for introduction of an encoding scheme that benefits from this multi-state variable signal space and transforms different types of data into NOF-encoded media. This encoding system aside from translating data from the digital format into optical nanostructures must also compress the data in an efficient way to reduce the number of optical nanostructures required to be fabricated for each data for the sake of system's cost efficiency(fabrication of nanostructures is an expensive procedure). Some important measure of using NOF in an encoding system is their ability to generate distinct colors in their diffracted spectrum which can be used as multiple states of variation for a unit information. Instead of having only two states of variation like binary integer based variables, a NOF can have 3 or more depending on the ability of the reading optics to resolve these colors in the reader's color-image. Through increasing the states of variation of the encoding variable, the entropy of the encoded data is measured with a smaller number and this lowers the number of code-words that source encoders such as Huffman require to encode the entropy of a sequence of data [2]. The challenges for manipulating the optical characteristics of the nano-optical features are both in physical tune-up of the nano-scale diffractive structures and in the signal acquisition system. Inherently, optical structures that produce a diffracted spectrum can be modelled as a linear system. The equation that governs the system defines the position and degree of diffraction of each wavelength based on the structure of the nano-optical system. Such linearity however calls for a tune-up when the number of optical structures and consequently the spatial dimension of the diffracted fields increase. In this thesis we have addressed the problem of having numerous optical nanostructures being fabricated in small distances with respect to one another and the appropriate tune-up of their multiple diffracted spectra through solving the linear two variable equation of angular

dispersion for incidence wavelength and grating periodicity instead of its original form which is a function of incidence angle and diffraction angle. The analysis allows for rewriting the angular dispersion function for two independent variables (wavelength and optical nanostructure periodicity) hence simulating the changes of diffracted wavelength in different periodicity values. The second challenge for using optical nanostructures in an encoding system is the signal acquisition and recognition. The diffracted spectrum of the NOF produces a multi-colour image that for a contrasted background can be extracted (data recovery) using standard image processing techniques. The scale of the structures however when too small creates an aberration for the sensor. This aberration can be defined as the mixing of diffracted colours in the sensor output. The degree of difficulty of colour extraction depends on both the optical tune-up of the diffractive nanostructures and the optics of the sensor. If the tune-up is considered optimal then use of smaller scale nanostructures requires more advanced optics for the sensor. The enhancement of the sensor's optics increases the price for a sensor design. We have addressed this challenge in the thesis via use of standard two-dimensional histogram analysis. The two-dimensional histogram based on a built-in MATLAB function known as accumarray allows for construction of a multi-dimensional vector field in which each colour value is first translated into CIE-LAB colour value and then become a vector with three values (Hue, Chroma, Occurrence frequency). The technique we used in this work needed to scale the LAB colour space values from their original [-128 128] range to a more appropriate (unsigned integer) scale for further analysis. Our analysis has targeted the extraction of each designated colour via referencing the simulated colour values based to simulated colours predicted using diffraction equation. Use of a vector field model referenced against a simulated (synthetic) colour map enables our algorithm to extract the desired colour along with shades which are close to the designated colour in Hue and Chroma value. Use of this method has eliminated the need for expensive optics for detecting the colours that have been used in the nano-optical medium and enables the decoding algorithm to detect colours using the readout signal of an off-the-shelf inexpensive flatbed scanner. The minimum size nano-structures successfully detected through the system were 20x20 square micron along with 20 micron distance in between each two nanostructures. We have detected three colours (Red, Green and Blue) from the aforementioned system.

The use of nanostructures and their diffracted spectrum as mentioned earlier in this chapter gives rise to a multi-variation random variable model that instead of the traditional bit (binary integer) system creating the base of current computation systems can represent data with more than two states of variation. Each distinct colour in the NOF can be regarded as a variation state and combination of these colours constructs a multi-variation state encoding system that has a much larger numerical representation range than the traditional bit. Aside from the numerical range in the case of a transmission setup (Optical transmission and reception) the benefit of transmitting variables with multiple variations states in oppose to only two the source encoder code-words can measure the data entropy with a much smaller value hence reducing the length of the code-words that are being transmitted. The aforementioned also enhances the transmission rate via transmitting more data value through each transmitted optical coloured signal. The inherent electromagnetic interference-resistance property of the optical signals can also benefit the transmission setup as to the fact that higher signal to noise ratios (SNR) can be achieved on the decoder side.

1.1. Synopsis

The state of the art information is presented in Chapter 2. The chapter will discuss the fundamental concepts behind encoding scheme that have been employed on Nanostructures introduced in [1]. It will briefly discuss the implementation of these encoding schemes. With main focus on data-encoding, the chapter is dedicated to state of the art schemes for digital data encoding using analog modulation and matching the standard definitions with optical signals acquired from the diffracting spectrum of a Nano-scale diffraction grating. Chapter 3 presents the design parameters of the interface between digital data and Nano-optical features as means for encoding. The chapter also presents system-level design of an encoder-decoder algorithm that accepts multi-format data and channels it into the encoder using standard compressor algorithms. The effects of the compressor algorithms have been discussed in detail. Further into the chapter there are optical design parameters calculated for arbitrary optics systems in order to design the Nano-optical features' periodicity. Chapter 4 presents the results and discussion regarding the effects of employing the Nano-optical feature encoding to

encode data on storage density and the readout signal quality regarding the signal to noise ratio of the acquired data.

1.2. Thesis Contribution

The main contributions to the project are the design and analysis of Nano-diffraction grating system and its signal spectrum along with theoretical derivation of the incident angles employed in the experimental parts. The design and implementation of system-level algorithms to receive, channel, encode and decode the input data have been of the specific contributions made in this thesis. The use of the standard compression platforms in order to decrease the bulk input data and the encoder-decoder platform for digital input to become optically stored have been the main focus of the contributions made to the work. The results analysis is presented at the end of the chapter 4. Chapter 5 is dedicated to investigating the future potentials of using Nano-optical periodic structures in data encoding and data transmission.

Chapter 2 Data Encoding

The state of the art data encoding techniques are categorized under two classes: 1) Data encoding for transmission 2) Data encoding for storage. The objective of techniques from both classes is modulation of a carrier in case of transmission encoding and a translator in case of storage encoding. The objective of this thesis is to use plasmonic structures fabricated in [1] for data storage. Hence the encoding for storage will be discussed more in detail than encoding for transmission.

2.1. Data encoding for Transmission

In data encoding for transmission the encoder is a mathematical algorithm through which the carrier which is a real-valued signal such as a wave is modulated. This modulation changes properties such as amplitude or frequency of the carrier proportional to the input binary data. For transmitting data such as images with numerical images greater than 0 and 1, the encoder will first translate these numbers into the binary space and after that it will modulate the carrier signal based on the variation of the binary signal.

Some examples of the state of the art encoding techniques used in data transmission are as follows [3]:

1)-Digital data encoding using analog signals (Modems)

Encoding schemes that rely on analog signals to transform and transmit signals use a carrier frequency. The data (binary or digital) is encoded through modulation of one of the following three parameters of the carrier frequency: a)- Amplitude, b)- Fundamental frequency and c)- Phase. Some schemes tend to combine these three in parts or in total to achieve higher encoding rates. There are several methods in which an encoder can manage to change the carrier frequency and enhance its bitrate and symbol rate (baud rate) during the flow of digital data. Common examples of Digital-data vs. analog-

encoder are QPSK (Quadrature Phase-Shift Keying) encoding, QAM (Quadrature Amplitude Keying) encoding, PSK (Phase-Shift Keying) encoding and DPKS (Differential Phase-Shift Keying) encoding. In most of these encoding schemes a diagram is being designed to map the streaming sequence of data into the mathematical (permutation) space of the encoder. As a result the transmission line does not have to deal with the data stream itself and hence error measurement algorithms can apply to the reception setup prior to the decoder (Figure 2. 1).

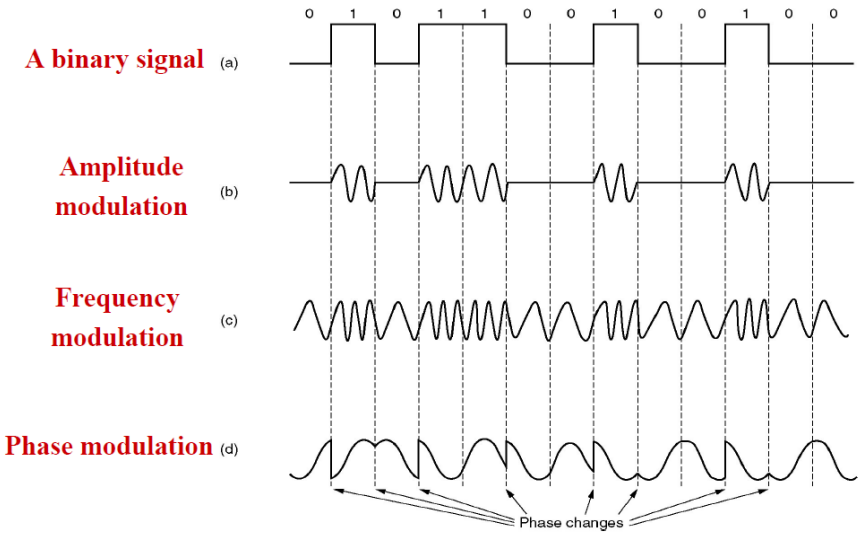

Figure 2. 1 Standard modulation of carrier wave parameters

2)-Digital data encoding using digital signals (Wired LAN)

Digital signals unlike their analog counterparts are less prone to misinterpretation by the decoder as to the fact that once achieved a certain threshold (e.g. Voltage) a digital signal can maintain its amplitude based on hard thresholding of the decoder and throughout the time it transmits within the channel. For an analog signal, every level of the transmitted waveform is valid whereas for the digital signal, as long as being in a certain range, only a few (two for binary encoding) levels are acceptable. An encoding scheme using digital signals to encode has the following parameters [4]:

Bit-time: Time for a transmitter to generate the equivalent of one bit

Signal Recovery: Array of digital information that are outputted by the decoder

Signal Resolution: How well can the transmitted signals over a given bandwidth on a certain channel.

The general scheme for such encoding setup is titles as line coding. In the line coding scheme, binary information are presented in various serial signalling formats called line codes. Graph below shows some popular line codes for digital encoding (Figure 2. 2):

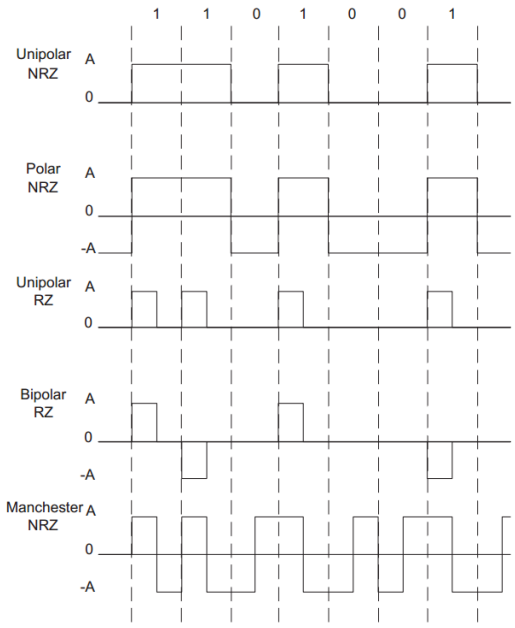

Figure 2. 2 Basic functions of standard line coders

3)-Analog data encoding using digital signals

The significance of this encoding method is the oversampling capability. Analog signals usually have limited frequency content which makes it easier to determine a minimum Nyquist sampling rate for them in order to have them fully reconstructed during decoding and demodulation. Generally speaking codecs can work both as means to convey information and to store and encrypt data streams. Given the attenuation property of an analog signal, use of digital signals to transmit and represent analog signals at discrete levels, means less need for amplification (which tunes up the noise as well) and better signal recovery for each bit of the digital representation. A codec as a result must perform three tasks:

1) Analog Signal Sampling

2) Sampled Signal Quantization

3) Quantized Signal Encoding

Some standard codec examples are given in Table 1 :

Table 1 Examples of standard encodings used in analog encoding with digital signals

Encoder's Brand	Application	File Extension
Windows Media	web , CD-ROM	WMV/AVI/ASF
Real Media	web, streaming	RM
Motion Picture Experts Group	digital video and audio, DVD, HD broadcast HD recording formats	MPEG

2.2. Definition of Data Field and Mathematical Definition of Data Encoding for Storage

Data is considered a field from which certain aspects or all of what exists in the field needs to be encoded and stored. This field is known in communication and engineering sciences as data field. Every system can have its own data field defined over a particular set of mathematical quantifications. Similar to encoding for transmission, in order to digitally store analog real valued data in a storage medium there has to be a signal whose parameters undergo modulation. The encoder can perform this modulation as part of a compression or expansion. The result of the modulation is a new sequence that has one or more of its innate characteristics varying proportional to that of the original (analog) data [5]. It is also necessary for the encoder to perform this modulation on a certain arithmetic basis hence once digitally stored; the data can still undergo arithmetic operation [6]. Similar to encoding for transmission, there should be a unit for storage. This unit is called a unit information carrier or simply unit information. The computer sciences model the unit information carrier as one bit which is also in a Boolean logic framework. There are quantities of unit information carriers in a machine arithmetic model where each transition between variables follows a true/false state and as a result each function that receives and transmits a single state of true or false also is a Boolean function. The Boolean algebra has full arithmetic space alongside a binary initial set. The aforementioned property of Boolean algebra and Boolean functions makes its arithmetic space (set of all bi-element sets and all functions operating on them) a suitable space for storing information using only two elements of a given system [7]. Because a logic set having only two distinct possibilities (e.g. true or false) is easy to replicate in a physical sense (e.g. on/off, current/no current, voltage / no voltage) it seems intuitive for modulating function to be a Boolean function [5]. For understanding the significance of Boolean nature of the modulating function it is also necessary to understand the representation of numbers in the set of data that is stored. Figure 2. 3 below show the relationship between an original (analog) data set and the stored data set. The function that maps in between the two sets is also the function that modulates the physical parameters of a unit information carrier in order for it to be stored.

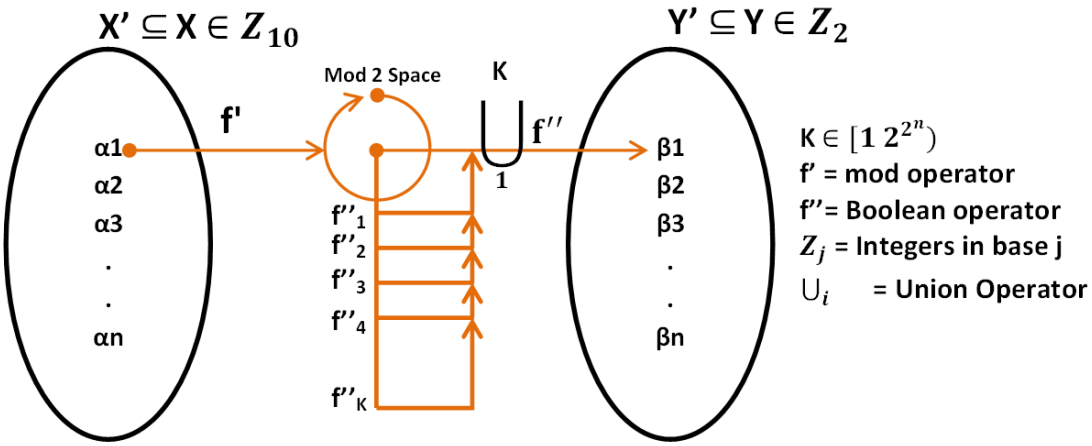

Figure 2. 3. Mathematical relationship between real valued decimal numbers and encoded binary set

For almost all computing systems, the unit information (translator) is a binary integer or bit hence the act of encoding-storage happens through assigning a binary representation to any symbol that needs to be stored in a storage medium (digital storage here). Diagram below shows the general representation for encoding different data in a digital storage (Figure 2. 4).

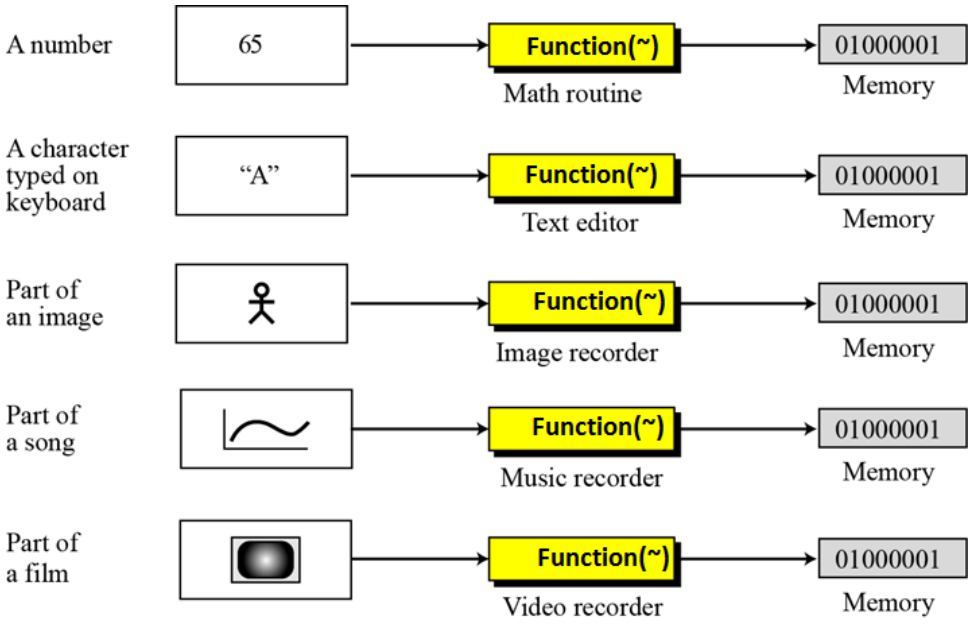

Figure 2. 4. Schematic depiction of data encoding and storage for binary storage media

Once the real valued (non-complex) data is translated into the space of the unit information, it is necessary for an encoding scheme to also measure the efficiency of the encoding procedure through the amount of physical space it requires to encode and store certain amount of data. Because analog data are usually measured in a base 10 (decimal) system, a transformation into the binary system expands the original data set. In order to perform an efficient data encoding, there are standard compression algorithms that are used to compress a data field before or after decimal to binary transformation (Figure 2. 5). These algorithms can be classified into two general categories:

1) Lossy and 2) Lossless algorithms

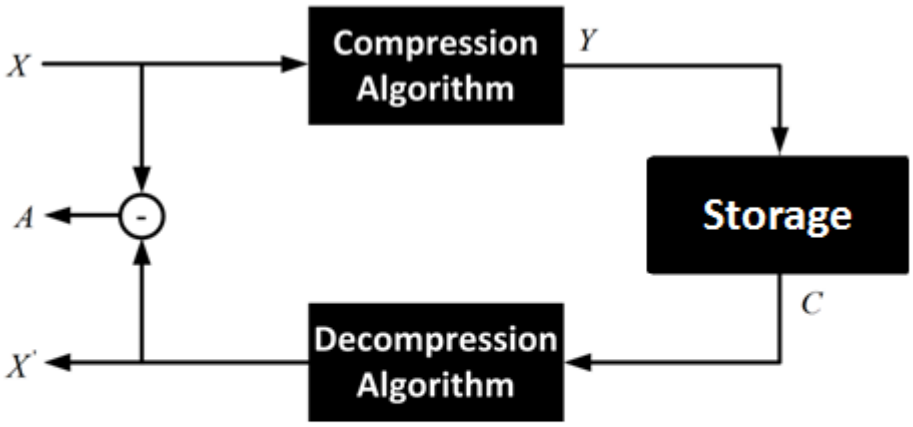

X=Input
Y=Compressed Input
X'=Reconstructed and decompressed input

$$\begin{cases} A = 0 \ if \ lossles \\ A \neq 0 \ if \ lossy \end{cases}$$

Figure 2. 5. Block diagram of a general compression algorithm with no transmission

Lossy Compression Algorithms

Some examples of most common lossy algorithms are given with brief descriptions below:

1) Uniform Scalar Quantization:

Is the way of compressing distinct values outputted by a source through partitioning of the input data range into intervals each being represented by a unique symbol or state. Each quantizer can be uniquely described by its partition of the input range (encoder side) and set of output values (decoder side). Quantization can be uniform. In a uniform scalar quantization the inputs and output can be either scalar or vector. The quantizer can partition the domain of input values into either equally spaced or unequally spaced partitions. The end-points of partitions of equally spaced intervals in the input values of a uniform scalar quantizer are called decision boundaries. The output value for each interval is the midpoint of the interval and the length of each interval is called the step size Δ [2] (Figure 2. 6).

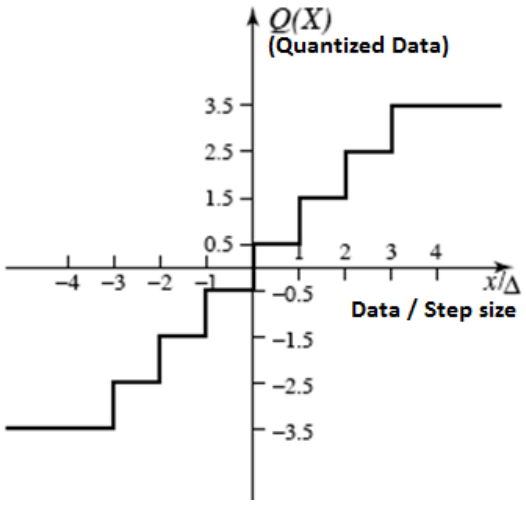

Figure 2. 6. Uniform scalar quantizer basic function representation

Assuming that the input is uniformly distributed in the interval [-Xmax, Xmax] the rate of the quantizer is $R = \text{ceil}(\log 2\ M)$. R is the number of bits needed to code the M output values where the step size Δ is given by $\Delta = 2\text{Xmax}/M$. For a uniform quantizer, the total distortion (after normalizing) is twice the sum over the positive data:

$$D = 2\sum_{i=1}^{\frac{M}{2}} \int_{(i-1)\Delta}^{i\Delta} \left(x - \frac{2i-1}{2}\right)^2 \frac{1}{2X_{max}} dx \qquad \textbf{2-1}$$

2) Non Uniform Scalar Quantization

A uniform quantizer may be inefficient for an input source which is not uniformly distributed hence the algorithm needs to use more decision levels where input is densely distributed to lower distortion error and use fewer where data is sparsely distributed. Total number of decision levels remains the same yet the quanitzer's output has less distortion error for a given sample. Some common non uniform quantizer examples are:

1- Lloyd-Max quantization that iteratively estimates optimal boundaries based on current estimates of reconstruction levels then updates the level and continues until levels converge.

2- Companded quantization in which Input is mapped using a compressor function G then quantized using a uniform quantizer. After transmission, quantized values are mapped back using an expander function G^{-1}.

3) Transform Coders

These algorithms transform the data through a transform matrix that translates data values into a different mathematical space than that of the data. This new representation of the data is then quantized using standard methods mentioned in the previous section to compress the data. After quantization the transformed data will be recovered through inverse transformation back into the original mathematical space it was taken from. Examples of transform encoders are [8]:

1- Discrete Cosine Transform (DCT)

DCT is a widely used transform coding technique Spatial frequency indicates how many times pixel values change across an image block The DCT formalizes this notion in terms of how much the image contents change in correspondence to the number of cycles of a cosine wave per block. The DCT decomposes the original signal into its DC and AC components, following the techniques of Fourier analysis whereby any signal can be described as a sum of multiple signals that are sine or cosine waveforms at various amplitudes and frequencies. The inverse DCT (IDCT) reconstructs the original signal. Its mathematical representation is as follows [2]:

$$C(u,v) = \alpha(u)\alpha(v)\sum_{x=0}^{N-1}\sum_{y=0}^{N-1} f(x,y)\cos\left[\frac{\pi(2x+1)u}{2N}\right]\cos\left[\frac{\pi(2y+1)v}{2N}\right] \qquad \textbf{2-2}$$

$$f(x,y) = \sum_{u=0}^{N-1}\sum_{v=0}^{N-1} \alpha(u)\alpha(v)C(u,v)\cos\left[\frac{\pi(2x+1)u}{2N}\right]\cos\left[\frac{\pi(2y+1)v}{2N}\right]$$

$$\alpha(u) = \begin{cases} \sqrt{\frac{1}{N}} & for \quad u = 0 \\ \sqrt{\frac{2}{N}} & for \quad u \neq 0 \end{cases} \qquad \alpha(v) = \begin{cases} \sqrt{\frac{1}{N}} & for \quad v = 0 \\ \sqrt{\frac{2}{N}} & for \quad v \neq 0 \end{cases}$$

Where N is the number of elements of the data file, x and y are spatial positions of a data value (e.g. an image data), u,v are frequency components of the decomposed data and α is an attenuation term to suppress the sequence expansion.

2- Wavelet Transform

A wavelet transform, similar to a Fourier Transform takes the image (or data) into the frequency domain with the slight difference that what it outputs is localized both in frequency and time due to an scaling factor that is calculated as a result of averaging the

entries in a particular window and a translation factor that is calculated due to altering the length of the window that scans the signal. The combination of the two brings about a collection of temporal frequency scattering of a signal in the wavelet space. The resulting small functions that interact with each window (interval) of the signal are called wavelets and they must have certain mathematical characteristics in order to be invertible. Wavelet transform is described mathematically through [2]:

$$\gamma(S,\tau) = \int f(t)\psi^{*}_{S,\tau}(t)dt \qquad \textbf{2-3}$$
$$f(t) = \int\int \gamma(S,\tau)\psi_{S,\tau}(t)d\tau dS$$

With the following condition for the frequency domain analysis:

$$\int \frac{|\psi(\omega)|^2}{|\omega|} < \infty \qquad \textbf{2-4}$$
$$|\psi(\omega)|^2_{\omega=0} = 0$$

Where $\gamma(S,T)$ is the wavelet transform of the data, ψ_{ST} is the wavelet notion and S, T are Scaling and Translation of the signal. $\psi(\omega)$ is the Fourier transform of the wavelet and must be zero at $\omega=0$ for a fast decay of the wavelet approximating moments.

2.2.1. Lossless Compression Algorithms

During a lossless compression, the algorithm relies on three types of data redundancies in order to perform compression. These redundancies due to the error free nature of the algorithm cannot be eliminated or ignored hence the algorithm must take notes or pieces of information (reconstruction clues) in order to further compress the code. Some of the typical redundancies in a dataset used by lossless compression algorithms are: Coding redundancy, Inter-pixel redundancy and Psycho-visual redundancy. Some standard categories of lossless compression are [2]:

1) Variable-Length Encoding

Also referred to as source coding, this class of encoder reduces the bit or code length redundancy in a set of data (or Image). The idea rises from the definition of entropy as an average measure of uncertainty of occurrence of symbol (data value) within a data field or from a data source. Each data field is usually described by the symbols that represent information and a probability density vector that defines how often each symbol is occurring in the field. By using the Shannon's entropy measure $H(X)$, the class of source variable length encoders assign variable lengths of binary code words to each symbol on the data field in order to achieve an average less amount of total code length in binary digits compared to a uniform assignment of code-words (Figure 2. 7).

r_k	$p_r(r_k)$	$Code1$	$l_1(r_k)$	$Code2$
$r_0 = 0$	0.19	000	3	00
$r_1 = 1/7$	0.25	001	3	1
$r_2 = 2/7$	0.21	010	3	0
$r_3 = 3/7$	0.16	011	3	01
$r_4 = 4/7$	0.08	100	3	10
$r_5 = 5/7$	0.06	101	3	11
$r_6 = 6/7$	0.03	110	3	000
$r_7 = 1$	0.02	111	3	001

R1	0.25 (01)	0.25 (01)	0.25 (01)	0.25 (01)	0.35 (00)	0.4 (1)	0.6 (0)
R2	0.21 (10)	0.21 (10)	0.21 (10)	0.21 (10)	0.25 (01)	0.35 (00)	0.4 (1)
R0	0.19 (11)	0.19 (11)	0.19 (11)	0.19 (11)	0.21 (10)	0.25 (01)	
R3	0.16 (001)	0.16 (001)	0.16 (001)	0.19 (000)	0.19 (11)		
R4	0.08 (0001)	0.08 (0001)	0.11 (0000)	0.16 (001)			
R5	0.06 (00000)	0.06 (00000)	0.08 (0001)				
R6	0.03 (000010)	0.05 (00001)					
R7	0.02 (000011)						

Figure 2. 7. Probability of gray level occurrence of a stream of image data and the corresponding source entropy approximation (zero-order entropy) for source encoding

Of the existing algorithms, Huffman class is the optimum encoder for code word redundancy reduction. The scheme in brief, pairs up the lowest probability symbols in the source and assigns a single symbol to the pair as the rest of the source is being coded. By sorting the probability of the new source (after pairing up all the lowest probabilities in the sequence) the encoder produces a library entry and moves on to the next cycle where it does the same to existing sequence. It can be shown that for a finite length symbol source, the Shannon's entropy measure bounds the upper and lower limits of an optimum code length as follows:

$$H(X) \leq L_X \leq H(X) + 1 \qquad \textbf{2-5}$$

H(X) : Source entropy of data X
Lx : Code length of data X

2) Lempel-Ziv-Welch (LZW) Encoding

This class starts with outputting a dictionary that must be transmitted along with compressed file from an encoder. By examining variable length sequences within the data segment, the algorithm generates a new dictionary entry and a new code-word every time it encounters a new sequence within the scanned data. The overall size of the code-words and the dictionary along with the encoded segment will have less bitrate due to the fact that the variable length summing of the symbol sequences has reduced the inter-value redundancy. The merit of this algorithm is the fast decoding procedure as to the fact that it does not rely on the probability mass function of the data and the source (Figure 2. 8).

Currently Recognized Sequence	Pixel Being Processed	Encoded Output	Dictionary Location (Code Word)	Dictionary Entry
	39			
39	39	39	256	39-39
39	126	39	257	39-126
126	126	126	258	126-126
126	39	126	259	126-39
39	39			
39-39	126	256	260	39-39-126
126	126			
126-126	39	258	261	126-126-39
39	39			
39-39	126			
39-39-126	126	260	262	39-39-126-126
126	39			
126-39	39	259	263	126-39-39
39	126			
39-126	126	257	264	39-126-126
126		126		

Figure 2. 8. An example of LZW encoding of non-frequent data stream

2.3. State of the Art Data Encoding for Storage

The encoding for storage is performed in two different ways in standard methods: 1)-Encoding for storage in computation devices (computers and microcontrollers) where the data is stored either temporarily or permanently in the chip random memory and/or bios unit. This encoding uses the potential difference between reference and a wire as an indicator for existence of a binary one or zero. 2)-Encoding for storage in magnetic storage media (analog media). In this storage scheme, the data are being represented using the polarity of the magnetic field. In this method the encoder uses positive or negative voltages to change the polarity of the magnetic particles in a magnetic particle field. The decoder reads the data by detecting transition regions known as flux reversals throughout the entire field which represent binary ones and non-transitioning areas representing binary zeros. During this procedure, the encoder first acquires the raw digital data and translates them into the domain of a wave. This wave is used to produce change of polarities in the magnetic medium. For efficient encoding and decoding the encoding scheme must have optimized parameters such as modulation order and modulation parameter(s) that are being affected in the storage medium. Some most practical and optimal encoding techniques for magnetic data storage are presented as following [8][9]:

1)-Modified frequency modulation encoding

2)-Run-length-limited encoding

2.3.1. Modified Frequency Modulation Encoding

The modulation that separates the binary raw data and the magnetic particles in the storage medium must determine the clocking of the input data. This means that the decoder must know when the polarity changes represent a one and when represent a zero. In this method the ones and zeros are represented with magnetic flux reversals and clocking bits that separate the beginning of one bit from the end of the other. Figure 2. 9 shows how data current is being translated into the storage medium magnetic polarisation.

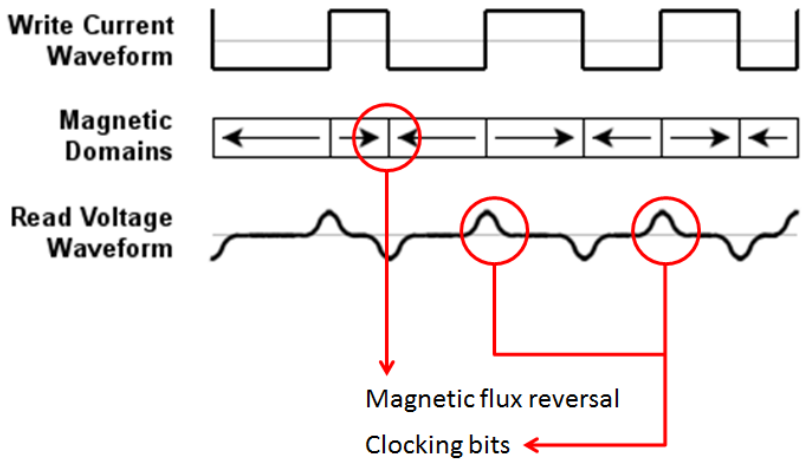

Figure 2. 9. Diagram of data encoding for magnetic data storage

The basis of modified frequency modulation encoding (MFM) is based on a precursor method known as frequency modulation encoding (FM) which is extinct since the introduction of MFM in 1970. The encoding scheme for FM adds two consecutive flux reversals for representing a one and a flux reversal preceded by no reversal to represent a zero. This method is modified in MFM via addition of flux reversals only when there are consecutive strings of zeros at the input. When there are ones involved no extra flux reversals (clocking bits) are inserted as to the fact that the decoder can identify the sequences represented by a reversal pointing out a one preceded and proceeded by zeros. This modulation technique adds up to the amount information that is the flux reversals created on the magnetic medium in order to clarify the bit string being encoded. There are usually physical challenges involved in data encoding for storage on the magnetic medium. These challenges can be summarised in the problem of magnetic field additivity. This property means that N number of magnetic dipoles (bipolar particles) cannot be distinguished from each other one by one when sensed by the readout circuit due to forming an added magnetic field N times stronger than each one alone. The industry hence pushes for introduction of material with higher magnetic field density per inch square for enhancing the data storage density on one hand and use of more complex algorithms that can modulate the reversal flux timing (clocking of the magnetisation) for error-free representation of more bits per flux reversal.

2.3.2. Run-Length-Limited Encoding

Run-length-limited encoding (RLL) takes MFM one step further. It considers groups of several bits instead of encoding one bit at a time. The idea is to mix clock and data flux reversals to allow for even denser packing of encoded data, to improve efficiency. The two parameters that define RLL are the run length and the run limit. The word "run" here refers to a sequence of spaces in the output data stream without flux reversals. The run length is the minimum spacing between flux reversals, and the run limit is the maximum spacing between them. The amount of time between reversals cannot be too large or the read head can get out of sync and lose track of which bit is where. The particular variety of RLL used on a drive is expressed as "RLL (X,Y)" or "X,Y RLL" where X is the run length and Y is the run limit. The most commonly used types of RLL in hard drives are "RLL (1,7)", also seen as " 1,7 RLL "; and "RLL (2,7) " (" 2,7 RLL"). Considering the spacing of potential flux reversals in the encoded magnetic stream, in the case of “2,7", this means that the smallest number of "spaces" between flux reversals is 2, and the largest number is 7. The encoder in RLL encoding first parses (separates using a certain standard) the input sequence then it uses clock bits (flux transitions) to encode the data. This way, the minimum number of clock bits are inserted into the data stream hence more data bits can be stored per square inch of the magnetic medium (Figure 2. 10)[9].

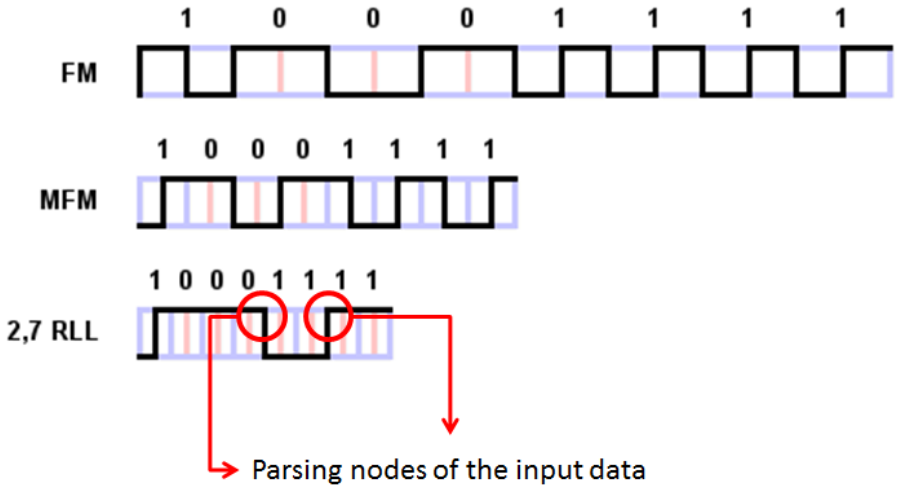

Figure 2. 10. Storage density per reversal flux increase from FM to RLL encoding

2.3.3. Optical Data Field and Current Optical Data Encoding for Storage

Current technology uses the digital domain parameters for both encoding and decoding the analogue information into and from the optical media. The state of the art system can be briefly described in the below graph (Figure 2. 11).

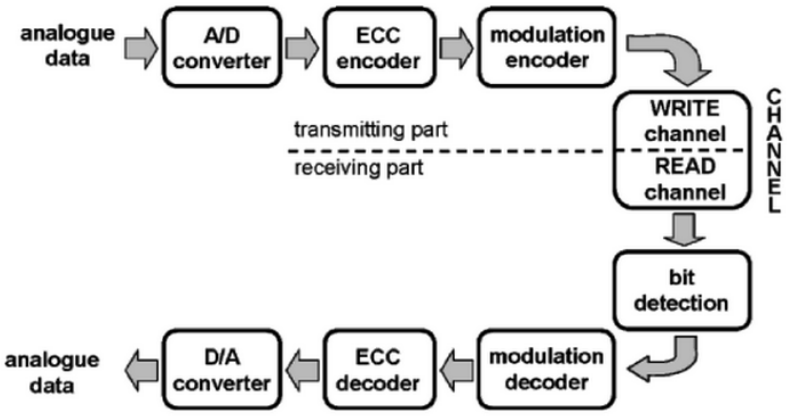

Figure 2. 11. Data encoding system with transmission properties (Optical Data Storage Ervin Meinders)

The optical data field can then be defined in two phases of the system; if the system relies on grid writing and patterning then the data field is defined on the physical layer. As a writer produces features such as grooves, rows or slits on the optical medium it also, by leaving certain spaces between the grooves, induces sequences which form tables and files that construct the data field [10][11]. One can distinguish between the physical data field, which is a result of file production through a digital system prior to the physical transfer onto the optical medium, and optical data field which is the total perceivable luminance flux through the optical sensor. Although there is no profound necessity for the two types of data field to be different from one another it appear so that in some cases through different field descriptions one can achieve more efficient compression and/or storage density. The recently employed concept of holography is an example of having separated the electrical domain (digital) data field from the optical data field (Figure 2. 12). In a holographic process the general idea is to not only record the intensity changes of the incident light by means of the photosensitive material but also to have the complete optical path of the incident light define that intensity distribution. The equation of an incident electromagnetic wave is described through [12]:

$$E = \hat{A}\cos(\omega t - \phi) \qquad \textbf{2-6}$$

It is the phase term that conveys information regarding the full path of the perceived photon [13].

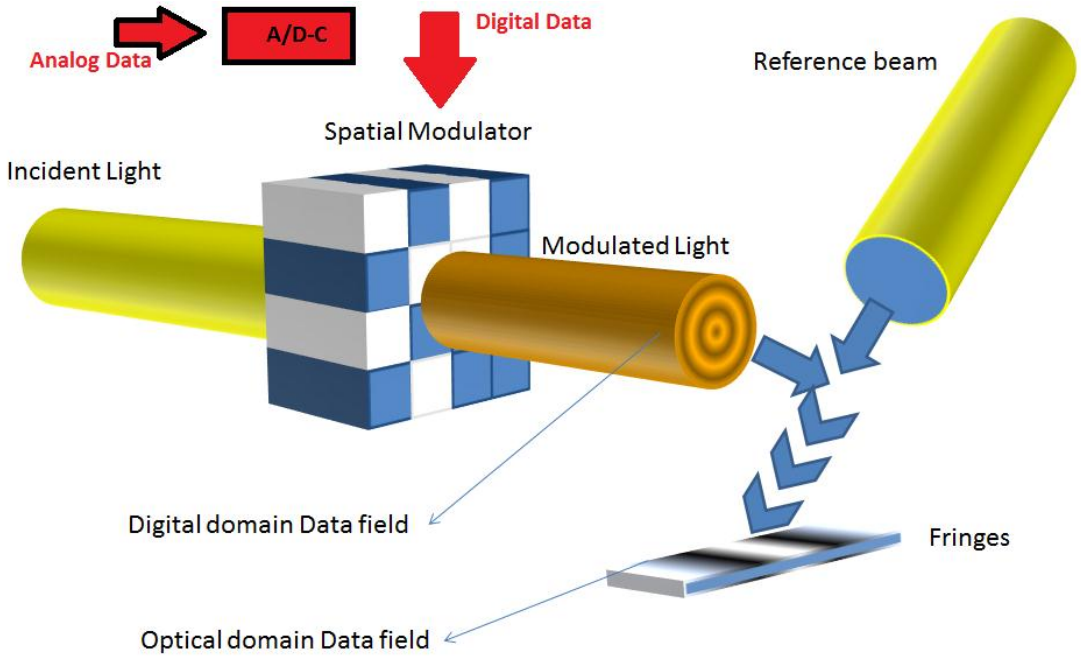

Figure 2. 12. An example of how the original (digital) and the successive optical data fields can differ; the fringe patterns of the interference create new data assortment hence a new field

2.4. Data Encoding for Storage in Authentication Industry

Authentication industry focuses on providing secure representation of personal or commercial data for both individuals and organisations. The type of security is dependent on the type of storage media and the capacity of information it possesses. Large data capacity increases the authentication system's accuracy on one hand and jeopardises the data security on the other. For large amount of personal data being securely stored on an authentication device such as a card, the data must be encrypted as well. It is also necessary implement types of media which resistant to external disturbances such as electric or magnetic field or both (electromagnetic field) as well as physical damages to the medium that can erase or corrupt the data. There have been many generations of data authentication systems which use different encoding methods to write and secure data. Some of these systems are simple and require no data encryption (e.g. 1D, 2D and color barcodes) whereas some other have higher level of security for protecting the data on the medium to be exposed to third party clients (e.g. smart cards). The state of the art authentication media are discussed briefly in this section.

2.4.1. Barcodes

This type of authentication media is a data entry streamline meaning that it shows a set of data (alphanumeric data) in a particular direction. It has the advantage of being printable on paper and easy to read via an optical reader setup. It also has lower levels of error during detection due to its simple mechanism of encoding. Barcodes are categorized based on the encoding dimensions. One dimensional barcodes offer length dependent storage on only one direction or dimension. The 2D barcodes have information recorded in more than one dimension (have data layout similar to a matrix). The recently implemented color barcodes take advantage of presenting colors as an extra encoding dimension as well. In general barcodes have following advantages and disadvantages [14][15]:

Advantages: Easy to print, Not language dependent, Low error rate, Variety of print methods, Full character set, Beam scannable

Disadvantages: Low capacity, Easy to acquire physical damage, Low data obscurity, No encryption

2.4.2. One Dimensional Barcodes

One dimensional barcodes are created using combined sequences of dark and light (black and white) stripes. The encoding or symbology of the barcodes is user defined. Each character in a sequence of the coded data is represented by a block of the dark and light spaces. The density of this medium depends on two factors: 1)-length along which data is encoded 2)-Optical accuracy of the reader that images the encoded data Figure 2. 13 shows a UPC (Universal Product Code) symbology for encoding sequence of digits as barcode.

Figure 2. 13. Code 39 barcode example

These barcodes are read and decoded via blind deconvolution process. The storage density of the barcode is limited by the amount of information intended to be printed as a code and the type of parity (error corrective symbols) that are added up to the code by the encoding symbology. In theory barcodes can store infinite amount of data if extended in a direction for infinite length. In practice their storage is limited to ~10 characters (alphanumeric characters) per inch. The barcode has low error rate yet it is up to the reader decoding software to correctly model the noise distribution of the readout signal and retrieve the encoded data. The barcodes therefore are not capable of storing much information and usually contain keys that redirect the decoder to a larger database for extracting more information regarding the coded medium. Figure 2. 14 shows a barcode readout signal reconstruction.

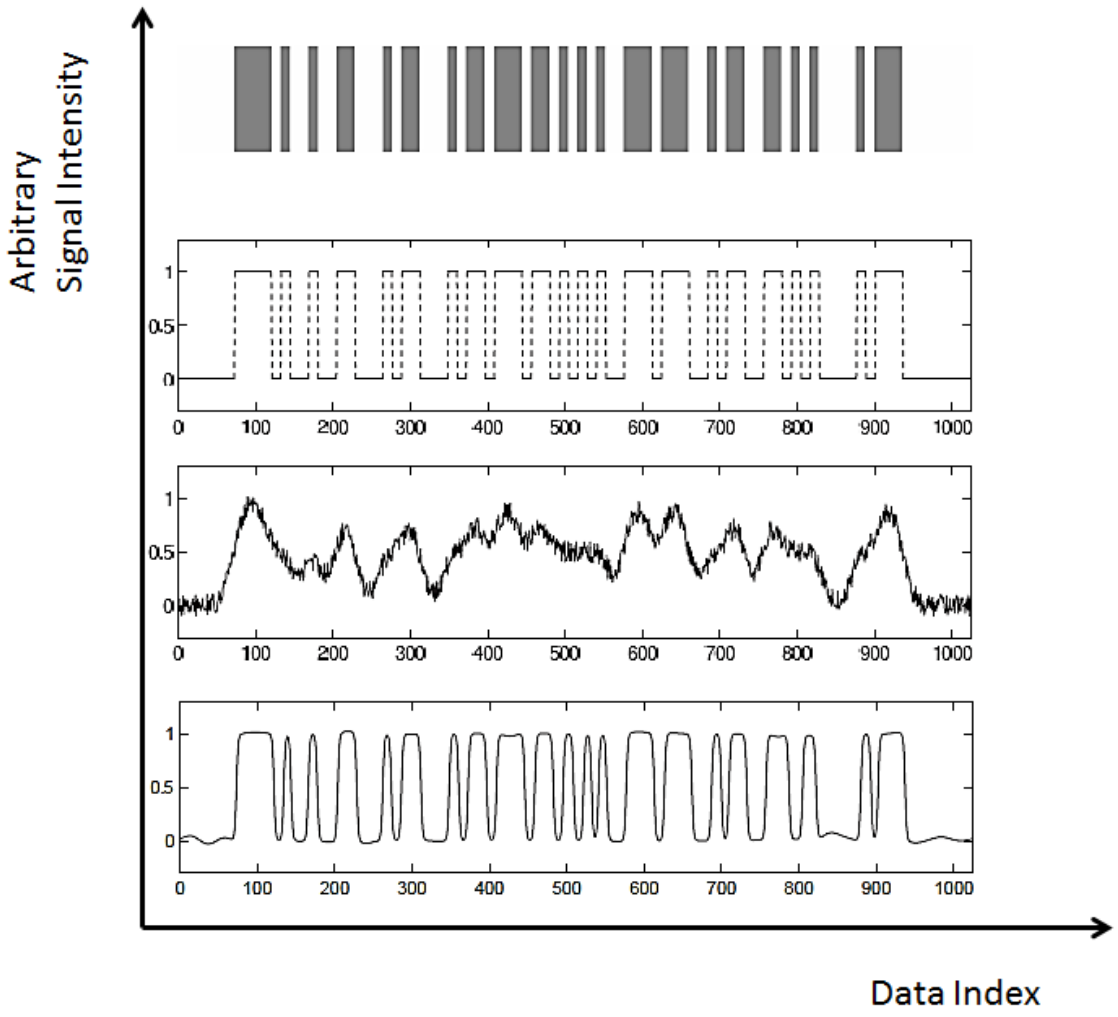

Figure 2. 14. Signal recovery process of a typical barcode decoding

2.4.3. Two-Dimensional Barcodes

Two dimensional barcodes are a second generation of barcode family with much larger capacity compared to the one dimensional barcodes. These systems are also termed as PDB (Portable Data Bases) due to larger data capacities they possess. Reading 2D barcodes is done via image processing and contrast enhancement of the acquired image from the encoded medium. 2D barcodes, similar to 1D barcodes are dependent

on how well the imaged encoded medium is resolved. The maximum data storage capacity for some most common types are presented in Table 2.

Table 2 Common 2D barcode systems and their characteristics

2D barcode	QR	PDF417	CM
Max capacity	3 KB	1 KB	32 KB
Error correction level	Levels 1~4	Levels 0~8	Levels 1~8
Barcode shape	Square only	Any rectangle	Any rectangle
Savable information	Text, symbols and small images	Text, symbols and simple images	Text, symbols, colorful pictures and even voice
Photoelectrical sensor (core part of a reader)	Made in Japan	Made in Japan	Made in China
Intellectual property rights	Japan	US	China

With maximum storage of 32 KB, 2D barcodes can allow for up to 2Kb/in^2 at 600 dpi scan resolution (Compact Matrix Code aka CM Barcode).

2.4.4. Smart Cards

Another type of authentication with higher level of security and data capacity is the smart card class. These media have more complex encoding and encryption implementation compared to 1D and 2D barcodes. The security measures of smart cards are related to both the type of data they carry, the amount of data on the card and decoding process. Some common examples of smart cards are:

2.4.5. RFID(Radio Frequency Identification) Tags

RFID tags carry an electronic chip that has information stored inside in the form of circuit structure where the response of the circuit when captured by the decoder reveals the information. These systems exist in two forms: 1)-Active tags 2)-Passive tags. Active tags have a source on the card that carries them (e.g. a battery) which keeps the circuit on all the time. As soon as the circuit and the decoder are in range the chip transmits its data to the decoder. The passive systems have also information stored in them in the form of integrated circuits. Instead of permanently transmitting the information the tags are powered up upon coming under a radio frequency wave propagation emitted from the decoder. The tag's response as a result becomes the transmission of the data stored in the circuit to the decoder. RFID tags outdo barcodes regarding the line-of-sight problem. In oppose to barcodes for which the decoder requires to "see" the encoded media, an RFID encoded medium can correspond with the decoder from a wireless range and does not require an exact one-on-one encounter with reader. This is very useful when the range of detection is increased. Currently the RFIDs come in sizes as small as $4mm^2$ in area and the highest storage capacity of about 128KB which translates into circa $2Kb/in^2$ data storage density [16] (Table 3).

Table 3 Characteristics of an RFID tag (Zebra Technologies)

Maximum Data Storage	Thermal Resistance	Reading Range at given Frequency	Minimum Tag Size	Radiation – induced damage
128 KB	-40° to +85°	3 f to 25 f for 125KHz-135MHz Frequency Range	2 mm x 2 mm	Yes

The range at which the RFID tags operate depends on the size of the tag hence for small tags the range cannot be exceeding a few inches. The amount of data stored by a tag is also limited by the size of the information-carrying circuitry hence for larger data storage larger tags are needed.

2.4.6. Magnetic Data Storage for Authentication Storage Media (Magnetic Stripe Cards)

Encoding techniques for magnetic data storage are not only used for mass storage purposes such as computer hard disk drives (HDD). It is also possible to encode data magnetically on stripes of magnetic material attached to portable media such as an ID card. The class of these media employed for authentication storage is referred to as smart card media and their main purpose is to store certain data which are encrypted as well to identify personal information of the card holder or to trace certain data or objects in a wireless grid. Smart cards using magnetic data storage are termed as magnetic stripe (mag stripe) cards. The encoding schemes introduced in section 2.3.3 in combination with standard encryption protocols are used to encode binary data on magnetic stripe cards. Figure 2. 15 shows the magnetic stripe card characteristics and data storage capacity [17].

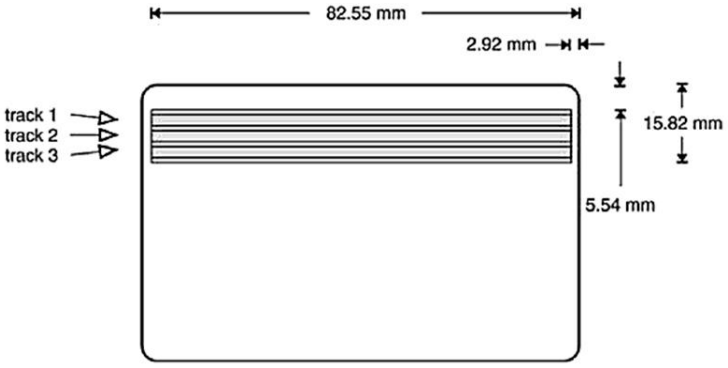

Property	Track 1	Track 2	Track 3
Data volume	79 characters max.	40 characters max.	107 characters max.
Data coding	6-bit alphanumeric	4-bit BCD	4-bit BCD
Data density	210 bit/inch (8.3 bit/mm)	75 bit/inch (3 bit/mm)	210 bit/inch (8.3 bit/mm)
Writing	not allowed	not allowed	allowed

Figure 2. 15. Characteristics of magnetic stripe card

The most imminent threat to magnetic stripe cards is an external magnetic field with intensity high enough to re-polarize the flux reversal within the magnetic field on the storage area of the card. Its advantages are: Machine readability, Immunity to external contagion and global standards and disadvantages are: Close-contact reading, Vulnerable to external magnetic fields, Low data capacity and vulnerable to side channel attacks.

2.4.7. Optical Memory Card

Optical memory cards have the largest capacity among the state of the art authentication data encoding for storage due to have been using the compact write/read technology on a card size medium. The storage density of the optical memory cards are high yet the card, due to the applied hardware for the reader the costs for enhancing the storage density rise to a point of non-beneficial manufacturing [17]. Optical memory cards store binary raw or encrypted data and can record a vast variety of information including text, images, sound etc. Some characteristics of optical memory cards are given in the following table (Table 4).

Table 4 Data Storage Density for Optical Memory Cards (Laser Cards Technologies)

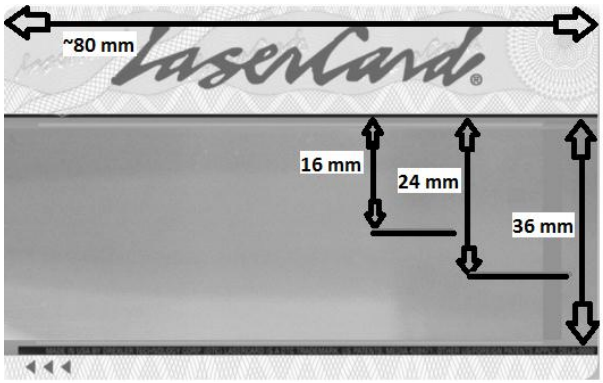

Card Optical Track Width	Storage Density
16 mm	622 Kb/in^2
24 mm	400 Kb/in^2
36 mm	244 Kb/in^2

Similar to CDs optical memory cards use a portion of their capacity for error correction (parity check) bits of data hence losing some of their storage capacity for actual data. Due to similar encoding and physical read/write mechanism to CDs, information presented on an optical memory card can become subject to unauthorized copy and replication (for writable cards). The information can also be debugged in binary format if they are encrypted during writing process. Overall optical memory cards are considered to be an expensive data storage system as well due to the material used for production and securing the optical tracks and the hardware used for reading the data [17][18].

2.5. Project Motivation

The current encoding schemes for storage mentioned in 2.4, encounter some issues regarding the storage density of the encoded medium as well as problems with respect to a class of attacks called side channel attacks. Side-channel attacks use the electrical signature (voltage or power) of the encoded medium to decrypt the data and to extract the sequences that are being encoded. Low data storage density allows these attacks to decrypt the secured combinations of data faster. Smart cards such as RFID tags and magnetic stripe cards are vulnerable to these attacks. Another form of data extraction from an encoded medium is use of exhausting search algorithms that can affect those type of authentication media with low storage density. A third way to extract data from an authenticated medium is to replicate the entire encoded medium onto another medium and perform debugging analysis. Authentication media such as optical memory cards which use CD-encoding technology can be decrypted this way.

Our intention through this work is to address these two issues (security and data storage density) via use of plasmonic nanostructures. The thesis introduced in [1] has presented plasmonic nanostructures which are capable of diffracting polychromatic (white) light in different wavelengths (colors). It also presents a rather fast fabrication process for fabricating the nanostructures using electron beam lithography (EBL). Following the focus of [1] we intend to investigate the application of the presented structures to encode data for storage purposes and measure the efficiency of an encoding system based on these structures regarding the storage density and data security. Through our simulation and experimental work we have proved that use of the plasmonic nanostructures as means to store data is an efficient way for storing large amounts of data in small spaces which are convenient for authentication media such as ID cards and other similar documents. The state of the art authentication media such as barcodes, RFID tags and optical memory cards all show deficiencies in either data storage density or their security.

We have shown that the nanostructures can be tuned to reflect or transmit certain wavelengths in a given direction and through combining them via a mathematical algorithm hence they can be encoded in such way that their decryption becomes extremely difficult and has high level of security. We also have shown that use of Nano-scale structures allows for much higher data storage density than state of the art authentication media. Our motivation is to design a system level implementation of the mentioned Nano-optical structures in order to encode data on authentication media. Through mathematical analysis via image processing techniques we have proven the use of inexpensive reading setups can extract the encoded data in lower SNR (Signal to Noise Ratio) and investigated the benefits of use of the mentioned plasmonic nanostructures on Shannon's Typical Element Set (set of most probable outcomes for an ergodic source of data) theoretically. Our motivation for the project is the employment of a Nano-optical storage implementation for data encoding for storage in order to enhance the security of the encoded data via removing the power analysis and side channel attack possibilities. It also has been a focus of the work to introduce an algorithm that receives and compresses data in an efficient way prior to preparing it for nanofabrication on optical medium. The objectives for this thesis can be summarised as follows:

1) Defining an appropriate encoding scheme for the Nano-optical structures

2) Defining an optical data-field using the diffracting spectrum of Nano-optical structures

3) Investigating the performance of an optical encoder using periodic nanostructures

4) Proof of concept for specific applications using the optically encoded data by means of the periodic Nano-optical structures

2.5.1. Defining an Appropriate Encoding Scheme for Nano-Optical Structures

An encoding scheme enables the encoder using the nanostructures to be efficiently employed in a way that during decoding the least amount of erroneous data is detected

by the decoder. Existence of multi-variable field parameters in optical media can enhance the way data is being encoded and modulated in a way to achieve less error rate during storage, transmission and less noise during recovery. In order to employ these characteristics of an optical field, an encoding scheme needs to be designed to incorporate the fixed or modulated variables related to the optical spectrum. In our case the encoding scheme needs to address the optical characteristics of the Nano-optical structures that we have intended to use in the experiment.

2.5.2. Defining an Optical Data Field using the Diffracted Spectrum of the Plasmonic Nanostructures

After designing the encoding scheme that will use the Nano-optical structures, we define a field (data field) based on which the encoding scheme takes real-valued data as input and transform these data into an arrangement of Nano-optical structures. The optical data field consists of an optical unit information that is the smallest unit of optical information that can be clearly represented by the optical medium and a modulation parameter that is the characteristic of the optical spectrum undergoing change to represent different information. By employing state of the art and novel Nano-fabrication techniques, it has become possible to transfer designs for optical medium encoding onto Nano-scale dimensions. This has become a motive for the project to design an optical data field constructed onto Nano-optical structure media.

2.5.3. Investigating the Performance of an Optical Encoding Scheme using Periodic (and Plasmonic) Nano-Optical Structures

Depending on the wavelength of the incident light the distance traveled by the wavelength without destructive attenuation is relatively much larger than an electrical signal such as a voltage. It also requires less power to maintain the field amplitude of an optical signal above degradation levels during signal transmission. These characteristics allow for high performances during data recovery. This thesis has investigated the levels of SNR at which full data recovery is possible over optical setups which have not been compensated for optical aberration. This investigation measures the ability of the designed encoding/decoding system using the full characteristics of the periodic optical

nanostructures during reflection of the diffracted spectrum of the incident reading light, to recover the color-based encoded data as a measure system performance.

2.5.4. Proof of concept for specific applications using the optically encoded data by means of the periodic Nano-optical structures

Once the encoding scheme and the optical data field are defined we can show that use of such encoding scheme allows for better and higher performance regarding some specific applications such as identity security applications in which the data that is been recorded on a portable medium such as a card, must be protected against any unauthorized users. The trials that have been made in this thesis allows for the proposed optical encoding system to securely encode information such as text, numbers or even images. The use of more than two variations states for the encoding unit information results in high storage density hence the data, in comparison to other encoding methods such as barcodes, occupies a much less physical space for storage (Figure 2. 16).

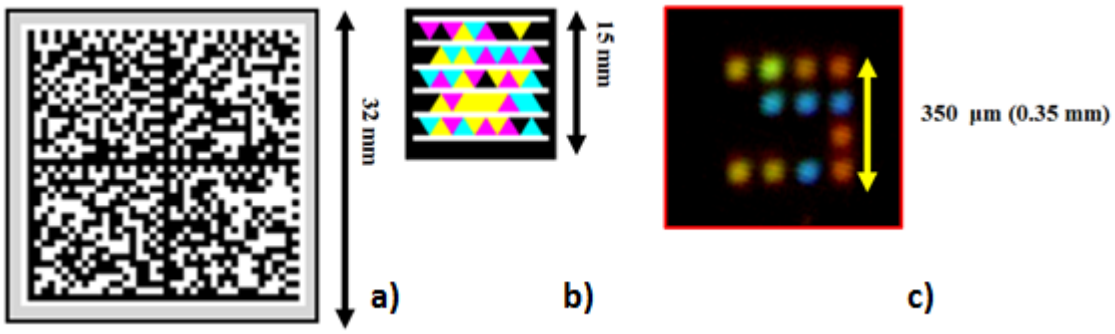

Figure 2. 16. a)-2D Barcode, b)-Microsoft Color-barcode and c)-NOF encoded representation of text:www.id-me.ca

Chapter 3 Simulation and Theoretical Analysis

This chapter presents the analysis made in order to define the signal we use by implementing a periodic nanostructures. Periodic nanostructures used in [1] act as Nano-order diffraction gratings that can diffract an incident polychromatic (white) light in different angularly separated directions. These diffracted spectra, if well resolved, can be imaged by an imaging sensor such as a CCD (Charged Coupled Device) or CIS (Contact Image Sensor) from distances far from the diffracting structures (in the Fraunhofer optical domain). In order to calculate the correct tuning factor and resolve the diffracted optical spectra in the sensor plane (image plane), we use MATLAB and linear optics to calculate the optical paths which are going to emerge from the periodic nanostructures both during transmission and reflection. The first step in our analysis is to define the dimensions of the periodic optical nanostructures and the dimensions of the signal received from them.

3.1. Defining the Physical Dimensions of the Periodic Optical Nanostructures and their Diffracted Spectrum

The periodic nanostructures under discussion act as diffraction gratings. The basic function of a planar grating system is to create an angular dispersion in different orders where the degree of dispersion of the light either transmitting or reflecting from the grating has an inverse relationship with the groove density (periodicity) of the grating. The term groove density is defined as number of holes, discontinuities or grooves in unit measurement (length). In the case of a regular grating system the groove density or groove frequency is defined as number of groove/mm whereas in the system under discussion as to the fact that the unit measurement in use is nm hence the term groove density is being defined as grooves /nm (Figure 3. 1) [19].

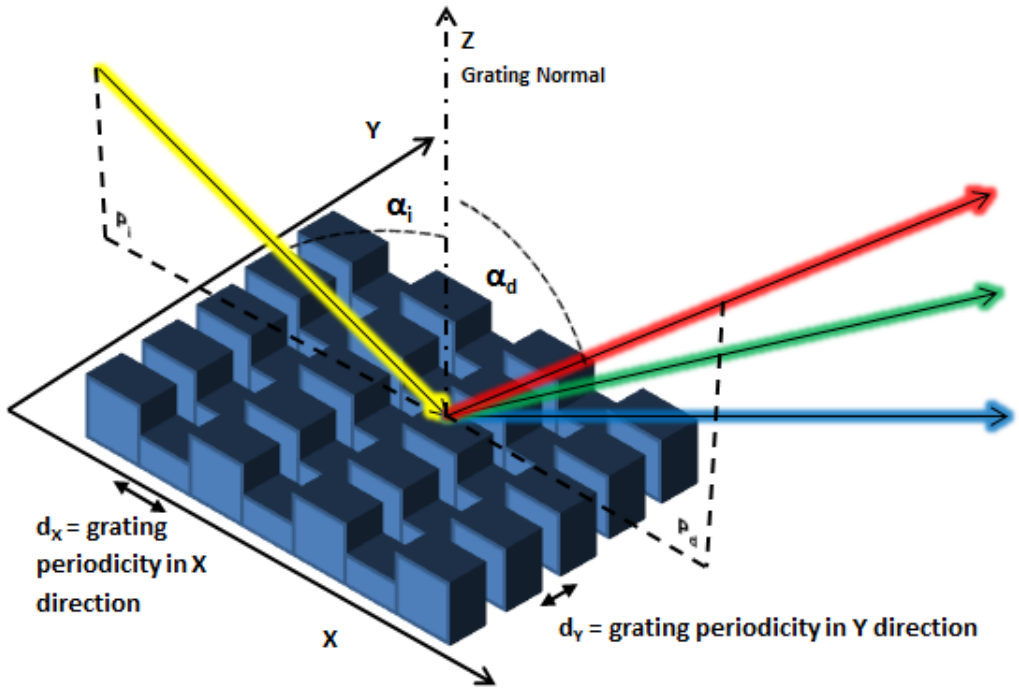

Figure 3. 1. Complete 3D diagram of a Nano-optical structure with in-plane incidence and diffraction

The procedure relies on defining a new storage system through introduction of a novel implementation of Nano-scale diffraction grating structures that contributes to thorough angular dispersion of a polychromatic incident light [19]. The data storage is a result of the encoding of any numerical value that has been mapped into the permutation space of these Nano-diffractive structures that will be referred to as Nano-Optical-Feature (NOF) throughout the document. The permutation space will be the space of all possible combinations of N number of NOF with varying array periodicities. The periodicity of a NOF will be a parameter that influences the angular dispersion of the diffracted wavelengths hence each NOF will diffract a specific wavelength at a specific degree of alternation with respect to the grating normal in the Z direction. Such characteristic is the foundation of this work in terms of choosing a certain angle (with respect to the grating's normal) and define the type or state of variation of the NOF based on the wavelength that is being diffracted in that particular direction There are the measures of separation or dispersion path differences between each wavelength [19]. This term is related to the dispersion power and resolving power of the grating. The resolving power of a grating is its ability to unambiguously resolve or distinguish between two adjacent peaks with similar amplitudes and different wavelengths. Theoretically the resolving power can be

used to optimise the grating parameters with the purpose of achieving certain resolution for the grating. This in practice is being also limited by the point spread function (PSF) of the sensor placed in the image plane (Figure 3. 2) [12].

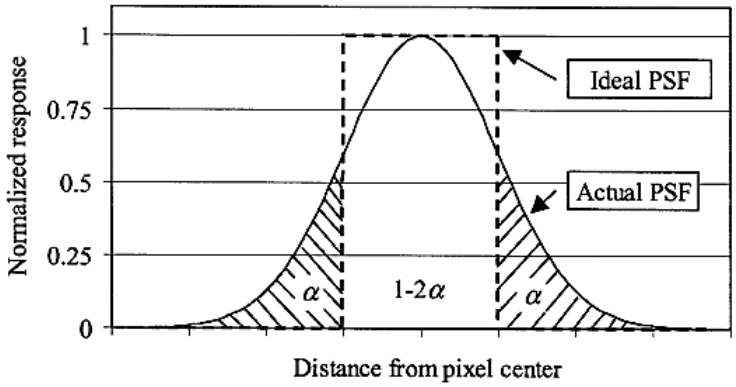

Figure 3. 2. Ideal and actual point spread function of simulated pixel response to TM (Transverse) field incidence. (Chengquan Huanga,*, John R.G.)

3.2. Defining the Encoding Scheme

An encoding scheme using NOF is a system that modulates an optical signal for data encoding for storage. The system has prominent parameters that describe its modulation procedure and allow for algorithmic handling of its input. These parameters are:

1) Signal Constellation

2) Carrier Signal (Translating Signal for a Storage System)

3) Signal Modulation Parameter

3.2.1. Signal Constellation

The signal constellation for NOF is based on the physical properties of planar diffraction grating being illuminated by white (polychromatic) light. The grating equation is a linear transformation that translates angles of incidence (radians) into three inter-related parameters: 1) Angle of Diffraction (Angle of output light compared to grating normal, 2) Wavelength (spectral property of the output light) and 3) grating periodicity (periodic

groove distribution over the surface of the grating). The diagram below shows the signal constellation of NOF (Figure 3. 3):

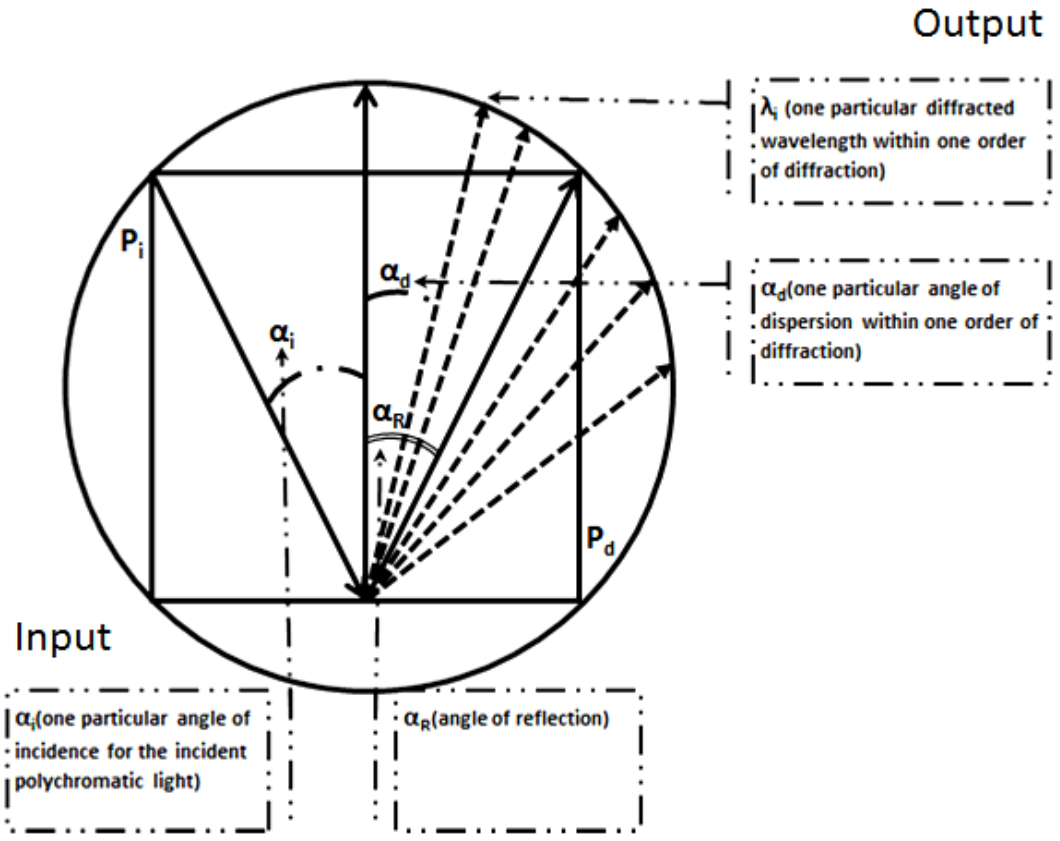

Figure 3. 3. Signal Constellation of NOF encoding system(describes input and modulated output of the encoder)

3.2.2. Carrier Signal

The carrier signal is white (polychromatic) light emitted from non-specific sources. Signal can be defined mathematically in the form of the visible range of the electromagnetic spectrum as:

$$E(r,t) = E_0 \cos(\omega t - K.r + \phi_0)$$
$$B(r,t) = B_0 \cos(\omega t - K.r + \phi_0) \qquad \textbf{3-1}$$
$$\nabla \times E = -\frac{\partial B}{\partial t}$$

Where E is the electric field amplitude, B is the magnetic field amplitude, $K=(kx,ky,kz)$ is the spatial wave vector, $r=(x,y,z)$, $\omega=2\pi f$ is the angular frequency and ϕ_0 is the initial phase in radians. The signal intensity is presented as [13]:

$$I = \frac{\mathcal{C} n \epsilon_0}{2} |E|^2 \qquad \textbf{3-2}$$

I = Signal Intensity
$\mathcal{C}$ = Speed of Light in Vacuum
ϵ_0 = Vacuum Permittivity
E = Light Electric Field

3.2.3. Modulation Parameters

Based on the signal constellation diagram and the signal mathematical description, what undergoes a change as the carrier gets diffracted through the grooves of a diffraction grating is dependent on which parameter of the grating equation is kept constant and which is let to vary. For simplicity, we define the system to have fixed angle of reception (hence the angle of diffraction is kept constant) and interpret the perceived signals as being modulated by the angular frequency to produce variable colors or wavelengths as interpreted by the spatial image sensor (Figure 3. 4). Transformation into signal domain is defined as:

$$x(t) = PR(D_i, b) = D_i^b \qquad \textbf{3-3}$$

$x(t)$ =Time domain acquired signal
$PR(.)$ =Permutation with repetition space of .
b =Constellation order
D_i =Encoding symbol

The order of the signal constellation depends on the number of available unit information in the encoding scheme. As an example a binary system employs 8 single bits to construct one byte and therefore the order of this constellation is 8. Some other example

of order in a constellation is the 8 symbol modulation in DPSK (Differential Phase Shift Keying) where each modulation order assigns a specific phase to a 3-bit packet of transmitting signals. In this work our constellation diagram in Figure 3. 4 allows for reception of different wavelengths at a fixed angular position. This translates into encoding symbols or states of variation of the unit information. The number of Nano-optical structures that exist in the encoding system is defined as the constellation order of our encoding system.

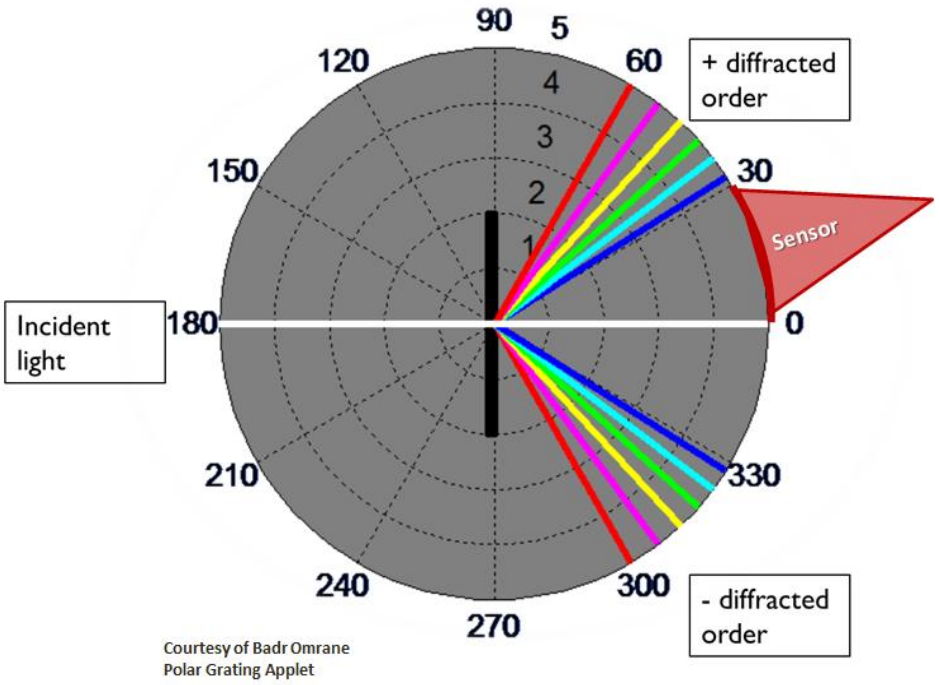

Figure 3. 4. Polar coordinates showing the way an image sensor may perceive the diffracted light from the nano optical features

The modulation is based on changing the angular frequency of the wave-front (light beam) at the sensor input by means of the periodicity of the NOF. Simulation below shows the values (wavelengths) the sensor receives at a particular angle of reception for three different periodicities while the sensor receives the diffracted wavelengths at a certain angle. The simulation is run in MATLAB using the theoretical conditions used in Fraunhofer diffraction model for a fixed angle of incidence and various periodicities defining generating different angles of diffraction: (Figure 3. 5)

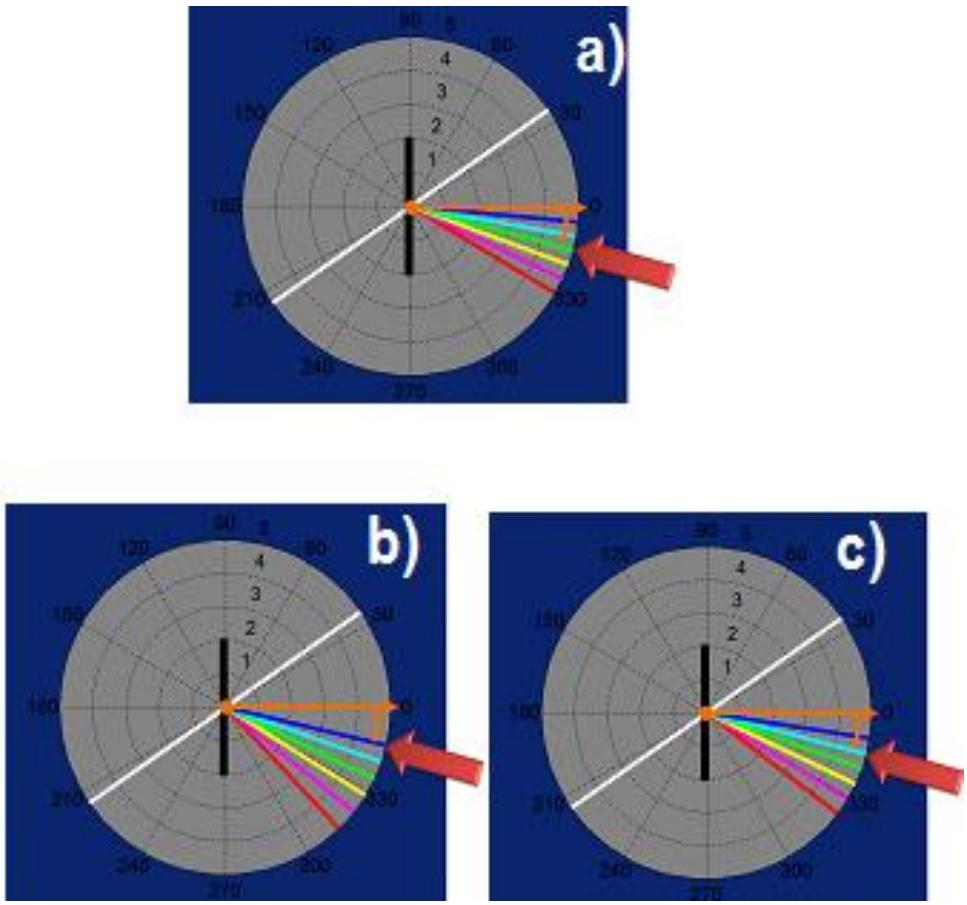

Figure 3. 5. a)-Green wavelength, b)-Blue Wave length and c)-Cyan color received by fixed angular position replace the initial signal (green) through change of grating periodicity

Table 5 shows the changes of the received wavelength for each periodicity at three angles of diffraction. If a sensor is positioned at β_1 angle, then the periodicities will be defined as following as a function of received wavelengths:

$$X\big(P(X=A)\big) = \sum_{j=0}^{M-1} \frac{m\lambda_i}{K} b^j = \frac{m}{K} \sum_{j=0}^{M-1} \lambda_i b^j \qquad \textbf{3-4}$$

$$K = \sin(\alpha) + \sin(\beta)$$

m =Order of diffraction

M =Symbol length

$P(.)$ =Probability of .

b =Constellation order

Tracing the values of wavelengths received by sensor at angle β_1 results in the derivation of The modulating parameter from Eq(3-4) is the ratio m/K. (A=Integer)

Table 5 Variations of a Signal outcome based o figure. 41 simulations; The angles of diffraction vary with wavelength

Wave length	Diff. Angle	NOF Periodicity	Wave length	Diff. Angle	NOF Periodicity	Wave length	Diff. Angle	NOF Periodicity
λ_1	β_1	d_1	λ_1	β_0	d_2	λ_1	β_{-1}	d_3
λ_2	β_2	d_1	λ_2	β_1	d_2	λ_2	β_0	d_3
λ_3	β_3	d_1	λ_3	β_2	d_2	λ_3	β_1	d_3

3.3. Simulating the Conditions for Optimal Angular Dispersion

The property we use to tune our best imaging conditions (aside from choosing an optimal optical solution for the imaging setup) is the Nano-optical structure's angular dispersion. The matching of angular dispersion and the wavelength perceived by the imaging sensor is the same for both slit-model-grating and the periodic Nano-optical structures due to the existence of periodic discontinuity in the optical medium [19] (Figure 3. 6).

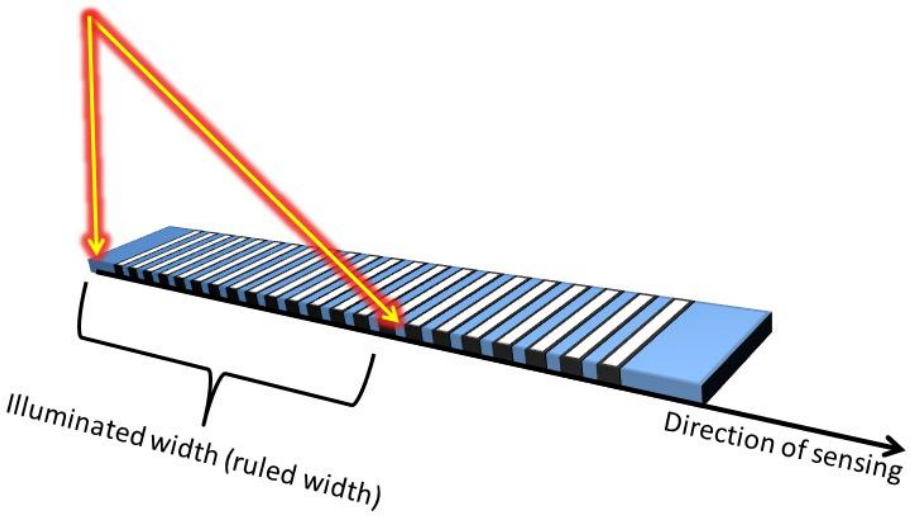

Figure 3. 6. The illuminated length of a grating defines its resolved spectrum as a function of its periodicity

For a slit grating model in one dimension the resolving power can be defined as:

$$R = \frac{\lambda}{\Delta\lambda} \qquad \textbf{3-5}$$

$$R = \frac{Nd(\sin(\alpha) + \sin(\beta))}{\lambda}$$

Nd =Ruled width (Illuminated width)

α =Incidence angle

β =Diffraction angle

N =Total number of grooves

d =Grating periodicity (pitch)

Without considerations for the imaging sensor and only based on the grating parameters one can acquire the differential form of the grating equation presented in [19] as follows:

$$D = \frac{\partial \beta}{\partial \lambda} = \frac{m}{d\cos(\beta)} = \frac{m}{d}\sec(\beta) \qquad \textbf{3-6}$$

For acquiring Eq(3-6) the angle of incidence is being treated as a constant as to the fact that the two angles of incidence and diffraction lie in a linear relationship. For acquiring an optimizer parameter one can expand Eq(3-6) further into:

$$D = \frac{m}{d\cos\left(\sin^{-1}\left(\frac{m\lambda}{d} - \sin(\alpha)\right)\right)} \qquad \textbf{3-7}$$

Using the identity:

$$\cos(\sin^{-1}(x)) = \sqrt{1 - x^2} \qquad \textbf{3-8}$$

And further into:

$$D = \frac{m}{d\cos\left(\sin^{-1}\left(\frac{m\lambda}{d} - \sin(\alpha)\right)\right)} = \cdots = \frac{m}{\sqrt{\left(\frac{1 - \sin(\alpha)}{G} + \lambda\right)\left(\frac{1 + sin(\alpha)}{G} - \lambda\right)}} \qquad \textbf{3-9}$$

$G = \frac{1}{d}$; m =Diffraction order

From Eq(3-9) we conclude that if the conditions for taking the derivative from the grating equation is imposed (fixed angle of incidence), the optimizer for angular dispersion is the grating frequency or reciprocal of the grating periodicity (Figure 3. 7).

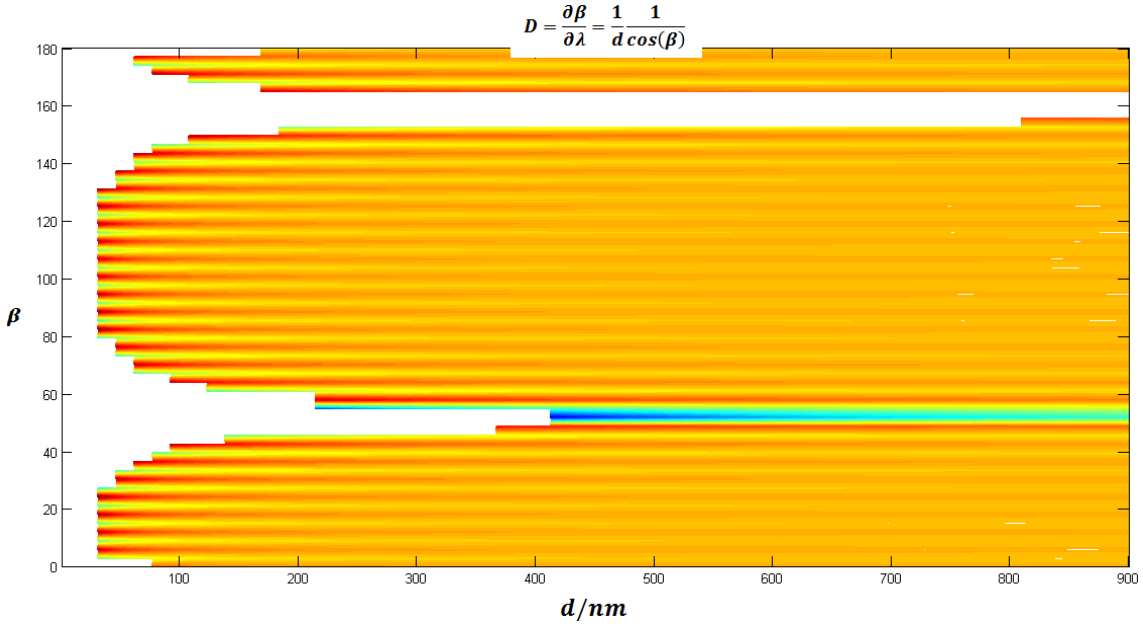

Figure 3. 7. Contour depiction of the dispersion of a grating; The high energy regions have maximum dispersion property

The high gain for angular dispersion occurs periodically in the grating. It also shows that some regions are discontinued in the contour plot. Another investigation for understanding the effects of the grating periodicity on the angular dispersion gain is through visualizing Eq(3-6) in 3D (Figure 3. 8). The 3D figure shows that if the dispersion versus periodicity graph is drawn using Eq(3-6) due to interrelationship between the diffraction angle and the incidence wavelength which is not present in it the graph results in undefined regions (discontinuities) and negative values (non-real dispersion).

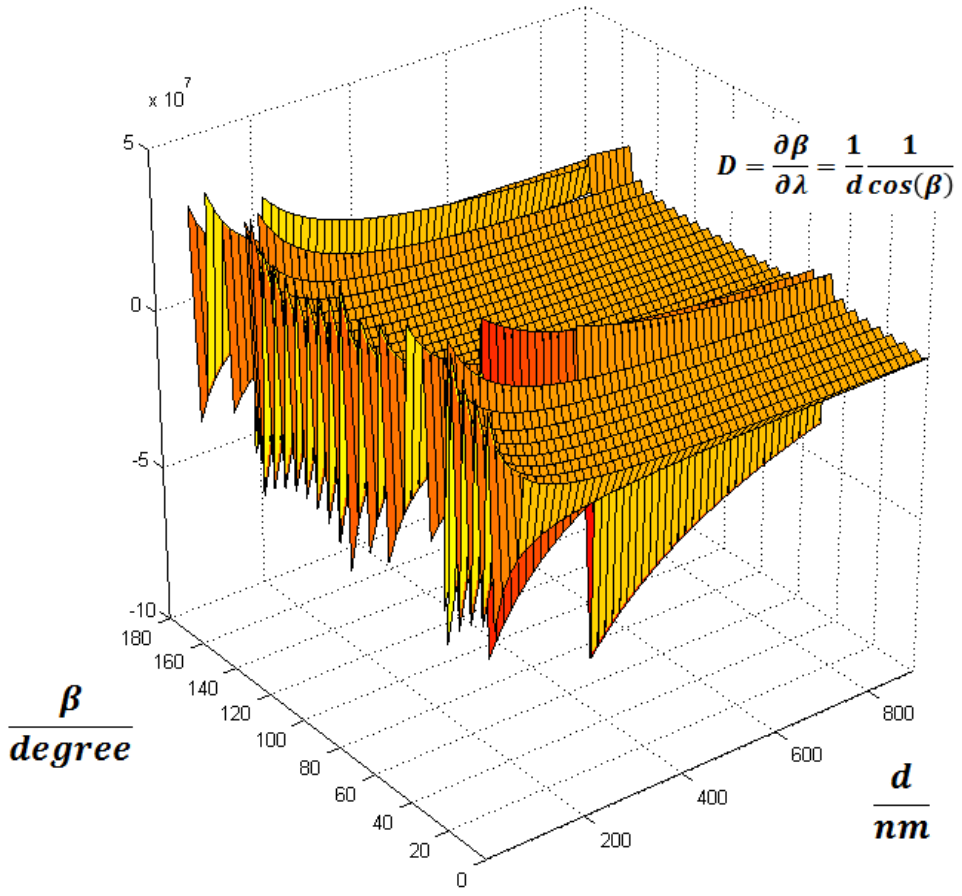

Figure 3. 8. Three dimensional depiction of Fig (43). The negative values may correspond to complex results which have no measurable physical property

Graphs below show the computer simulation for an approximation based on Eq(3-9) for different values for the fixed term $\sin(\alpha)$.As Figure 3. 8 shows, the effects of the changes of different angles of refraction on the dispersion is cyclic which corresponds to the cyclic nature of the phase (and consequently the amplitude for a non-decaying propagation) of the incident field. The overall transformations of the dispersion with respect to both grating periodicity and diffraction angle can be shown through Figure 3. 9. As shown in Figure 3. 9, using Eq(3-9) corrects the relationship between the angular dispersion and the incidence wavelength in oppose to what is resulted from Eq(3-6) in Figure 3. 8. Further derivation results in an estimation of the way D or partial changes of angular dispersion with respect to partial changes of wavelength, alters as a function of grating periodicity and the incident wavelength. Eq(3-9) is a result of careful derivation [19] with respect to changes of the wavelength. Through the latter procedure the angle

of incidence is treated as a constant, hence by using the alternate form of the dispersion Eq(3-9) we can observe what are the effects of independent changes of the incident wavelength on the angular dispersion (Figure 3. 9).

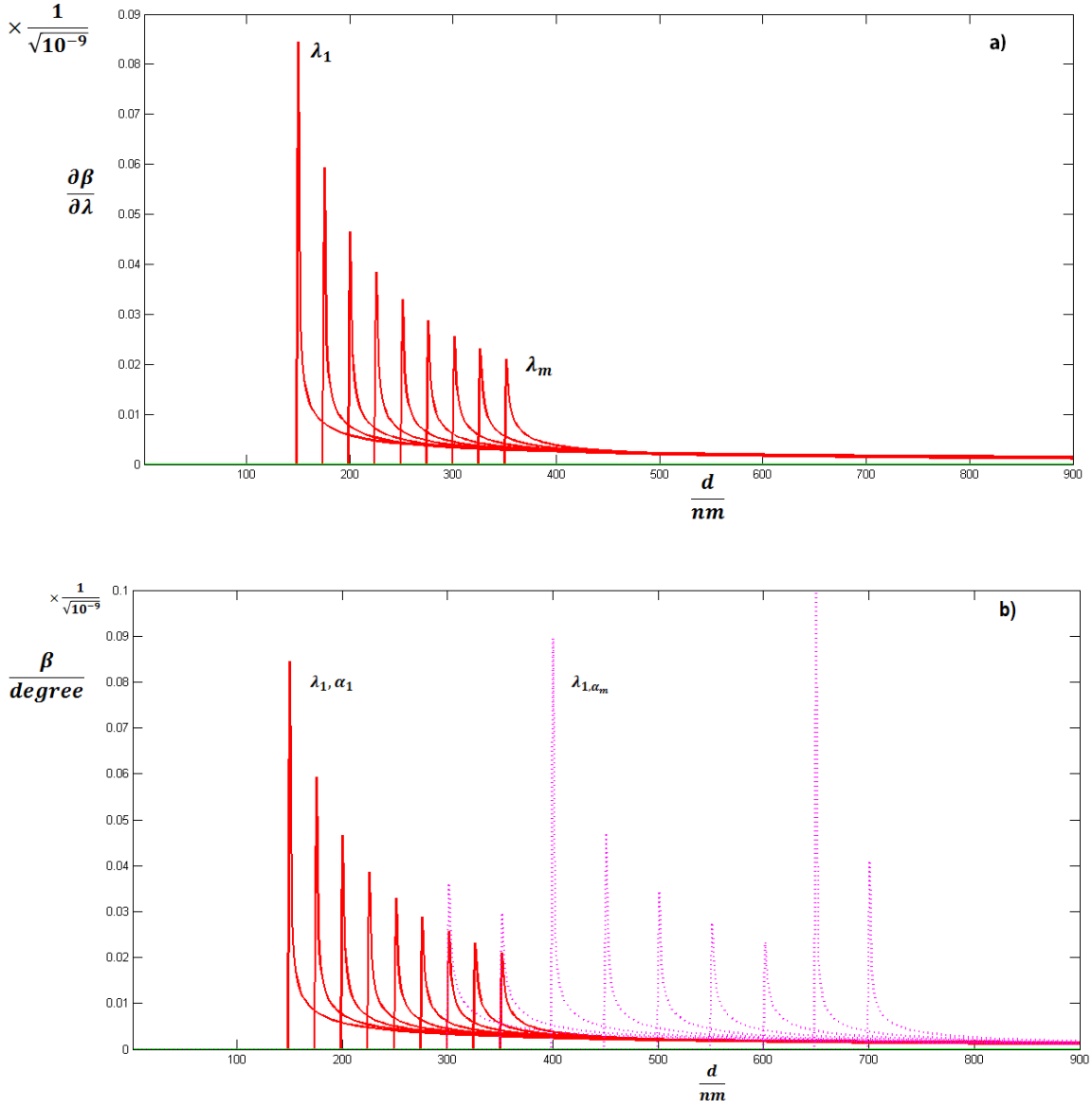

Figure 3. 9. a)- angular resolution for single angle of incidence b)-for multiple angles of incidence

Graphs in Figure 3. 9 indicate that depending on the grating periodicity and the angle of incidence as two independently varying variables, the rate of change of angular separation between different wavelengths (the grating dispersive resolution or angular dispersion) varies. According to Figure 3. 10, for a spectrum of distinct wavelengths such as that of the visible light (between 300 to 700 nm), the dispersive behaviour of the grating has a peak at a given periodicity. These peaks do not occur naturally at the periodicities close or equal to each wavelength yet via tuning the angle of incidence the dispersive peaks can be placed near the grating periodicities that also mimic the wavelengths of interest. Figure 3. 10 shows the dispersion peaks tuned up for grating periodicities between 400 to 900 nm.

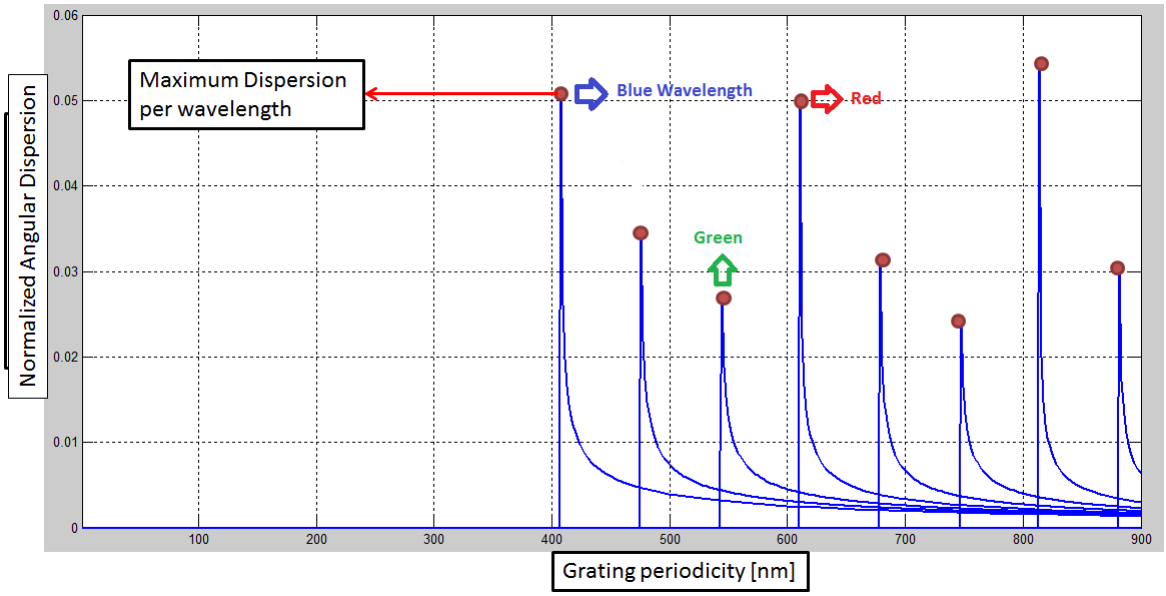

Figure 3. 10. Periodicities corresponding to the maxima of the graph range from 400 to 900 nm for simulated grating angular dispersion; at each maxima the grating is most sensitive to shifts in incident wavelength.

3.3.1. Defining the Periodicities for NOF

The grating incidence angles are chosen based on the imaging trials and the interaction with the angular resolution and the angular dispersion of the gratings. Due to an unknown point spread function of the imaging device and its angular resolution the choice of incidence angles was simple made based on how well resolved the images form with different periodicities. The Trials were first performed through fabrication and

imaging a reference array. The figures below show the diagrammatic and actual imaging of the reference array (Figure 3. 11).

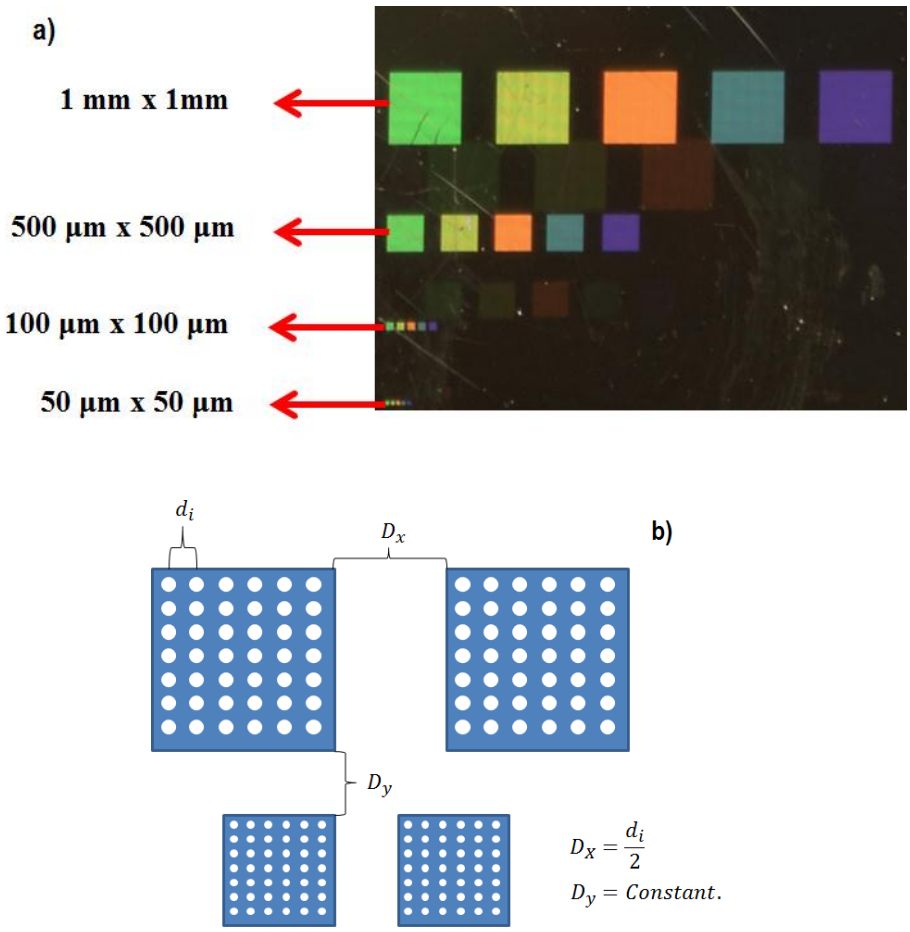

Figure 3. 11. a) Imaged Nano-optical optical features fabricated in columns to determine angular dispersion b)- The design parameters of the fabricated model

3.3.2. Encoding with Higher Counting Bases

Data encoding with binary counting system is proven to be an efficient method for encoding and storing real-valued analog data in a storage medium. The bi-state random variables that can either be one or zero are usually modeled through two distinct states of magnetization in a magnetic medium and/or two different optical signals that are being reflected from an optical medium. This allows for miniaturization of the physical structures that are supposed to produce these states efficiently. For the readout, due to the existence of only two states (signals, symbols or phase shifts) the confidence area is

considerably high while if not a hundred percent one signal, then it has to be the other hence there are good chances of decoding (demodulating) when the probability (or error probability) of either one of the sates is known. With such benefits why should there be an encoding system that employs a higher-variation-state random variable (each bit is considered a random variable mathematically) for data storage? In order to answer this question we divide the encoding process into two stages: 1)-Expansion 2)-Encoding Numerical Range.

1) Expansion Rate

During encoding a numerical value must change base to get translated into the modular space of the encoder system. Generally, a numerical value X is represented through the following form:

$$X = sgn(X) \oplus \sum_i D_i b^i \qquad \textbf{3-10}$$

$$sgn(X) = \sum_j \widehat{D}_j b^i$$

$\oplus$= Concatenation operator

$i, j \in \mathcal{N}$

D and $\widehat{D}$ are ranks of the numerical value and these are usually the parameters that are stored in a physical storage medium. During encoding the following relationship governs the expansion rate of the encoded data (Simple translation without source coding):

$$R_{exp}(X) = \frac{\sum \lceil \log_b x_i \rceil}{|X|} \qquad \textbf{3-11}$$

$R_{exp}(X)$ =Expansion rate of set X

X =Set of real-valued numbers (integers)

x_i =Element of X

$|.|$ =Cardinality of . (number of elements in .)

b =Counting base of the system

Adding to the states of variation of a unit information for storage via an encoding system means less physical space needed to store the transformed data. There are boundaries for how efficient the decrease will be as the number of variation states increases hence one can decide first up to what extent is it efficient to increase the variation states of the unit information carrier of the system second what is the cost of employment of more physical aspects into a bit (Figure 3. 12). The figure shows the expansion rate of a linear sequence of positive integers that has 1000 as its maximum value. The expansion rate is calculated for $b=[1,\ldots,10]$. The progression shows the rate of expansion for this sequence for unit information that ranges from 1 to maximum 10 states of variation. The solid lines show the rounded (upper boundary) values for the rate by which the sequence is expanded.

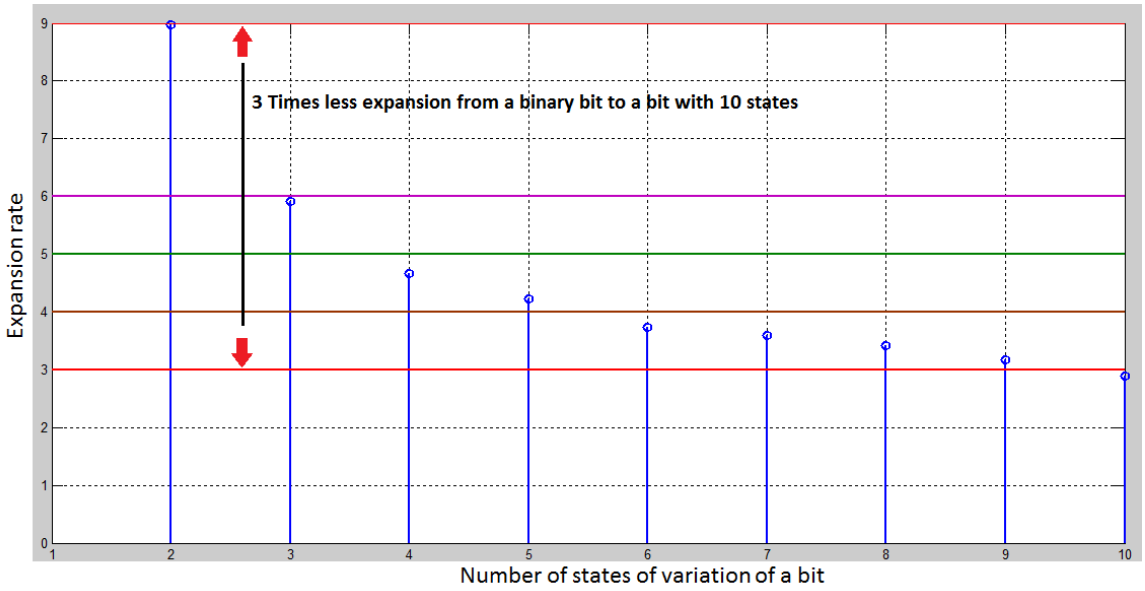

Figure 3. 12. Data expansion rate bounded by upper and lower limits as a function of bit-variation states

This figure indicates that e.g. for a sequence of monotonically increasing numbers (integers) with a maximum value of 1000, by encoding each element of the sequence using a bit that has ten states of variation compared to a binary bit, the sequence expands by a rate circa three times less hence the total number of unit information needed to be stored for such sequence drops by a factor of three.

2) Encoding Numerical Range

A simple derivation shows that for any number greater than 2, how the range of represented data in the storage system would be affected:

$$N + 1 = 2^M$$
$$N' + 1 = m^M$$
$$N' + 1 = m^M$$
$$N' = \left(\frac{m}{2} \times 2\right)^M - 1 = \left[\left(\frac{m}{2}\right)^M \times 2^M\right] - 1 = \beta \times 2^M - 1 = \beta N - 1$$
$$\forall\, m \geq 2 \;\; \beta = \left(\frac{m}{2}\right)^M \geq 1 \quad \therefore \quad N' > N$$

3-12

$m, M, N, N' \in \mathbb{N}$

$M =$ Number of bits

$m =$ number of states of variation of the bit

Figures 3.13 & 3.14 show the degree to which an encoding system can represent a numerical range using $m=[1,..,10]$ and $M=[1,..,10]$.

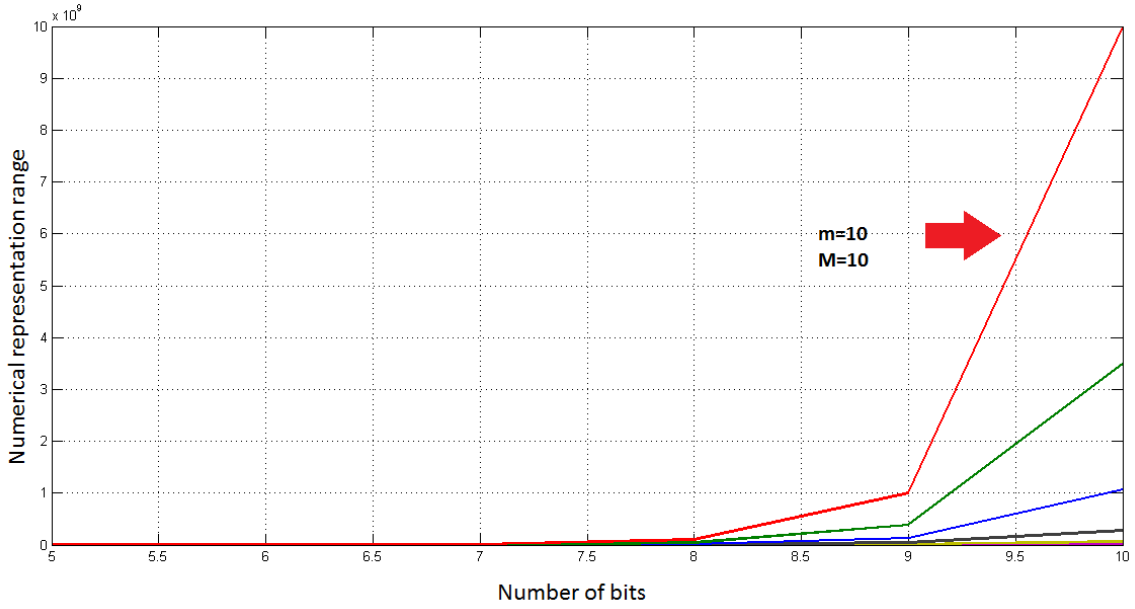

Figure 3. 13. Progression of the bit representation range as a function bit sequence length and variation state

Such diagrams allow for estimation of how efficient can it become for an encoding system to increase the states of its unit information. In Figure 3. 12, choices of 6,7,8,9 and 10 for the number of variation states are all having and expansion rate bounded between 3 and 4(the encoded data will expand 3 to 4 times the size of the initial data) hence it is economical to choose the lowest number (6) to employ less modulation parameters to the unit encoding system and also achieve only 3 to 4 times expansion in oppose to 9 times expansion using a binary bit.

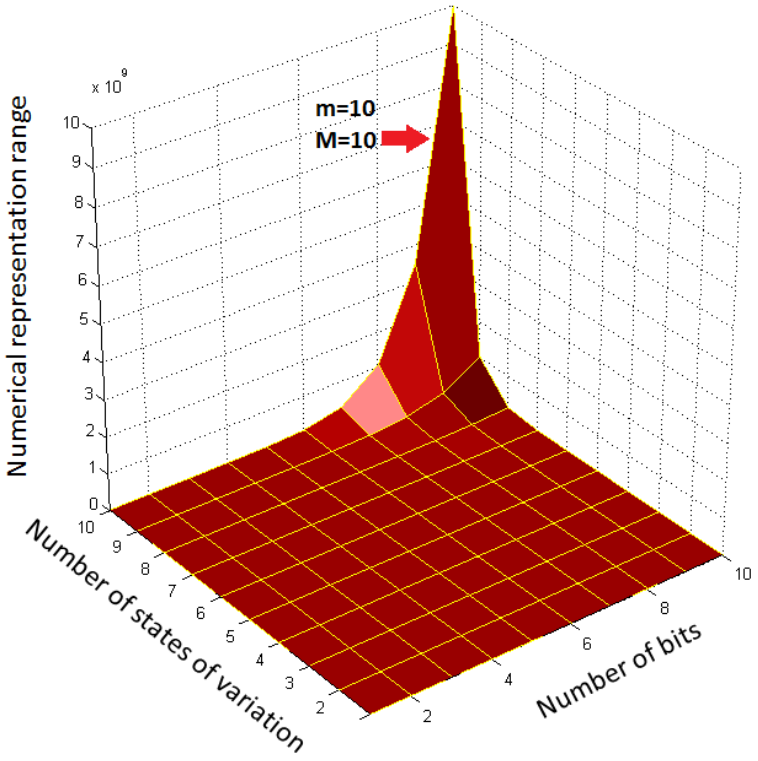

Figure 3. 14. Surface plot showing the peak numerical value representable by a 10-state bit string of length10

The result of Figure 3. 12 is that via choosing 4 or 5 states of variation the expansion rate of a sequence of decimal integers from the range [0 1000] will drop from 9 times the expansion down to ~4.5 times expansion. This decrease in the expansion rate is directly proportional to the decrease in the amount of space which is required for encoding and storing a given sequence of data. We choose 4 states of variation as a result of similar expansion rate decrease between 4 states and 5 states of variation so that the encoding bit will have 4 states: Sate “0”, Sate “1” , State “2” and State “3”. We match the simulated periodicities from Figure 3. 10 to these states so that each state is represented by a specific periodicity that mimics a particular wavelength (color). The four states chosen for this work are then represented as: 1)-State “0” =no grating 2)-State “1”=450 nm grating (Blue) 3)-State “2” =560 nm grating (Green) 4)-State”3”=650 nm grating (Red). Applying these periodicities to Eq(3-4) allows for modulation of an integer value into a combination of periodicities which will reflect their designated color, hence mapping from integer values (digital values) into the analog domain of the diffracted spectrum of the NOF.

The next step is to define an algorithm that receives data as an input and outputs the encoded data using the NOF permutation space (combination of the four states of the plasmonic nanostructures). The next section describes the designed algorithm part by part and describes each block of the algorithm in detail.

3.4. System Level Implementation of the Nano-optical Encoder

The system level analysis focuses on an interface between an input (digital for this matter) and an output that will be in the format of fabricated NOF as a result of the aforementioned transformation in (Eq(3-4)). Because the interface requires a precise element-wise modulation and due to cost and time boundaries of Nano-fabrication procedures the first step in the interface is the implementation of an efficient compression algorithm. Compression techniques have been reviewed in (2.3.2). Based on the existing standards we choose to implement a combination of lossy and lossless compressors to both decrease the bulk of the input data as much as possible while maintaining a fair psycho-visual(human-based visual quality) fidelity criteria for the reconstructed data after being read from the optically stored data. The scheme that has been implemented is shown in the Figure 3. 15 below:

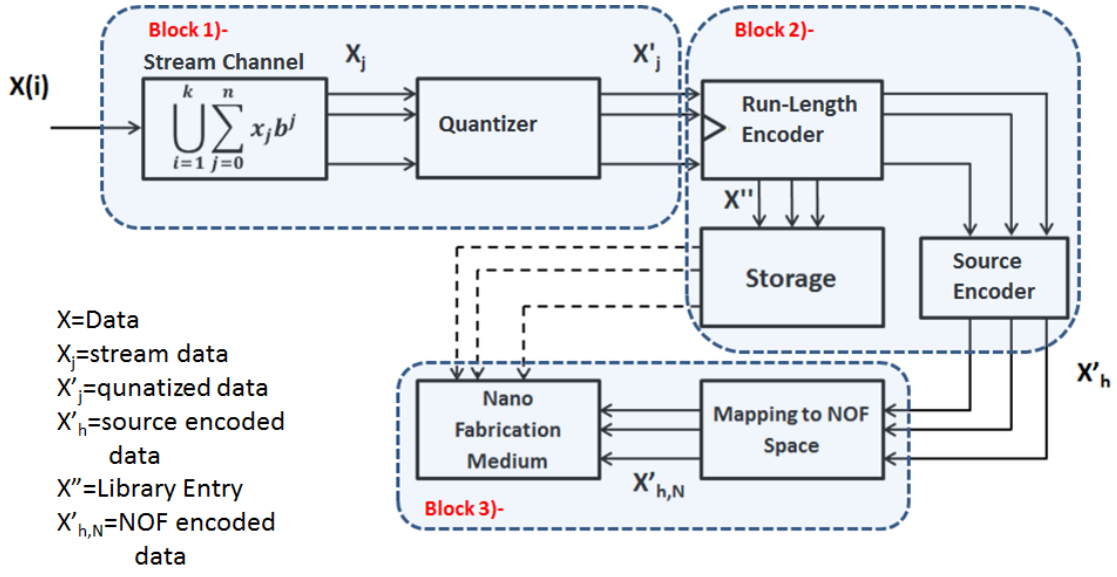

Figure 3. 15. Complete block diagram of NOF encoding system

A modular analysis of the system is presented in the following section:

3.4.1. Block1)-input streaming and quantization

The first block assigns a threshold to how much loss will be endured by the input via measurement of SNR(Signal to Noise Ratio) and PSNR(Peak Signal to Noise Ratio) (for Images), based on which the level of quantization is determined. The inputs that have been chosen for this project are 5 images and one text out of which three images and the text have been successfully encoded, optically stored and recovered. The remaining two due to Nano-fabrication limits have been set aside for future trials. Figure below shows the input images and the PSNR and MSE values for the quantization section. The blue line indicator has given the Rose criterion for PSNR related to image compression using lossy algorithms (PSNR>=20)(Figure 3. 16).

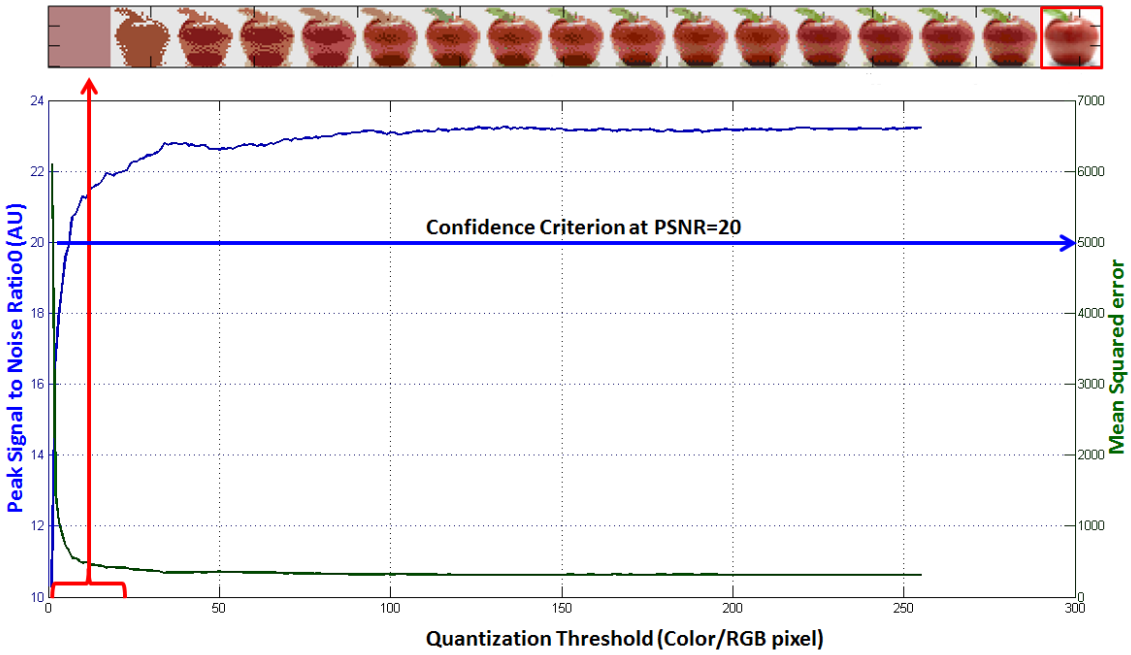

Figure 3. 16. The psycho visual comparison between different degrees of quantization for an input image. Red frame denotes the original quality

The encoding of two larger images yields larger number of nano-optical elements needed to be fabricated. Due to high hourly costs for both using the electron-beam lithography machine and the developer material used to post-process the nano-optically encoded data we resolved in encoding only three of the five initial images. In order to demonstrate the performance of the encoder in compressing and encoding both the un-fabricated images we present their equivalent compression ratios for three different compression levels.

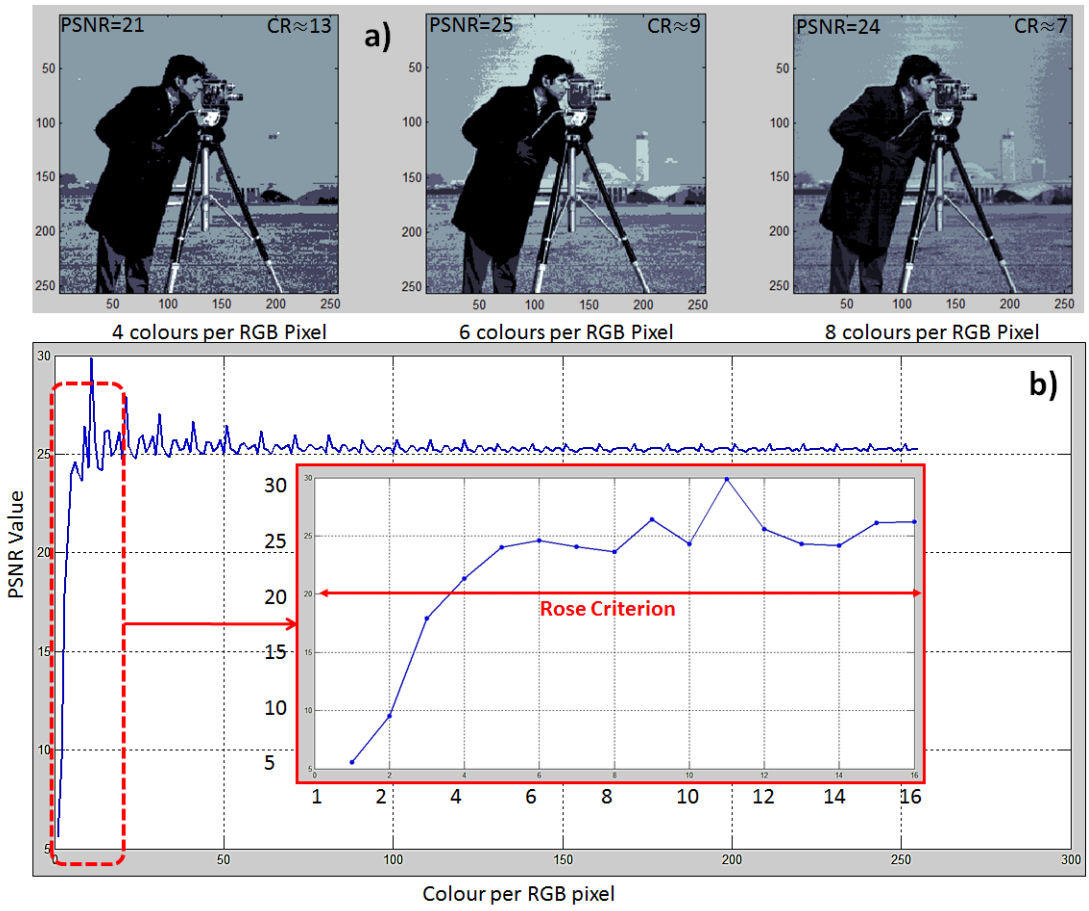

Figure 3. 17. a)-Different versions of cameraman image compressed by NOF encoder b)-PSNR for the encoded image using [1 255] colors per RGB pixel quantization.(The rest of the algorithm uses lossless encoding)

The number of optical arrays required for image 'Cameraman' exceeds 5000. Although as shown in Figure 3. 17 the compression ratio achieved by the algorithm is high yet fabricating 5000 arrays for the sake of this thesis project is merely un-economical. Figure on the next page shows similar information presented in Figure 3. 18, for image 'Lena' :

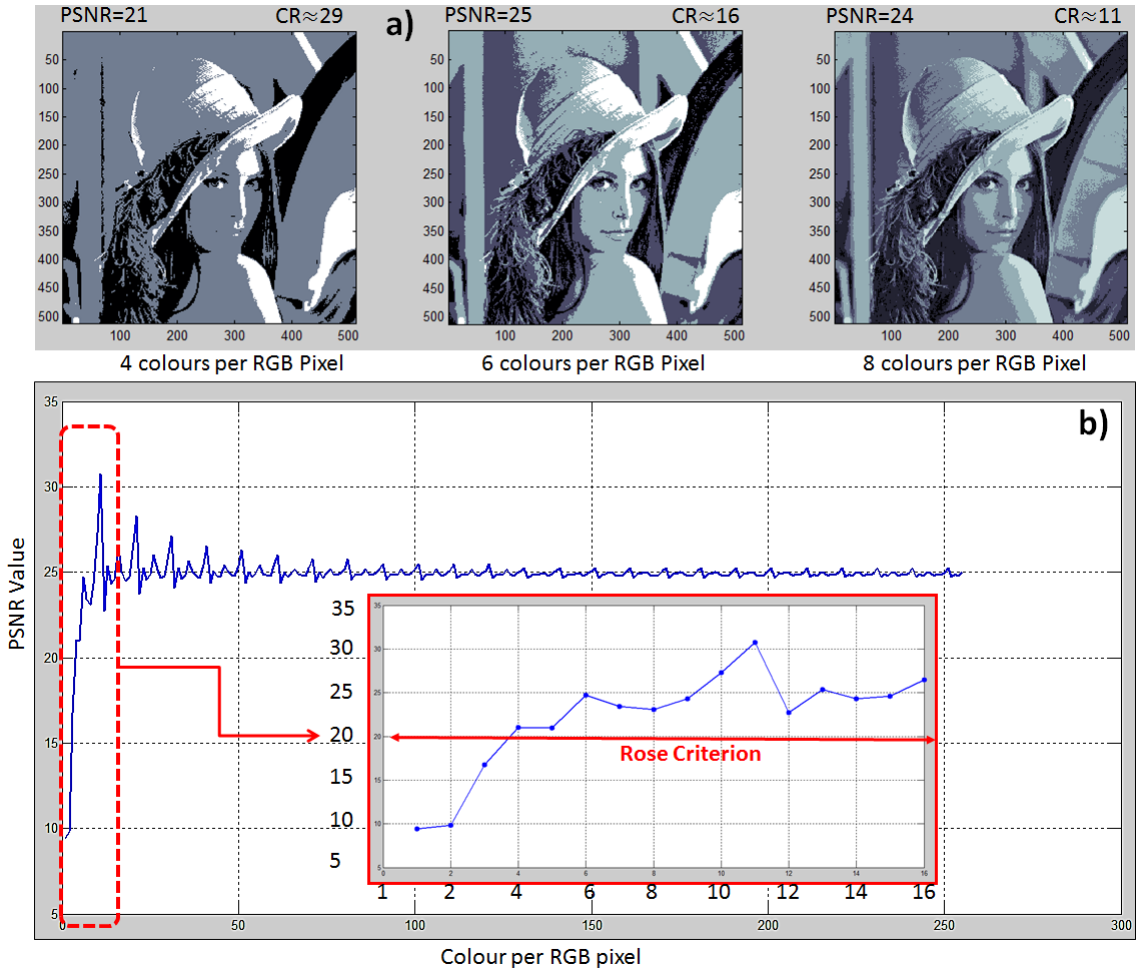

Figure 3. 18 a)- Different versions of lena image compressed by NOF encoder b)-PSNR for the encoded image using [1 255] colors per RGB pixel quantization.(The rest of the algorithm uses lossless encoding)

The number of optically storable elements required to be fabricated for the image 'lena' with results presented in Figure 3. 18 is circa 24000. This number is too large and cost inefficient for fabrication during this master's thesis. The compression ratios presented for these images on the other hand show more than 3 fold decrease in all the cases presented in Figure 3. 17-18 and along with PSNR greater than 20 we conclude that the perceptual quality of the two encoded and not fabricated images is acceptable for encoding using our proposed encoder.

The stream channel is a filter that either allows for progress of the data into the quantizer if data value is unsigned integer or 8-bit binary format, else the filter uses a 8-bit bitwise shift and streams the data in the following format: 1)-most significant bit stream 2)-least significant bit stream[§] into the quantizer. The input stream channel has also a decision block which can send queries to a buffer that accepts whatever extra (yet not invaluable) information that exceeds the quantizer or the stream channel`s tolerances for the type of the data that shall be further inputted into the system. This way, some of the stream's information can be selectively stored to allow for a security check over whom or what can access the stream at any level further than the stream channel (Figure 3. 20). The figure below shows the input images to the encoder. The ones with a red indicator are those having been fabricated (Figure 3. 19).

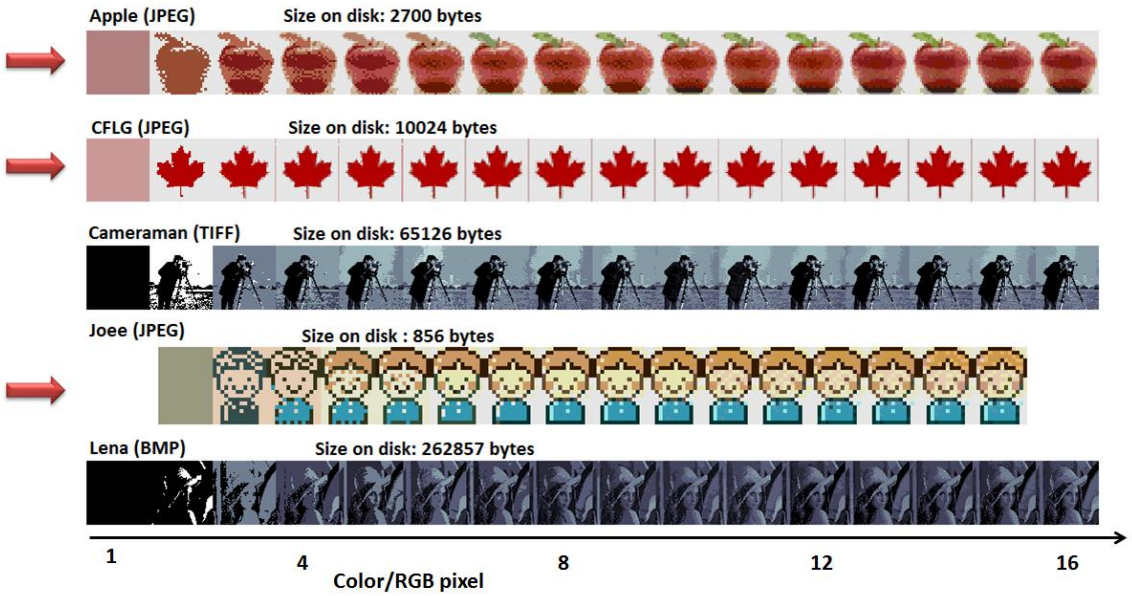

Figure 3. 19. The sample images each being quantized up to the confidence criterion marked in Fig(3.16)

[§] The least significant bit (lsb) is the bit position in a binary integer giving the units value, that is, determining whether the number is even or odd and the most significant bit (msb, also called the high-order bit) is the bit position in a binary number having the greatest value.

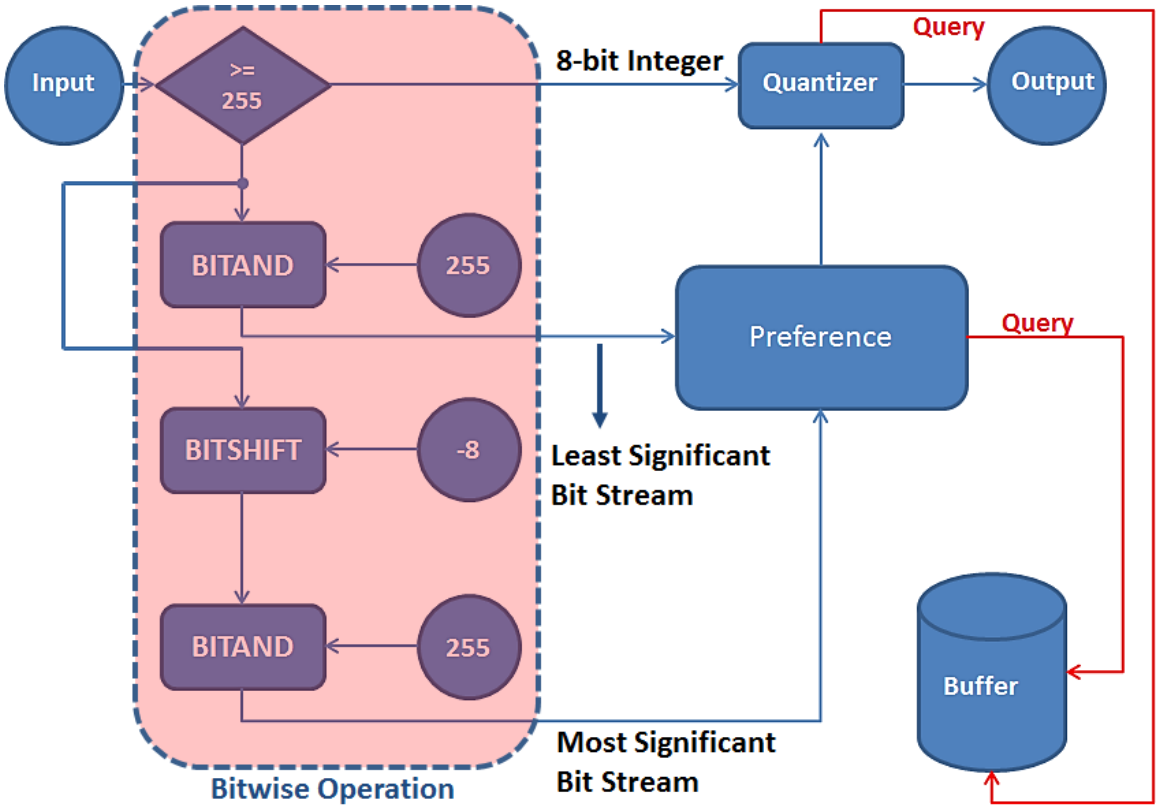

Figure 3. 20. Stream Channel Diagram; BITAND and BITSHIFT denote bitwise operation for maximum 8-bit value occurrence probability

3.4.2. Block2)-Run-Length Encoder and Source Encoder

The output of the quantizer passes through a two-phase run-length encoder in order to decrease the bulk of the data before source encoding. Both the encoders in this block are considered error free and/or lossless hence there is no measure of SNR or PSNR defined for the data at this stage. The compression ratio however is considered. The run-length encoder (RLE) performs a comparison between de-ranking the input values into integer streams if the end result of an estimation is better, else it runs the data through and streams the scanned data into the source encoder in the following format: 1)-unique set; these are the symbols that have been counted and stacked together, 2)-counted set, these are the numbers for which each symbol has been repeated. The graph shows the measure of RLE for a data stream after being compared through the RLE and De-Rank & RLE block and the source encoder (Figure 3. 21).

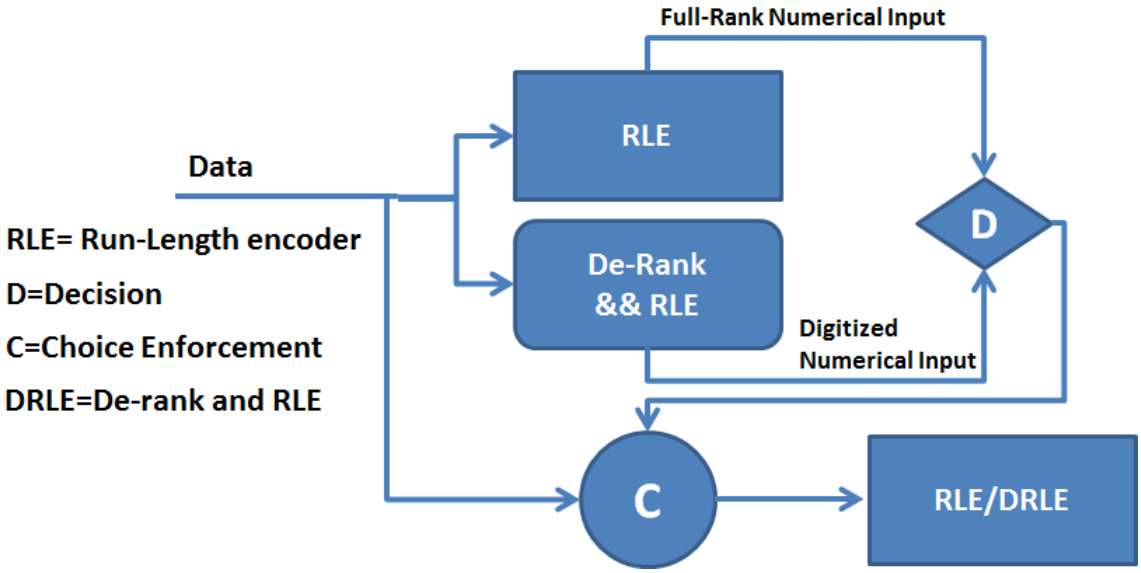

Figure 3. 21. Run-Length Encoder Decision making Diagram

The source encoder receives the data from the RLE and based on whether or not the user has defined a library entry chooses the encoder. In the case of library and also for better compression the source encoder runs the data through a Huffman encoder and then sends the decomposed and encrypted library to the storage (HDD), else the source encoder chooses an arithmetic encoder that leaves no library behind and then sends the encoded data to NOF permutation space transform block. In an extreme case, due to having fabrication limits the three optically encoded images have been chosen to leave a library behind. This way, the number of optical elements to be encoded on the optical medium becomes quite limited and easy to handle during the fabrication process.

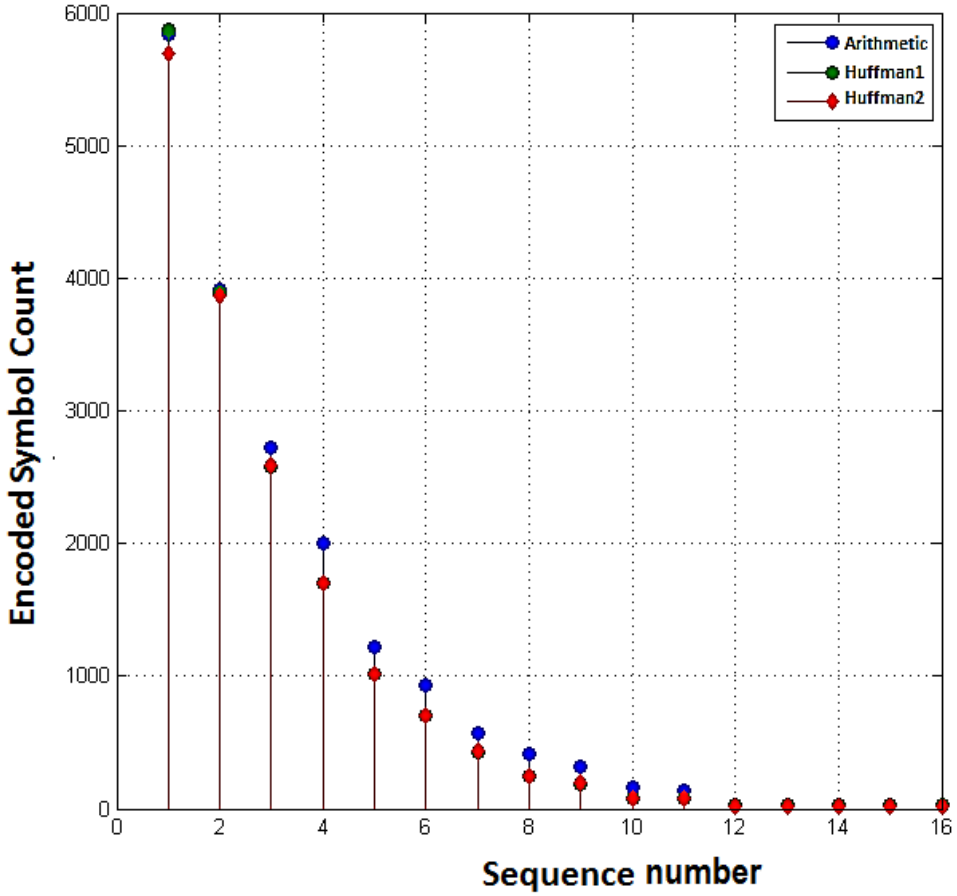

Figure 3. 22. Encoding symbol count comparison for 2 Huffman and one arithmetic encoder for variable length integer sequences

Figure 3. 22 shows the symbol count for 16 multiple streams and the number of encoded symbols outputted by two Huffman algorithms and an Arithmetic encoder. Based on these results the only difference between the two algorithms, Huffman and Arithmetic is due to the existence of a library for the Huffman encoder. As mentioned, for fabrication trials due to limits of fabrication procedures a recursive Huffman encoder is being applied that produces a relative large library yet minimizes the size of the NOF encoded data. Figure 3. 23 below shows the multi-state decision making of the algorithm to whether or not apply recursive Huffman encoding with the cost of increasing the library size or not. The preference is what user can directly define into the system while the states are connected to other true/false outputs from other modules.

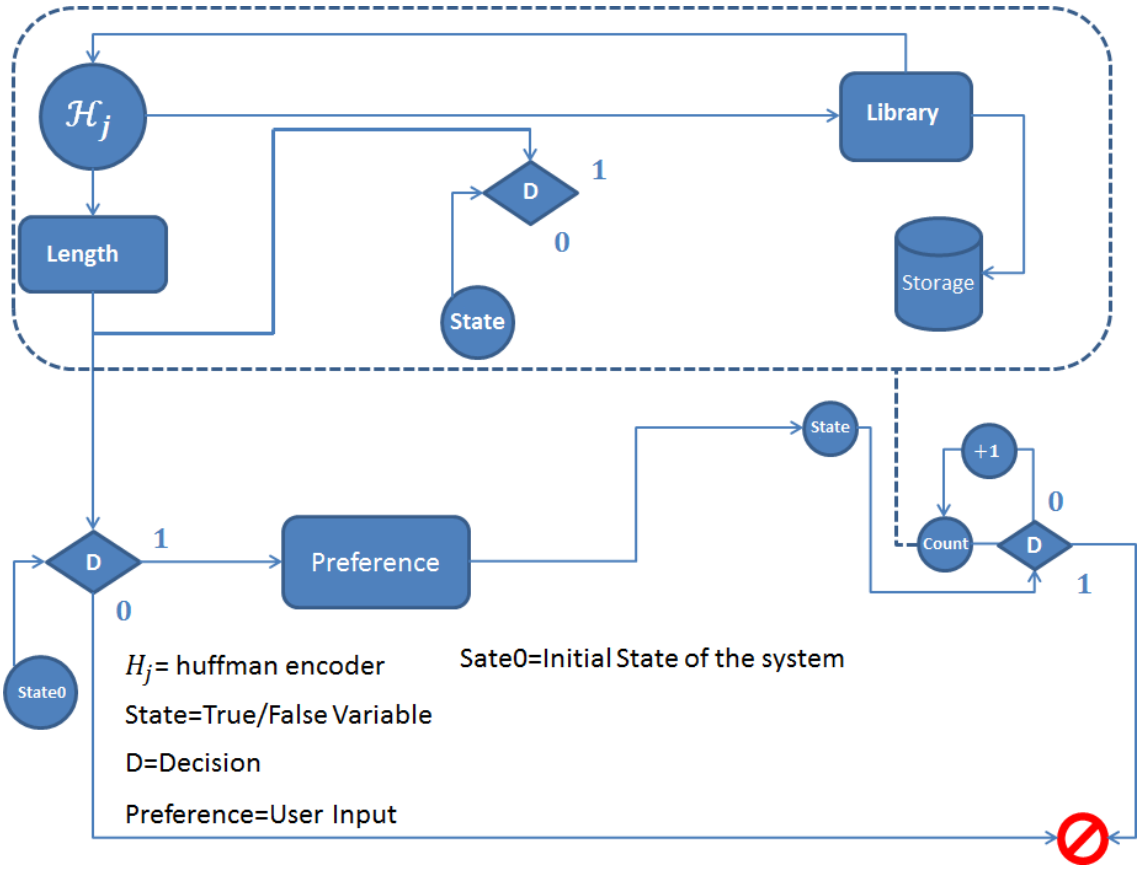

Figure 3. 23. The Huffman Recursive Loop Decision Making Diagram; initial state is one loop per data cycle

3.4.3. Block3)-Mapping to NOF space and Nano-Fabrication

This system block receives the source encoded output of the Huffman(or Arithmetic) encoder and applies a linear transformation as mentioned in (3.1) to translate each value of the data into the NOF permutation space:

$$X\big(P(X=A)\big)=\sum_{j=0}^{M-1}\frac{m\lambda_i}{K}b^j=\frac{m}{K}\sum_{j=0}^{M-1}\lambda_i\,b^j \qquad \textbf{3-13}$$

A Library (in case user defined states) will reside in a storage space for further data reconstruction followed by a two phase generation of electron beam lithography-compatible scripts that are result of application of a novel algorithm developed by

CiBER, and further translated into CAD format for the electron beam lithography (EBL) system to perform the final stage of the process and that of fabrication of the NOF (Figure 3. 24).

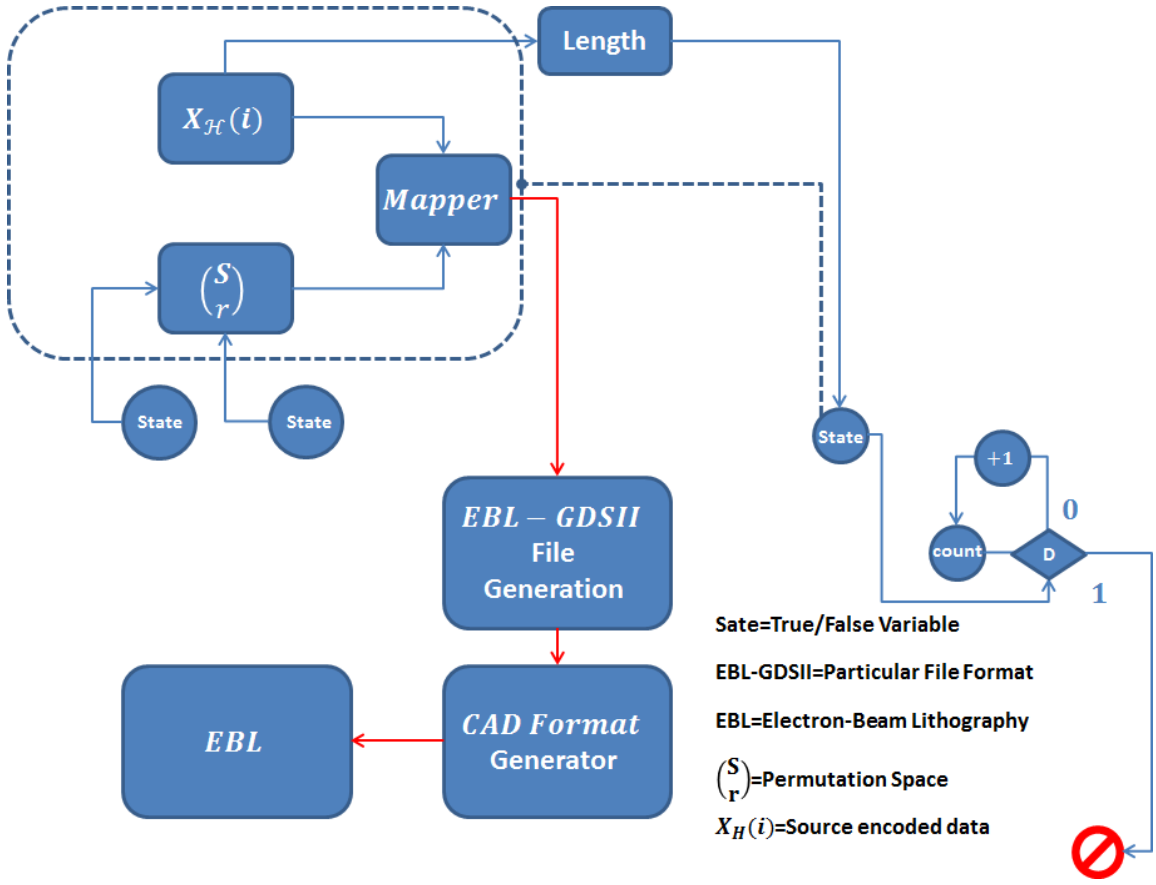

Figure 3. 24. Translation and Fabrication Module Diagram

3.4.4. Overall System Design

The final stage of the NOF encoding procedure is to input the encoded data into the software developed by CiBER for generation of Nano-optical feature. The software is part of the general algorithm that has been designed for designing and patterning Nano-features, it accepts integer values in a range defined by the user interface of the software and turn the input data into text file format with an EBL readable structure (GDSII). The file will finally be CAD transformed as to the fact that the EBL system uses an XY stage in order to transform the designed pattern or “write” the Nano-optical

feature patterns onto a substrate. The Nano-array-design software is a research project currently underway by CiBER research team (Figure 3. 25).

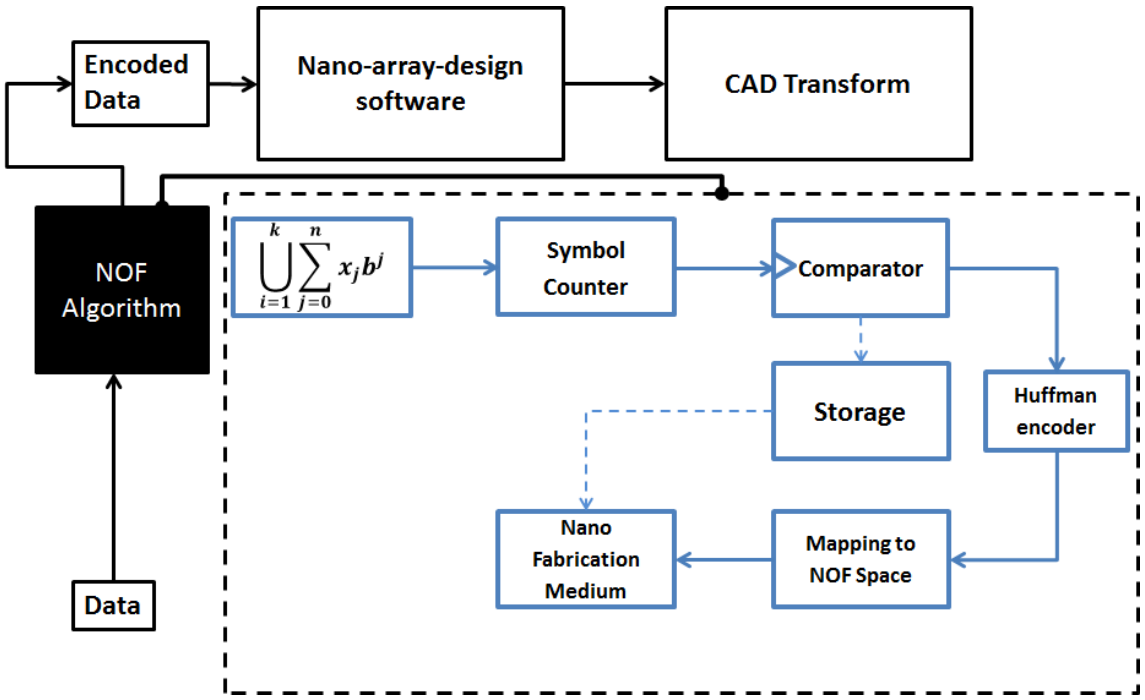

Figure 3. 25. System block diagram including the design software for transforming the encoded data into EBL readable templates

Figure 3. 26 and Figure 3. 27 on the show a full-detailed block diagram of NOF encoder and decoder system that have been described in the modular analysis in previous pages.

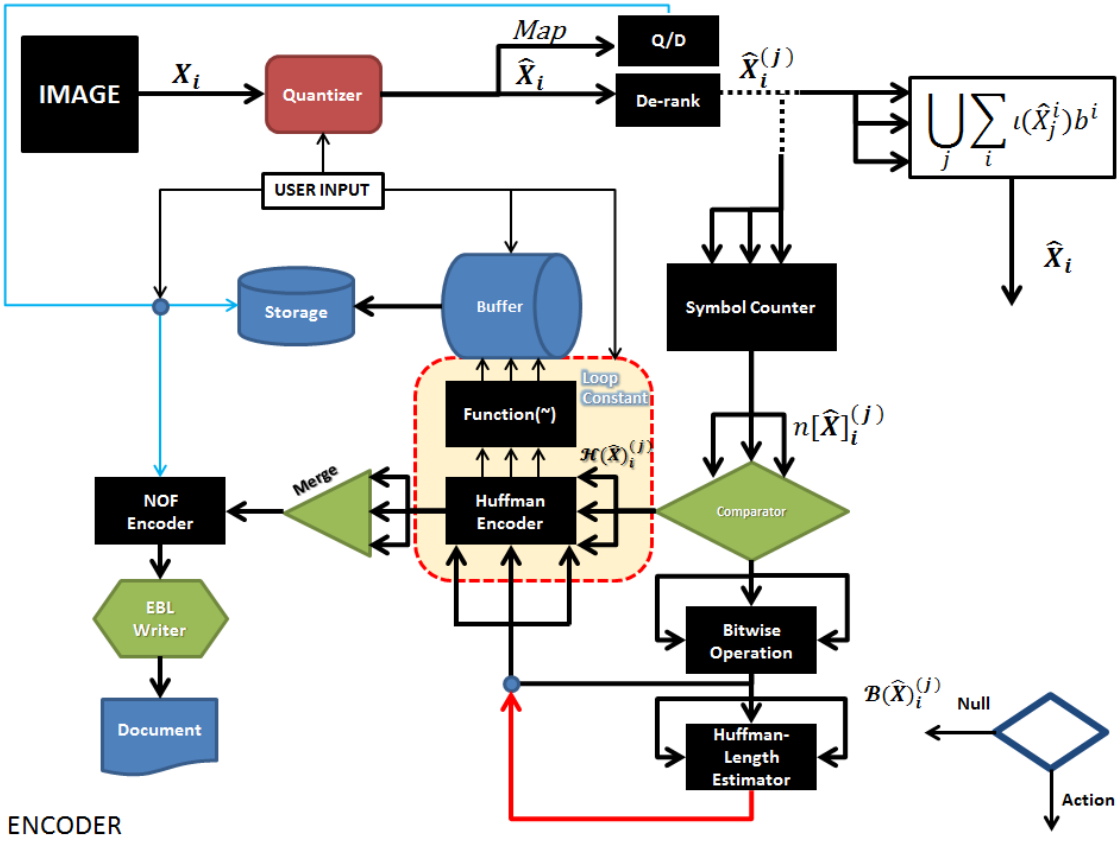

Figure 3. 26. NOF Encoder block diagram

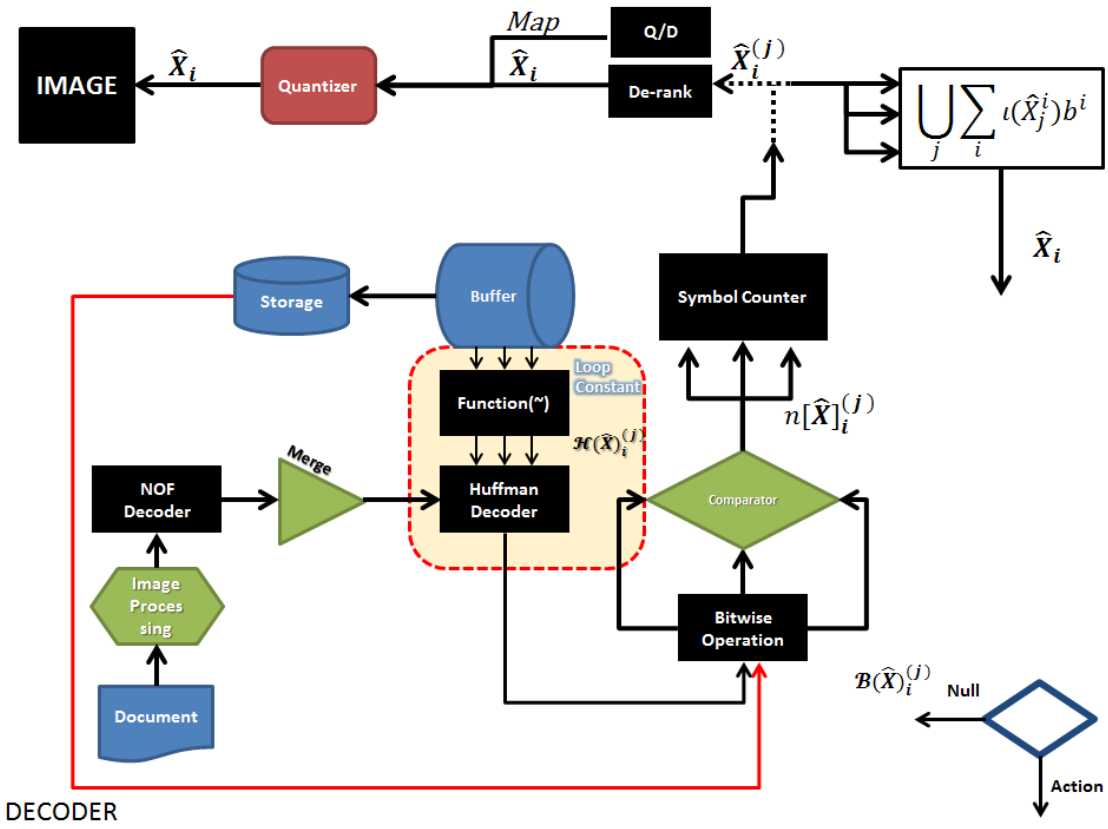

Figure 3. 27. NOF Decoder block diagram

The NOF (Nano-Optical Feature) encoding system in summary receives numerical values which will be streamed through an entry-level channel that allows (and converts) all input into 8-bit integer formats and after quantization and compression, it transforms the data into CAD-Readable Graphic Database System file format II (GDSII) and turns the data into machine EBL-compatible machine readable data for Nanofabrication.

Chapter 4 Experimental Results and Discussion

The experimental setup for encoding data has been the electron beam lithography(EBL) setup at 4D-Labs located in Simon Fraser University's Physics department (Figure 4. 1) and the trials have been three color images of various sizes and the text (www.ID-ME.ca) all encoded using the NOF encoder algorithm. As mentioned earlier due to minimization of the optical nanostructures that were needed to be fabricated on the optical medium for encoding, the algorithm chose to perform the source coding using Huffman coding with 5 repetition loop to decrease the size of the data encoded on through EBL leaving libraries that were stored in a buffer (HDD or other storage media) for data reconstruction.

Figure 4. 1. The EBL setup at 4D labs located in Simon Fraser's Physics Department

The figure below shows the file transformation from integer (8-bit unsigned format) to the GDSII pre-text format that is EBL machine readable. Each colored rectangle shows the file format of the transformed data related to the block with similar color arrow (Figure 4. 2).

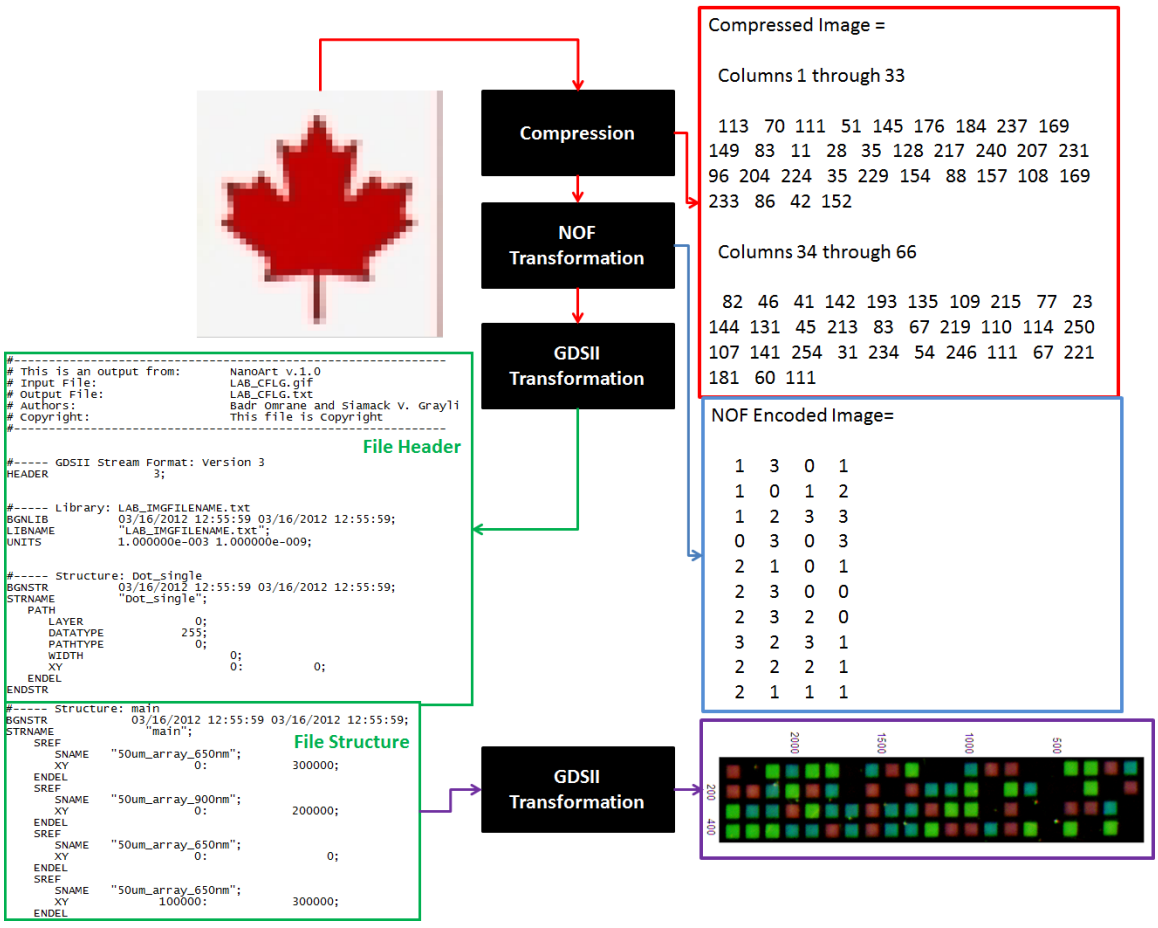

Figure 4. 2. Depiction of different stages of NOF encoder outputs until EBL machine readable file

The data recovery has been performed using two different methods for signal acquisition: 1)-Transmissive signal readout 2)-Reflective signal readout

4.1. Transmissive Signal Readout

Transmissive signal read out relies on the surface plasmonic resonance signature of the NOF encoded arrays. In order to detect a full range spectrum of the transmitted light we used an inverted microscope (courtesy of Dr. Karen Kavanagh SFU 4D Labs) and

recorded the spectral response of the encoded data using a computer. The recorded spectra were then analyzed for peak plasmonic resonance peak detection that matches the fabricated arrays' periodicities. In a transmissive system, the sensor is placed in the exit plane of the grating. As a result if the system of Nano-hole arrays is coated with thin metallic layers the incident angles will eventually provide the momentum matching conditions for the surface plasmonic standing waves Eq(2-6) and the transmission field has a resonant peak proportional to the Nano-scale grating groove periodicity. The experiments did not further expand using the effects of surface plasmonic resonance and the contribution of surface plasmon polaritons to an optical signal due to a requirement for high resolution lens apertures and objectives for resolving the signals. The reference array shown in Figure 3. 11 is also been examined using a high resolution microscope to investigate effects of surface plasmonic resonance in the spectral response of arrays with various periodicities (Figure 4. 3).

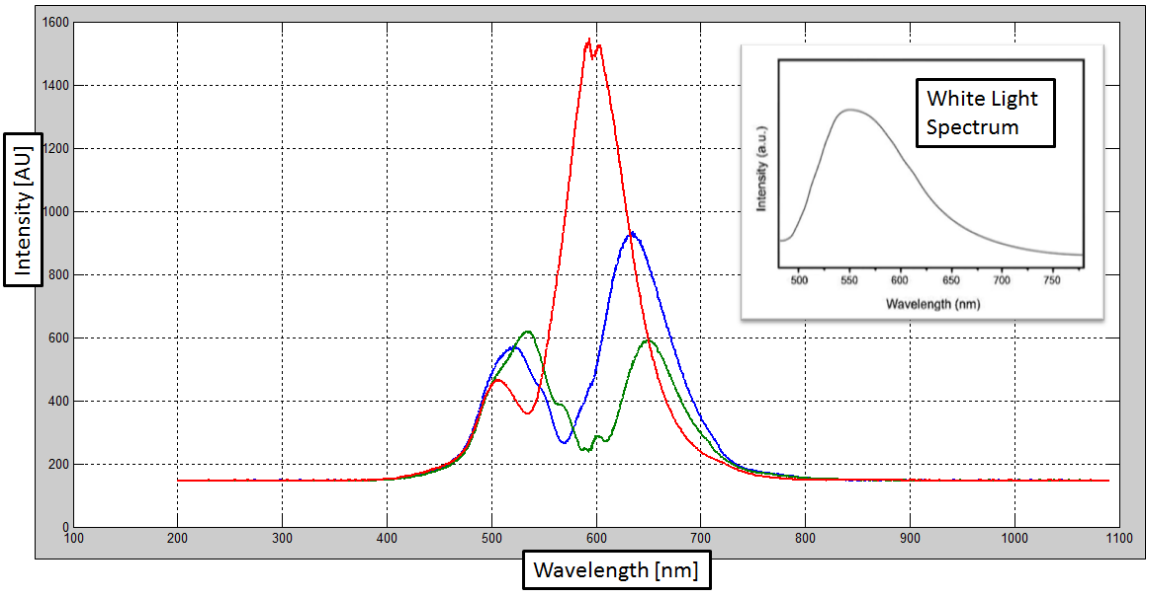

Figure 4. 3. Spectral readings for three adjacent Nano-optical features with well-resolved extra ordinary transmission peaks

The graph above shows that from each periodicity arises a different spectral peak compared to others. These peaks correspond to the resonance conditions that have been met under the boundary and momentum matching equation presented in Eq(2-6). The measure of variation is the wavelength at which the peak response occurs. The enhanced transmission (EOT section) enables miniaturization of the gratings in order to

achieve higher storage density but the susceptibility of the acquired signal due to sensor limitations (spectral resolution) does not allow for fix thresholds to tag different periodicities. This work simply resigns further discussions on optical data storage using EOT based Nano-optical features and gives some measure of comparison based on a reference array presented in Figure 3. 11. In this method the storage density depends on the spectral resolution of the system which in turn is a function of optical system of the imaging sensor. Figures 4.4 & 4.6 show the spectral responses for similar arrays which vary in size by 3 orders of magnitude.

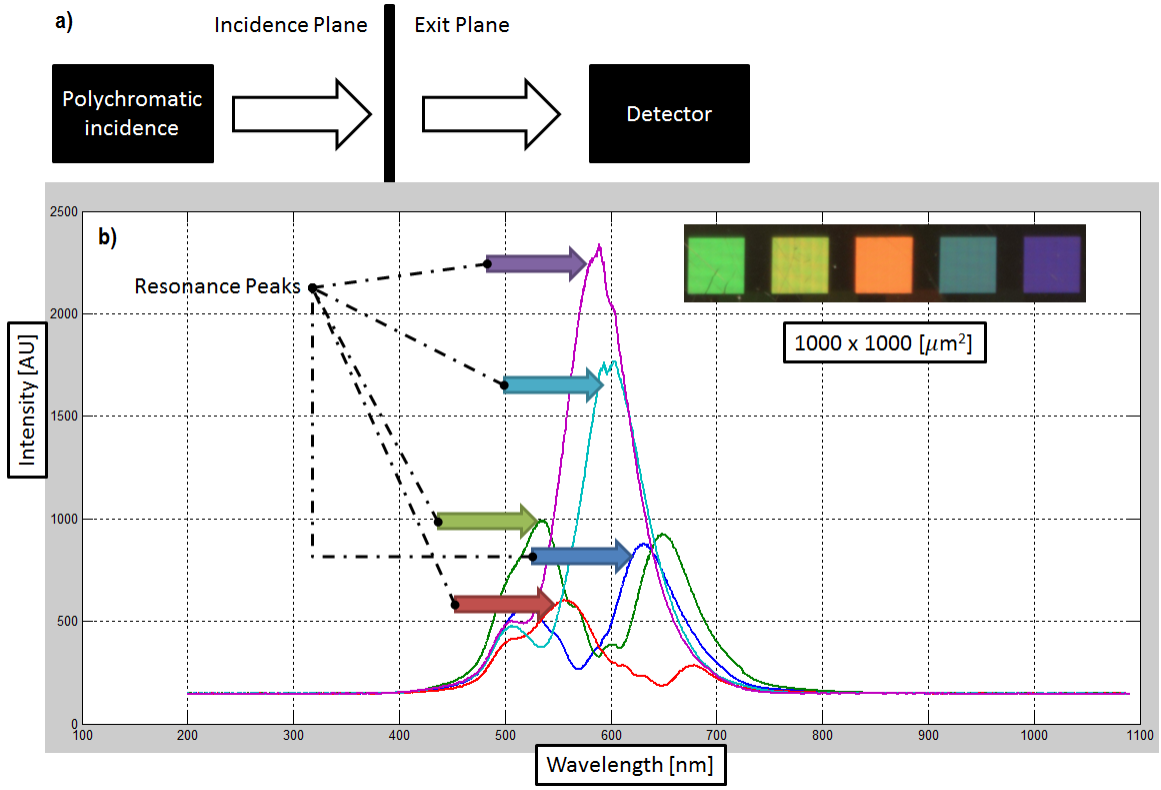

Figure 4. 4. a)-Sensing Block Diagram for Transmissive Plasmonic and b)- Spectrum of NOF and well resolved spectral responses for Nano-optical features with 5 different periodicities

Figure 4. 4 shows how each NOF spectral response is being received by the spectrometer for a combination of arrays with 5 different periodicities. The degree of resolution of the spectral response depends on the well-separated plasmonic peaks for each array.

Figure 4. 5 below is the experimental setup for transmissive signal detection. The system used is an inverted microscope (Make: Reichert-Model No. 325 098) and a computer to record the spectral responses through a spectrometer (Make : Tidas 400MP-Unpolarized Spectral Range 360-780nm).

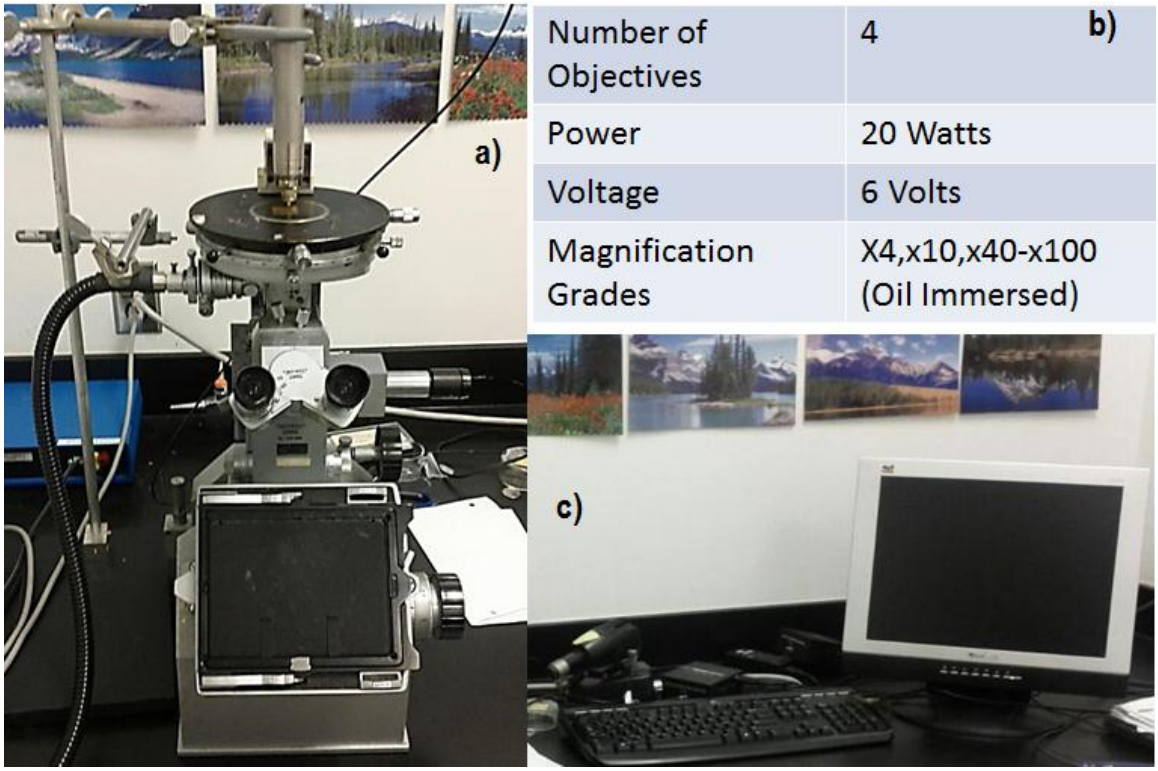

Figure 4. 5. a)-Inverted microscope combined with a spectrometer b)-Microscope specs and c)-the computer used to record the spectra

The use of the spectrometer with an unpolarized spectral range of 360nm to 780 nm has been matching the range of spectral response (plasmonic response) predicted by the periodicity of the NOF (450nm-650nm) which produce plasmonic peaks in the same range as the periodicities for square shaped NOF.

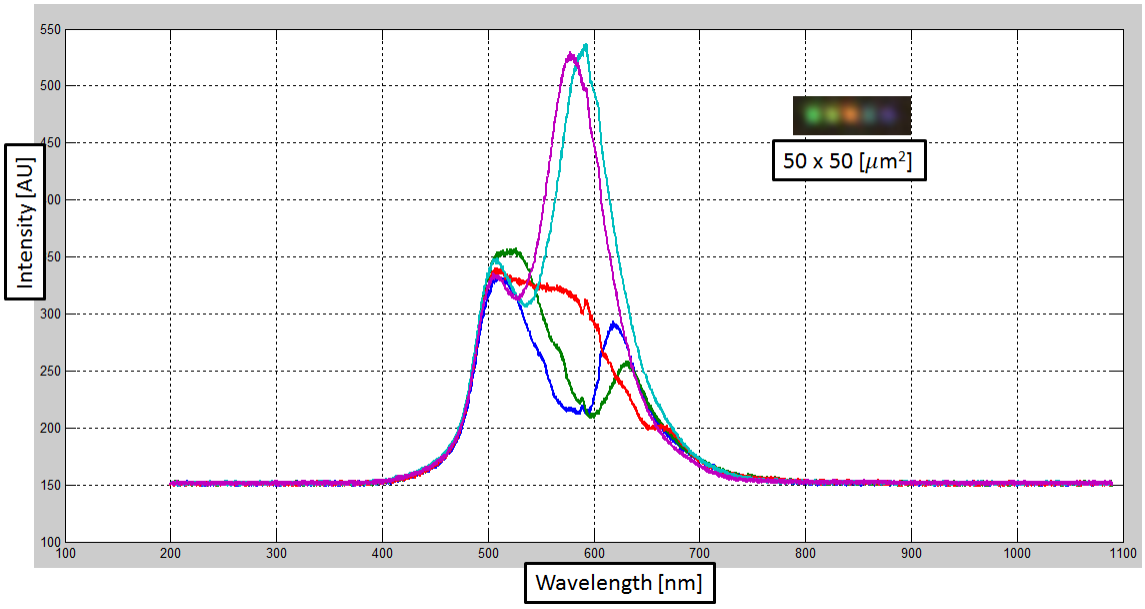

Figure 4. 6. Unresolved spectral responses for Nano-optical features with 5 different periodicities

The transform that takes the real-valued quantities into the signal domain for transmissive signal is defined as the overall (sum or integral) of the propagations of periodic structure being illuminated as a function of its reciprocal lattice vectors G_x, G_y. For a square array as one used in Figure 3. 11 the reciprocal lattice vectors are the same, hence the resonant wavelength as a function of the grating periodicity is calculated through the following equations Figure 4. 7 [20][21]:

$$\lambda_{SPR}(m,n) = \frac{a_0\left(\sqrt{\frac{\epsilon_m \epsilon_d}{\epsilon_m + \epsilon_d}}\right)}{\sqrt{m^2+n^2}} \qquad \textbf{4-1}$$

$$|\bar{G}_X| = |\bar{G}_Y| = \frac{2\pi}{a_0}$$

$\bar{G}_X$, $\bar{G}_Y$ =Reciprocal lattice vectors

a_0 =Nano-grating periodicity

m, n =Spatial coordinates for an array

λ_{SPR} =Resonant (peak) wavelength

ϵ_m, ϵ_d =Metal and dielectric permittivity

An approximation of the signal perceived by the sensor shall account for changes in the metal permittivity as a function of the incident field angular frequency as well hence Eq(4-1) can be written for separate wavelengths :

$$\lambda_j(m,n) = a_0\sqrt{\epsilon_d}\int\int_{m,n}\left(\sqrt{\frac{\epsilon_m(\omega_j)}{\epsilon_m(\omega_j)+\epsilon_d}}\cdot\frac{1}{\sqrt{m^2+n^2}}\right)dm\,dn \qquad \textbf{4-2}$$

And the total transmissive signal perceived by the sensor can be written as:

$$\lambda_{Signal}(m,n) = a_0\sqrt{\epsilon_d}\sum_{j=0}^{M-1}\int\int_{m,n}\left(\sqrt{\frac{\epsilon_m(\omega_j)}{\epsilon_m(\omega_j)+\epsilon_d}}\cdot\frac{1}{\sqrt{m^2+n^2}}\right)dm\,dn \qquad \textbf{4-3}$$

ω_j =Angular frequency at wavelength j

ω_j =Angular frequency at wavelength j

M = Constellation order

Figure 4. 7 shows the spatial distribution of resonance peaks as orthogonal lattice directions m and n.

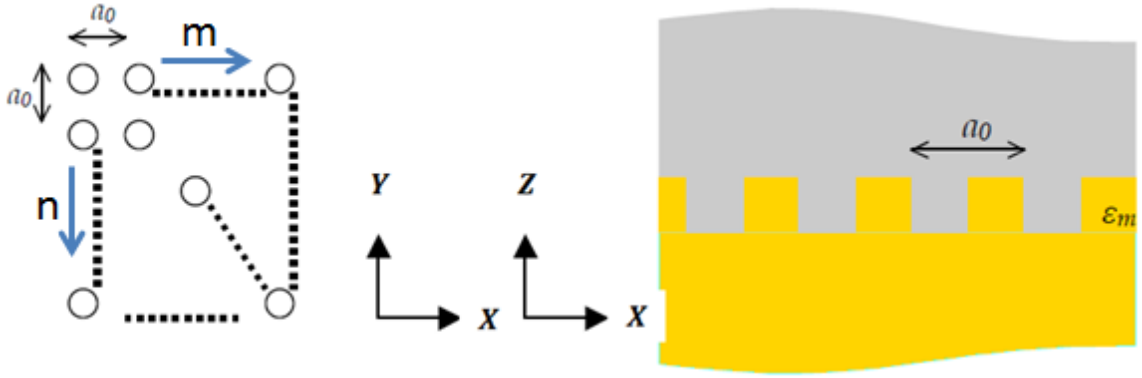

Figure 4. 7. Position and direction of the resonance peaks in a square lattice

The signal collection direction means to have a sensor recording the spectral responses of the NOF in either m or n direction which construct an orthogonal (perpendicular) coordinate system as shown in Figure 4. 7 .

4.2. Reflective Signal Acquisition

A reflective signal is acquired as collection of the diffracted orders. Depending on the periodicity and what has been discussed in (3.2) these responses were captured via scanning the arrays with a flat-board scanner setup with maximum resolution of 9600 dpi. Scanners use a cylindrical lens to collect the back-reflected light from the scanning object while a light source (usually a polychromatic source) at an angle is incident on the scanning object. The back reflected light is gathered at an angle normal (or other) to the scanner's bed. For a diffraction grating under the scan, this collection angle translates into a grating-periodicity-dependent diffraction angle for the fixed angle of incidence and hence what received by the scanner image sensor (CCD or CIS) is the result of pixel by pixel collection of particular wavelengths (colors) to form an image.

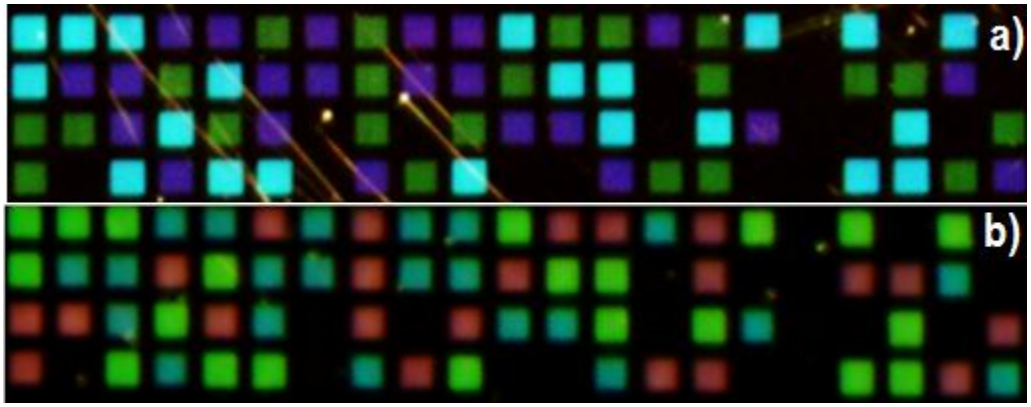

Figure 4. 8. a)-NOF Encoded data scanned using in-plane incidence and b)-out-of-plane incidence

As shown in Figure 4. 8 above, the colors perceived by the sensor can vary into distinguishable colors if the plane of incidence changes. Changes in the plane of incidence can be translated into an angular term ε for which the cosine value affects the diffracted orders (Figure 4. 9) [19].

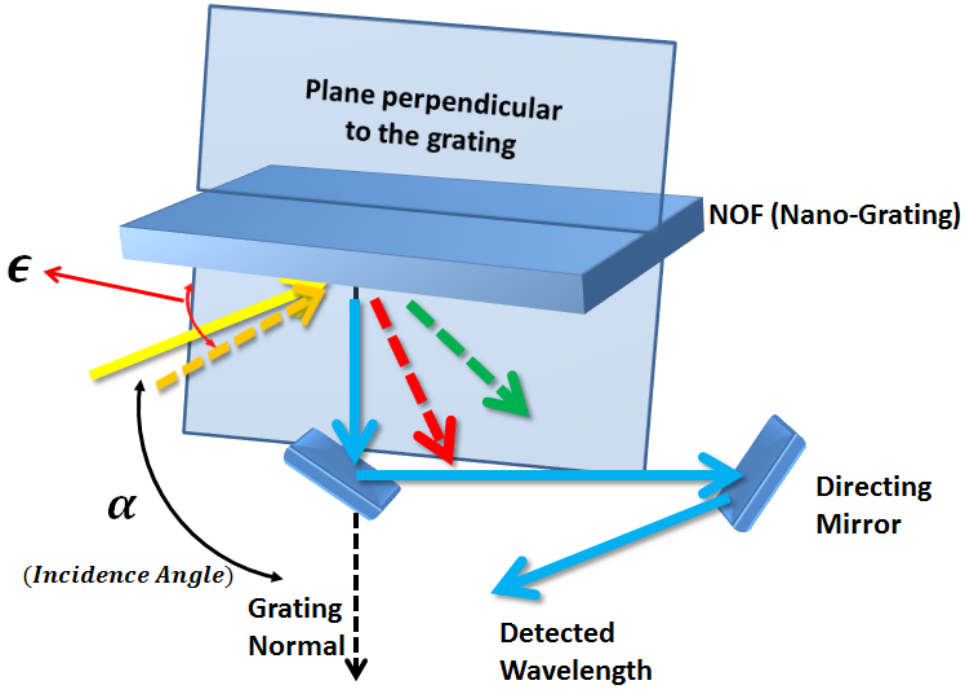

Figure 4. 9. Proposed implementation setup for an in-plane (solid) and out-of-plane (dashed) angle of incidence deviated by ε.

The implementation of Figure 4. 9 is shown in the experimental setup in Figure 4. 10:

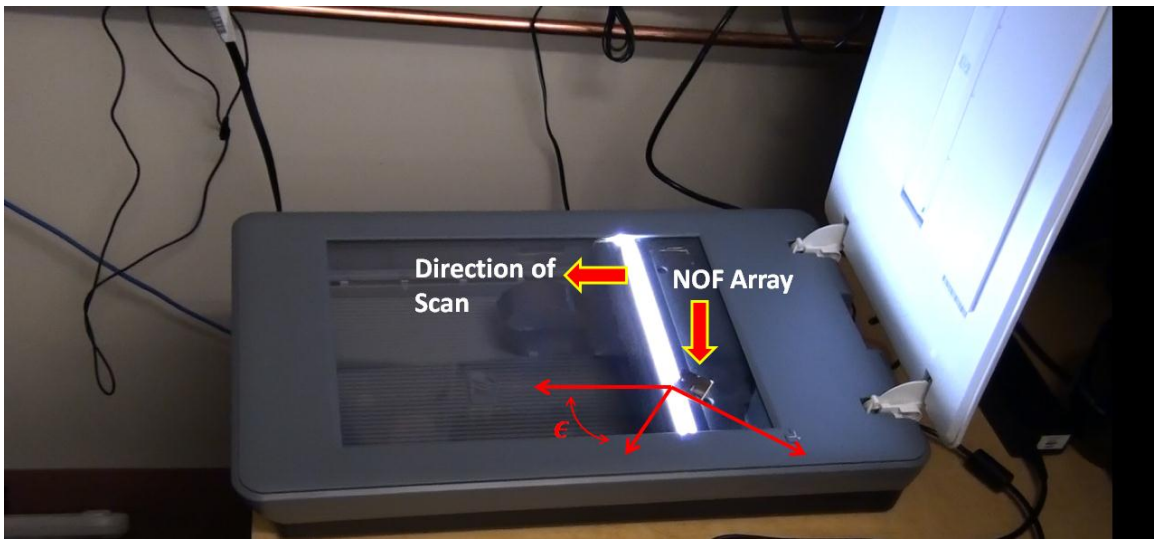

Figure 4. 10. Implementation of out-of-plane incidence (canonical diffraction) for NOF using flat-board scanner

The storage density of the stored data was measured over the recovery of the stored data from the largest sample (Tagged as “Joee”) encoded via 200 x 200 um arrays down to the smallest sample(Tagged as “CFLG”) stored with 50 x 50 um arrays of Nano-optical features. The signal acquisition is shown in Figure 4. 11 & 12.

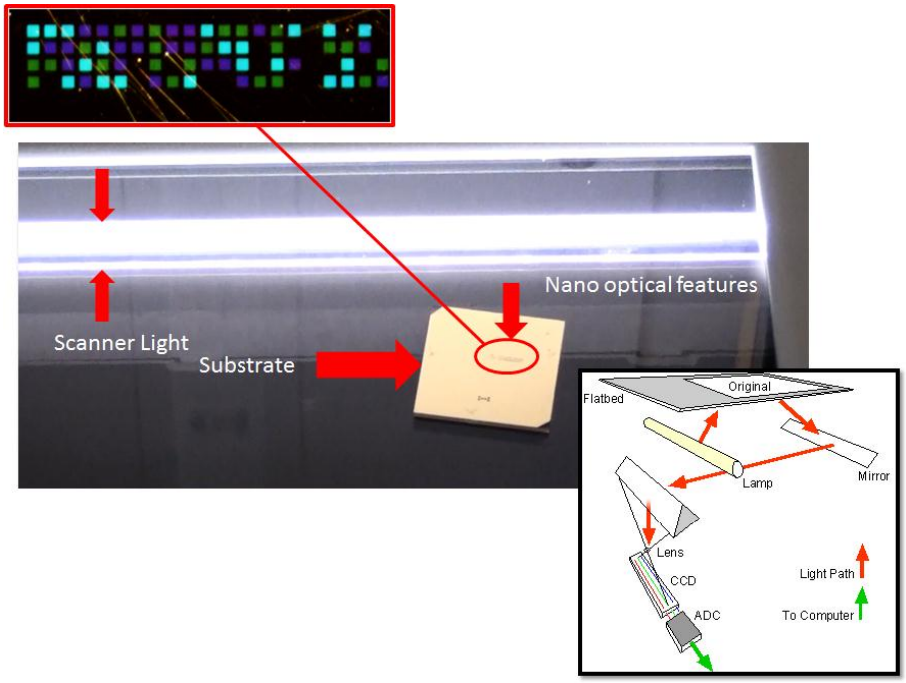

Figure 4. 11. The sensing setup for the reflective diffracting spectrum of the NOF. The inclined angle of sensing can be translated into errors for the calculated angle of incidence for clarity and error correction

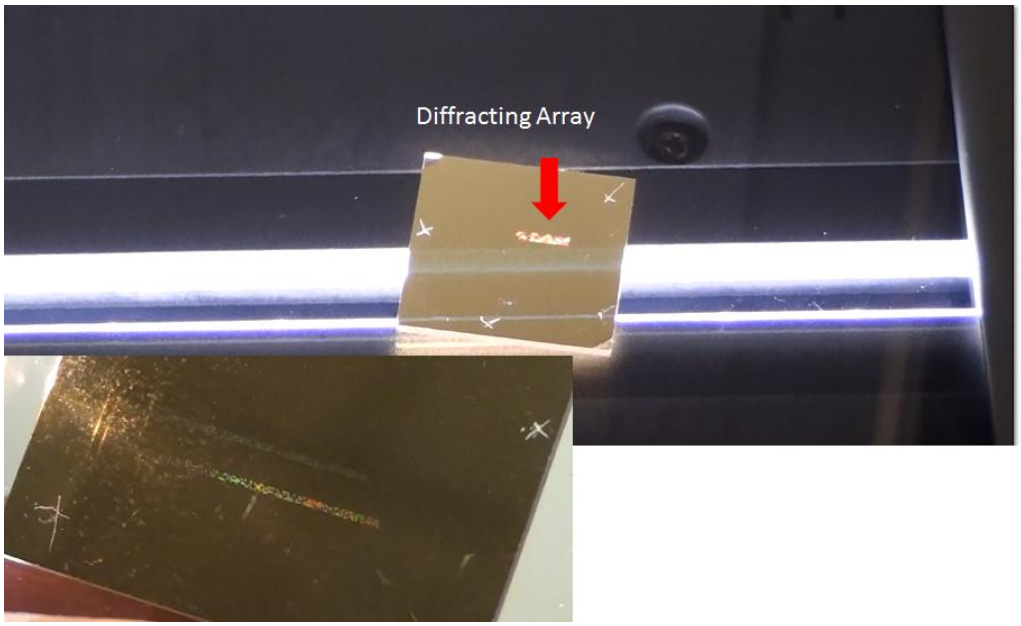

Figure 4. 12. NOF in reflective sensing setup and during diffraction. The temporal scan interval is being ignored in spectral calculations

The storage density of a reflected signal (excluding the effects of EOT and surface plasmonic resonance in the acquired signal) is a result of diffracting light under a certain angle. The acquired image can then be investigated with respect to how well each Nano-optical feature can be separated from an adjacent one or how well the boundaries in the color space can be resolved. Figures below show the storage density achieved through down scaling the Nano-optical feature sizes over the encoding process.

Figure 4. 13. a)-Acquired storage density with large 200x200μm^2 arrays b)-18-folds increase in the storage density via encoding with 20x20 μm^2 arrays

The storage densities presented in Figure 4. 1 can vary if the inter-array distance increases or decreases.

4.2.1. Encoded Data Reconstruction

After producing a readout signal for the Nano-optical feature based encoded data, image processing techniques were implied to achieve a separated color image from the acquired image. As a result of the color segmentation, the encoded matrix is recovered and the data can be fed into the main compressor platform of the algorithm in reverse order to be regenerated. In brief the recovery procedure can be summarized in:

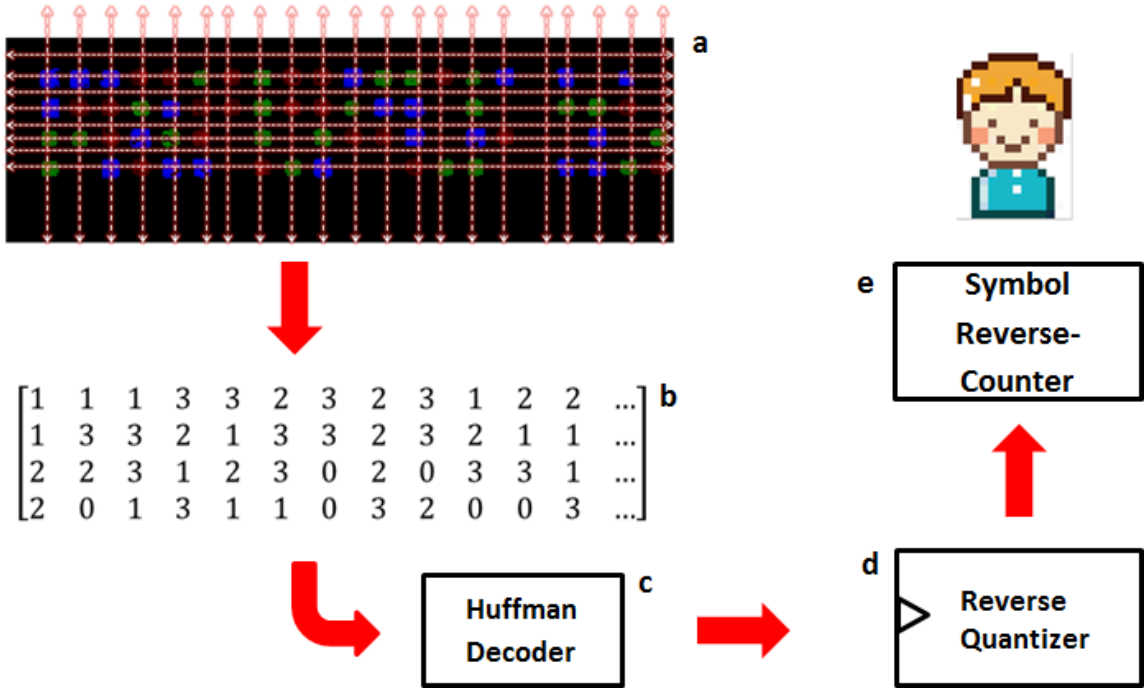

Figure 4. 14. Visualisation of the data recovery using a)grid scanning b)numeral evaluation c)Huffman decode d)reverse comparison e) reverse symbol counter (from left to right)

This part of the project can be a stand-alone module that could be either receiving feedback from the main algorithm regarding how to reconstruct data in case of a library that decrypts the optical data or simply perform reading and extraction of the numerical data that has been outputted by the compression algorithm (Figure 4. 14).

The procedure for data recovery is divided into the following steps:

a) Image Dimension Approximation

The image from the sensor is in the TIFF format hence the first step for data recovery is to perform a color segmentation process in order to extract the dominant colors in the medium. The steps to do so are as following:

1- Using the fabrication and scan coordinates of the substrate isolating the encoded area(Figure 4. 15-4.16):

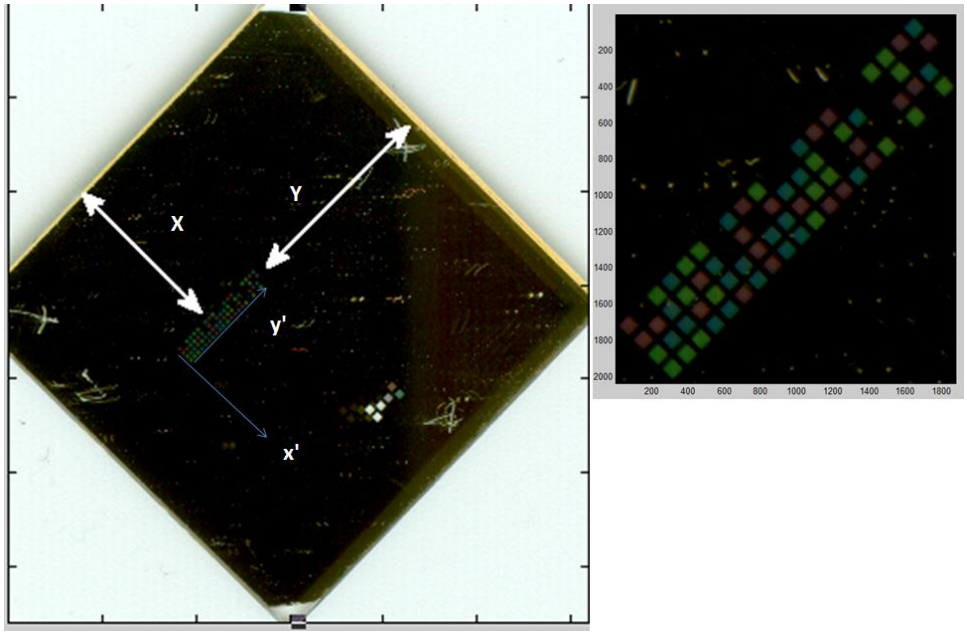

Figure 4. 15. Original Image outputted by the scanner and its fabrication and scan coordinates

2- Rotating the image to vertical – horizontal axis and isolation of the encoded area is performed using bi-cubic interpolation function to isolate the fabricated image area from the rest of the scanned image

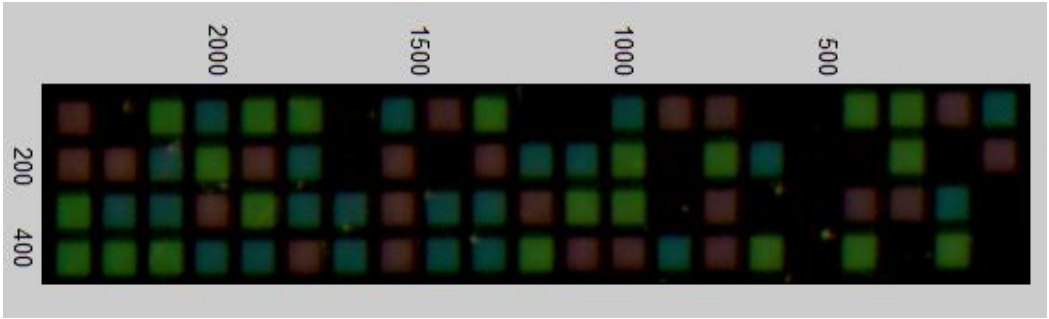

Figure 4. 16. Isolated encoded area for data reconstruction

3- Two-Dimensional Histogram Construction using color information in L*a*b (Color-Segmentation)

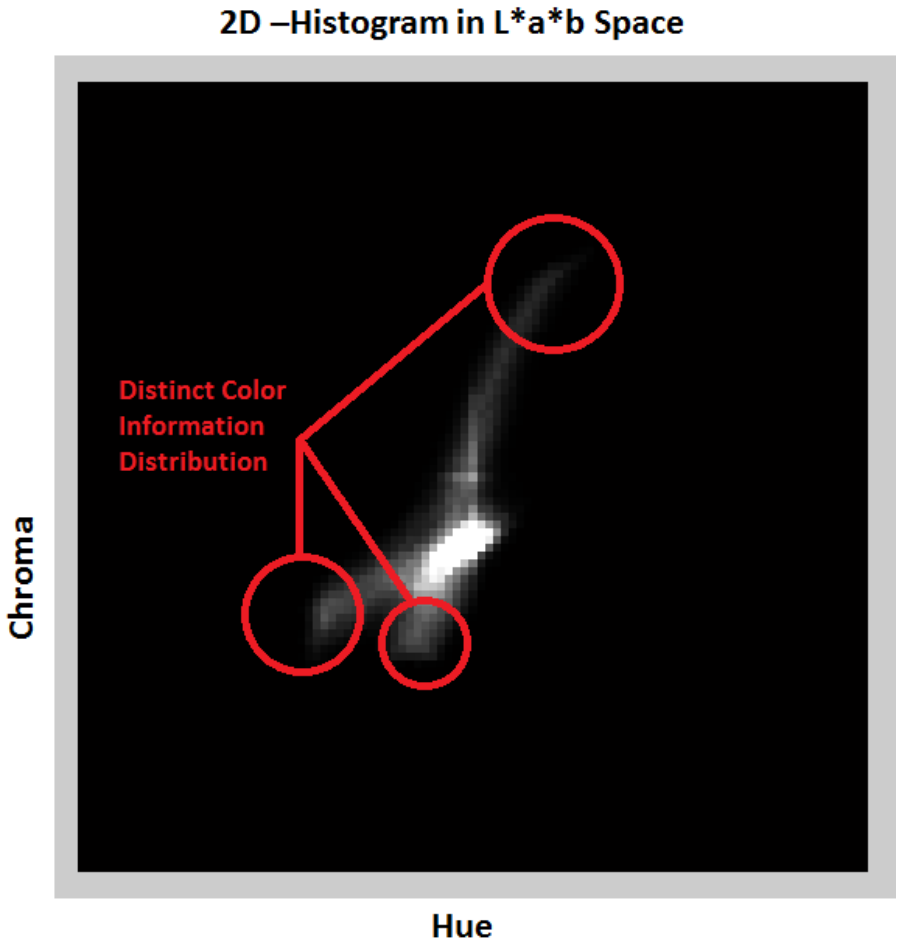

Figure 4. 17. Hue-Vs. Chroma information accumulated to form orthogonal 2D space. Each point in this space corresponds to a spatial distribution of colors

Through definition of a 2D histogram and due to the angularly well-resolved and well-dispersed diffracted spectrum by the NOF, this information is found to be spatially scattered across the 2D space of the Histogram in Figure 4. 17. In a 2D histogram the number of points in the Hue-Chroma Space(2D distribution of image color information) is tuneable hence a visually user-defined parameter can be set to monitor the distribution of the color information and decide for more or less points included in the histogram (histogram bins). In case of occurrence of undesirable effects such as mixed points that represent more than one color group, spatial filters such as averaging or blind deconvolution was performed to create stronger contrast and amplify the edges of the acquired image [22][23] (Figure 4. 18).

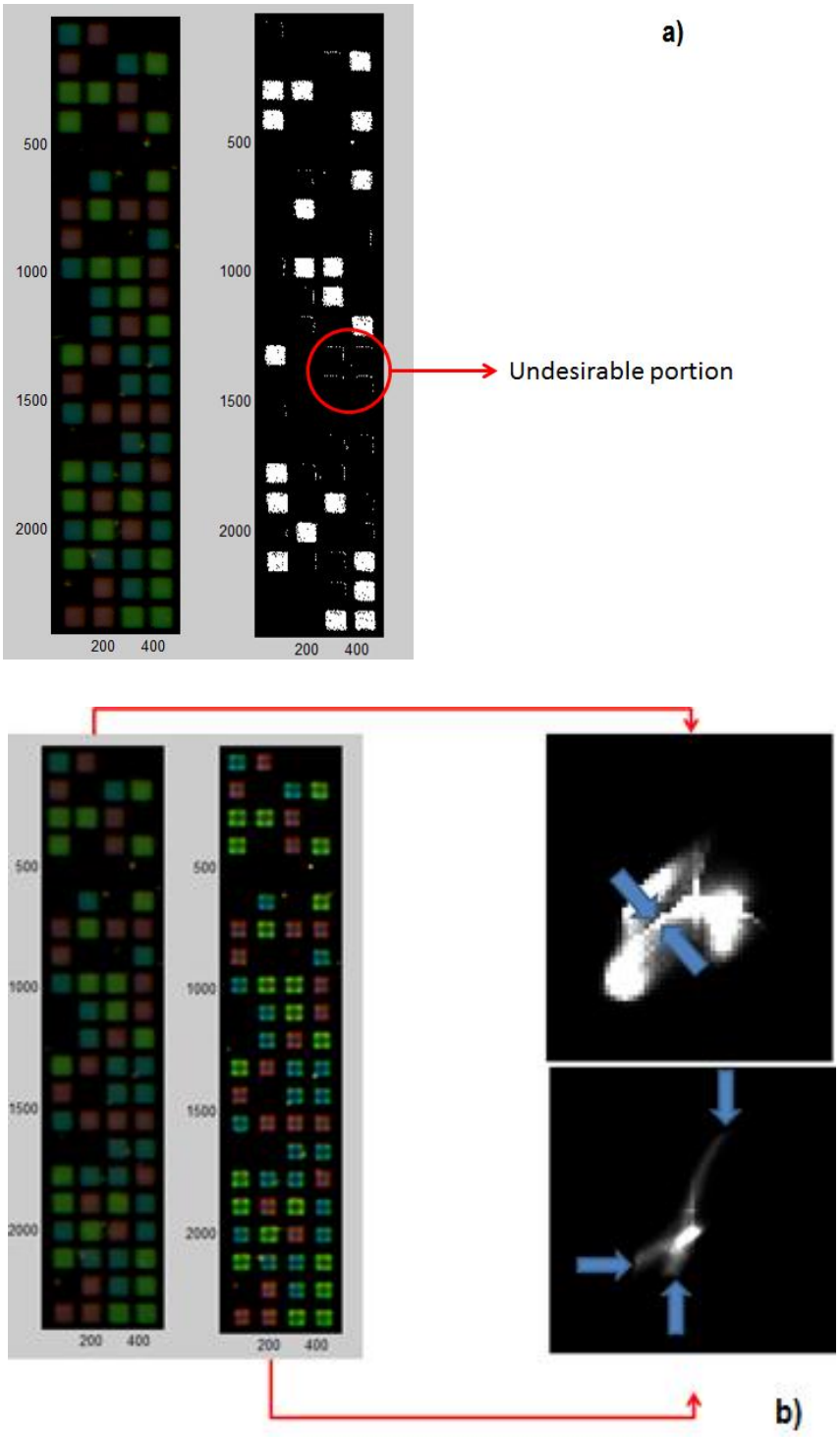

Figure 4. 18. a)-Effect of noise on the color extraction (segmentation) procedure; b)-use of averaging filter and a blind deconvolution for edge preservation sets the color data more visibly apart for extraction

4- Extraction of Isolated Color-Channels using acquired color-masks from 2):(Figure 4. 19)

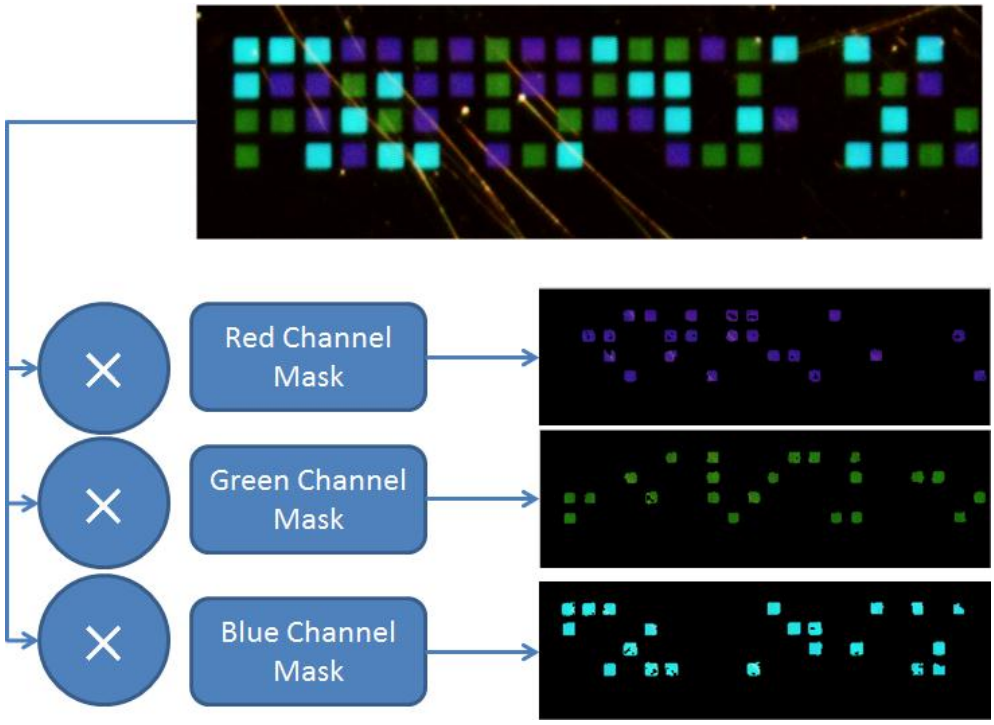

Figure 4. 19. The image being decomposed to its major color-content using mask-multiplication

The next step after the color-isolation is to merge the isolated single-valued images to form a tri-color sample (Figure 4. 20):

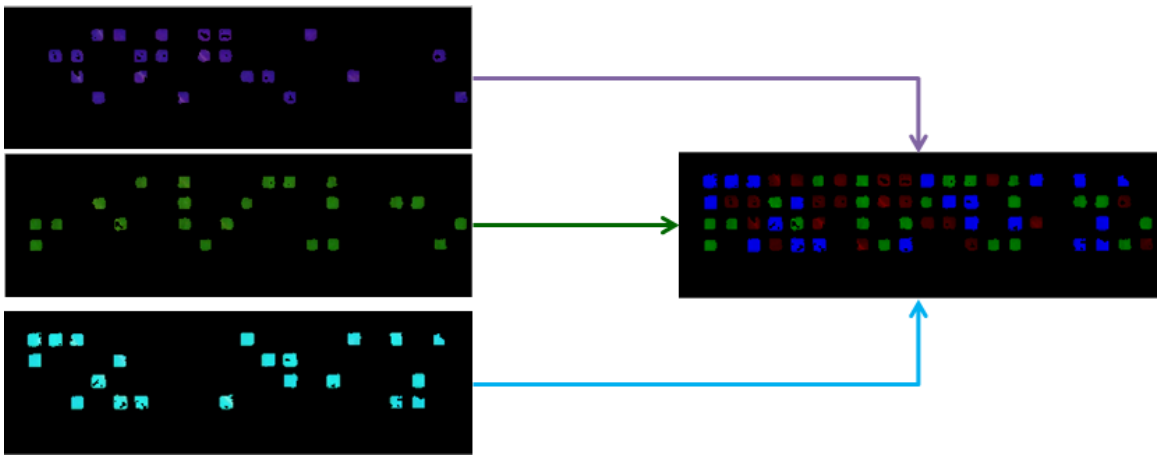

Figure 4. 20. Three dimensional concatenation of the single color images

5- Grid-Scanning the Tri-Color Sample and Data extraction

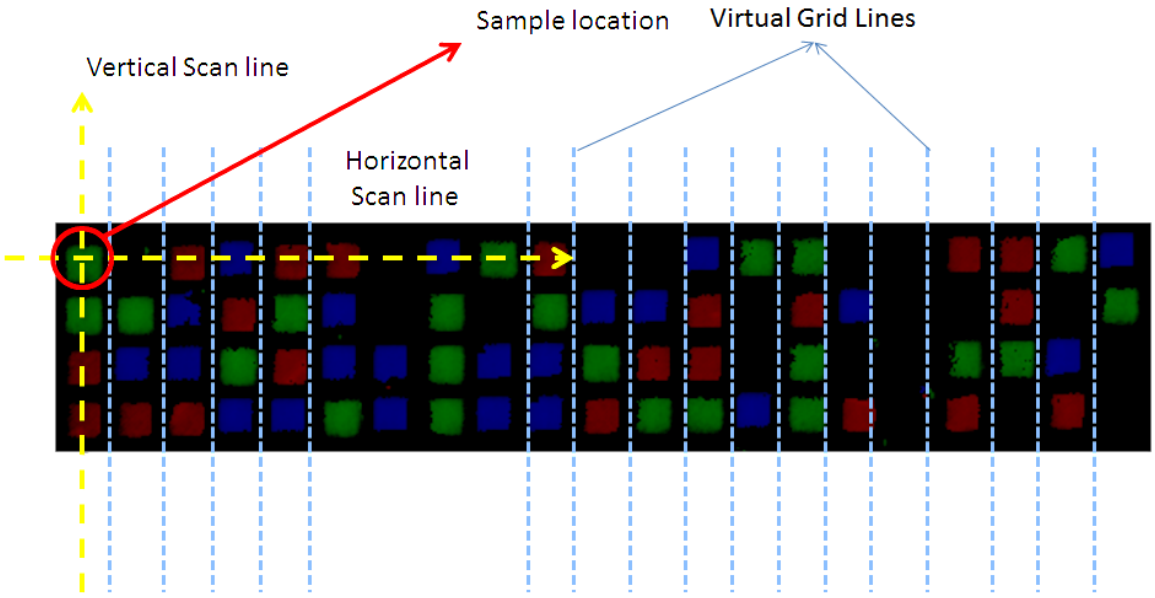

Figure 4. 21. The scan lines intersect at the center of each cluster of color data hence one sample is picked out

As shown in Figure 4. 21, through scanning within a virtual grid that is the result of known number of optical elements in the acquired image, the algorithm samples at each direction and compares the values at the intersections. If the values at each cross-scanning intersection are unequal the algorithm readjusts the virtual grid and performs the scan one more time. For each trial, the algorithm calculates an error factor that is the number of cross-scanning until the false result per total number of cross points in the current grid. If the error factor exceeds a certain threshold (user definable) the algorithm declines the image and requests a new scan. The result of a complete sample-cross-scanning is a matrix that contains the optically encoded data. This matrix returns to the original data via reverse NOF-transformation, reverse RLE, source decoding and finally reverse quantization.

4.2.2. Encoded Results

An overall 4 trials were successfully made in order to optically modulate and encode data in the form Nano-optical features with varying periodicity and in the form of arrays of periodic Nano-structures. Throughout this chapter the results of optical encoding are presented and results are being compared to some commercially available data storage media for finite-length, low-cost, high-security data storage. The results are presented in the following table (Table 6):

Table 6 Images stored using recursive source encoding within NOF algorithm along with their space on optical material and library size on disk

File Name	File Size	Compression Platform	Compression	Library Size
Joee	280 bytes	Lossy/Lossless	47.556	0.82 kB
CFLG	2026 bytes	Lossy/Lossless	16.3387	0.23 kB
Apple	10.4 kB	Lossy/Lossless	75.4928	0.21 kB

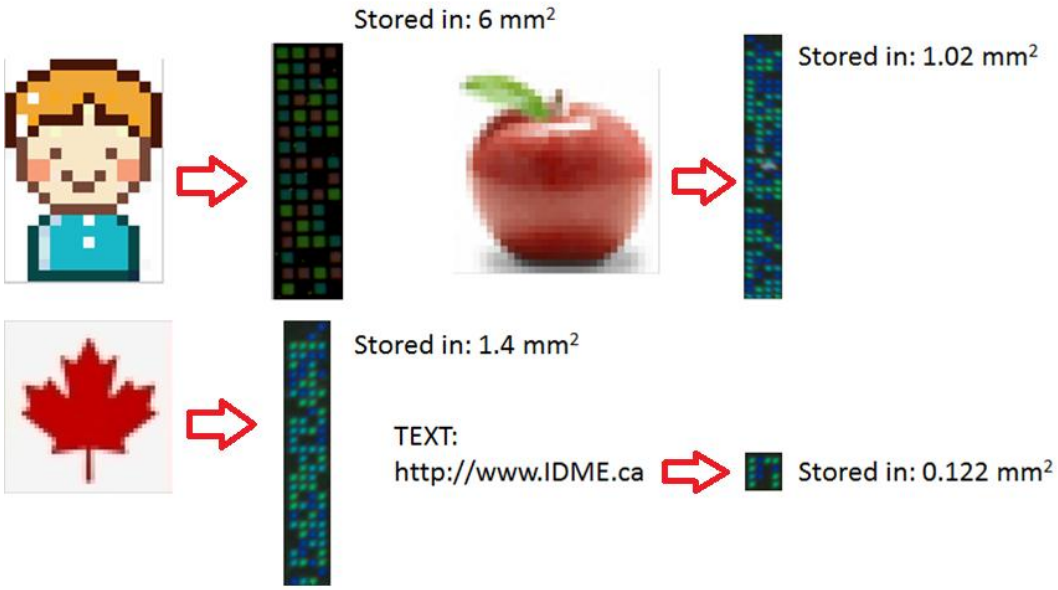

The large compression ratios are the consequence of recursive Huffman loop on the encoded data, hence storage of relatively large libraries. These trials have been all targeting an economical fabrication of the NOF and not an efficient data storage capacity for the compressed data libraries. It can be deducted through the results of this work that through increasing the modulation order of the input data (adding more colors to the

states of variation of NOF) and employment of higher-resolution optics both the dimensions and amount of data storable on an optical medium can be decreased and increased respectively. The comparison between the final trial in which a simple text has been NOF-encoded with barcodes of different kinds to encode the same text shows the great advantage regarding machine readability and physical storage dimensions between NOF and a common commercial application for authentication data storage (barcode)(Figure 4. 22).

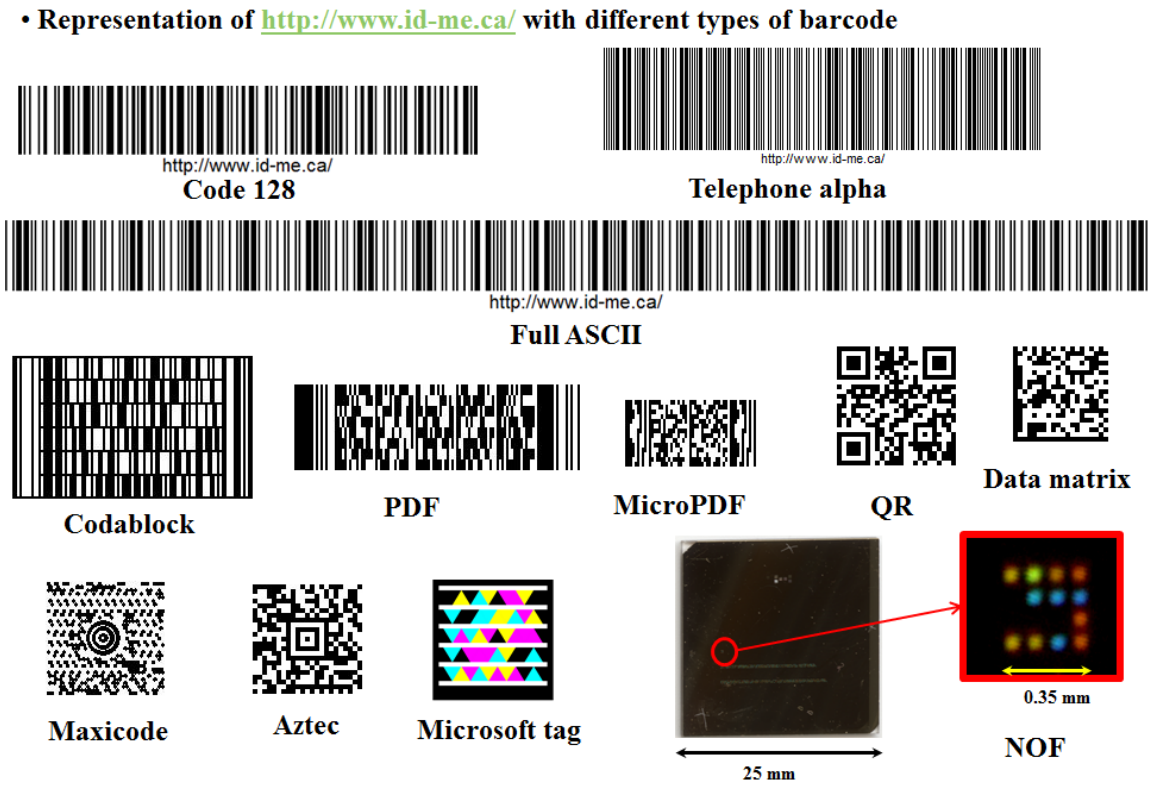

Figure 4. 22. Physical representation of a common text by different barcodes and NOF. NOF shows a sheer decrease in storage space as to the fact that all barcodes are presented in actual size

4.2.3. NOF Encoding Performance as an Authentication Storage Medium

The results presented in this chapter show two important advantages for using NOF to encode data: 1)-Optical Security and 2)-High Storage Density. These two factors make NOF encoding an optimal choice for using NOF encoding for authenticating documents, cards or other media. In comparison to state of the art techniques, NOF presents an extra layer of security and that of angle-dependent color spectrum (Figure 4. 23). Table 7 compares previously reviewed encoding for storage techniques with NOF:

Table 7 Overall comparison between NOF encoding and some standard examples for authentication encoding for storage

	1D Barcode	2D Barcode	Mag-Stripe Cards	RFID Tags	Optical Memory Card	Compact Disk (CD)	Nano-Optical-Features (NOF)
Max. Storage density	645 b/in^2	21.6Kb/in^2 **(Claimed by Syscan-China)**	2.87 Kb/in^2	165 Kb/in^2 **(Reported by Zebra Technologies)**	622 Kb/in^2 **(reported by Laser Card Technologies)**	0.9 Gb/in^2	806.5 Kb/in^2
Side-Channel Attack	Immune	Immune	Vulnerable	Vulnerable	Immune	Immune	Immune
Software Decryption (Cracking)	Immune	Immune	Immune	Immune	Vulnerable	Vulnerable	Immune
Encryption	No	Yes	Yes	Yes	Yes	Yes	Yes
Directional Reading Optical Security	NA	NA	NA	NA	NA	NA	Yes
Radiation Damage	Immune	Immune	Vulnerable	Vulnerable	Immune	Immune	Immune

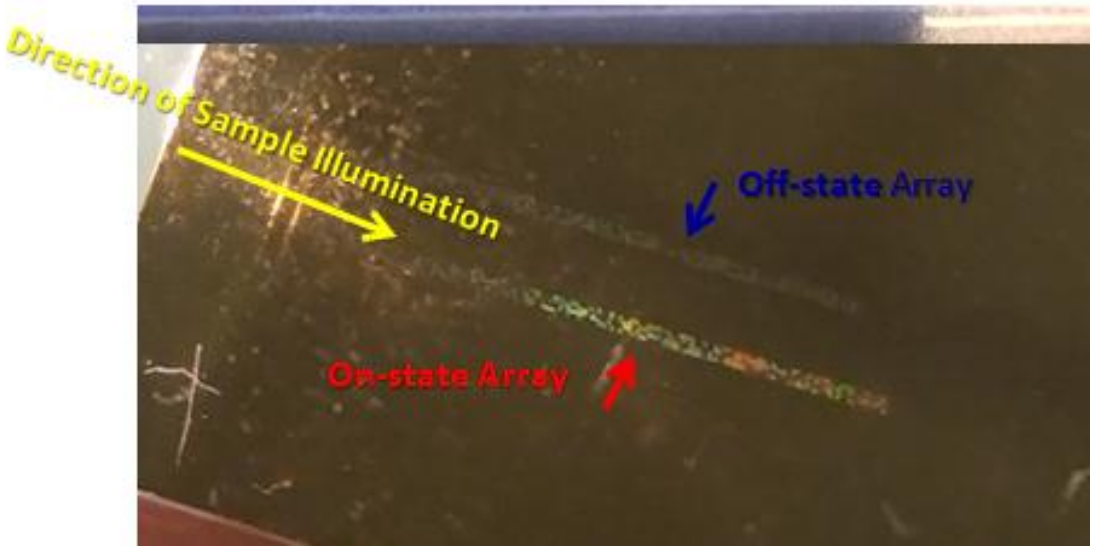

Figure 4. 23. Directional readout of a NOF reader sensor can be employed as a measure of security where only colors at a certain wavelength range can be accepted as a readout before the system decodes the data

The presented data in Table 7 along with wavelength dependent decoding possibility and directional optical security of the NOF encoded data makes it a suitable encoding scheme for data encoding for storage applied in authentication media such as credit cards, ID cards, Passports etc. aside from the machine readable security features, NOF encoded data provide a first-hand visual security layer since small grating nature of NOF data reflects and diffracts light efficiently so that the features are visible even with unaided vision (Naked-eye). The immunity of NOF encoded data due to their optical nature to radiation damage and side-channel attacks makes them a smart choice for high-security data encoding for storage (Figure 4. 24).

Figure 4. 24. An example of NOF encoding for authenticating official documents

In contrast to barcodes that require an encoding symbology for decoding information, NOF has a numerical range that accepts almost any input and allows for large encryption possibilities using combinations of different characters or letters and numbers (Figure 4. 25).

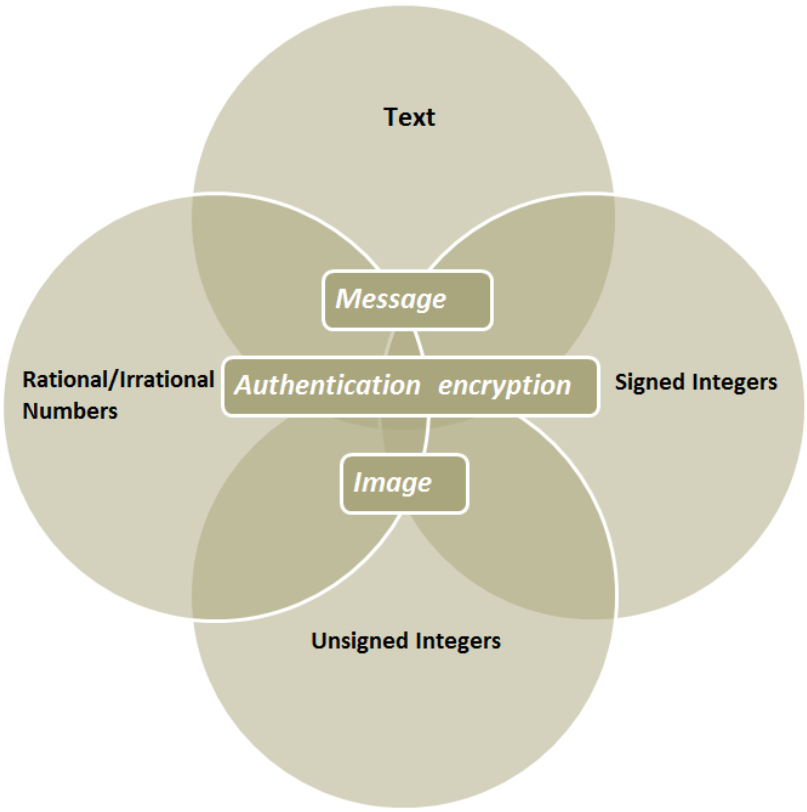

Figure 4. 25. Mathematical quantifications of a security check system parameters to produce encodable data

4.2.4. Comparison between NOF and recently reported Nano-Optical Multi-State Data Encoding Systems

There has been various reports on use of Nano-optical structures and particularly those range below the diffraction limits for an optical reader (half of the wavelength with high-end optics) to encode multi-variation state bits. These reports usually target those media which are capable of withholding changes made to them through an illumination of a polychromatic or monochromatic beam. These media can also contain additional degrees of storage that can be affected via modulating other beam parameters such as phase, polarization and etc. In trials presented in [24], the encoding system has

employed a five-variation-state-bit (penta-bit) in order to encode distinguishable information by use of mono-chromatic incidence beam (Nd:YAG Laser with wavelength of 532 nm) as writing means and azo-polymer (azo-moiety Disperse Red-1) blended into poly-methylmethacrylate (PMMA) with a 25% molar concentration as the optical medium. Both encoding and decoding processes are done via NSOM (Near-Field Scanning Optical Microscopy) and the Table 8 shows the parameters of the encoded data using this report. The encoded bits show variation states as changes made to the voltage signal received by the NSOM as a result angular shifts with respect to the birefringence axis of a linearly polarized reading light (laser). The experiment reports bit storage density of circa 1.9 Gbits/in^2 calculated based on the given minimum distinguishable bit distance between every two adjacent penta-bits (distance is given as 300 nm). The storage density calculated from this report is very high yet it has been nominally calculated for a case of actual storage of maximum 4 bits and the background (zero state). Figure 4. 26-b & 4.26-c shows the NSOM contrasted image and the related voltage signal for the encoded states (Original from the report). Amid the minute spot size for each penta-bit, the medium in which the bits are stored is a polymeric medium undergone isomerization. The latter has not been tested for bit-rot effects in time longer than a month mentioned in the report. The measure of changes in the state of the bit is the shifts induced in the birefringence axis of sub-wavelength volumes on the surface of the polymer. This measure of change can become highly erroneous if the readout signal is not being corrected for reader noise that tends to appear as convolutions with the acquired signal. The use high NA (Numerical Aperture) for acquiring the results is directly related to very high costs for a reader device hence imposes the problem of cost-efficient machine readability.

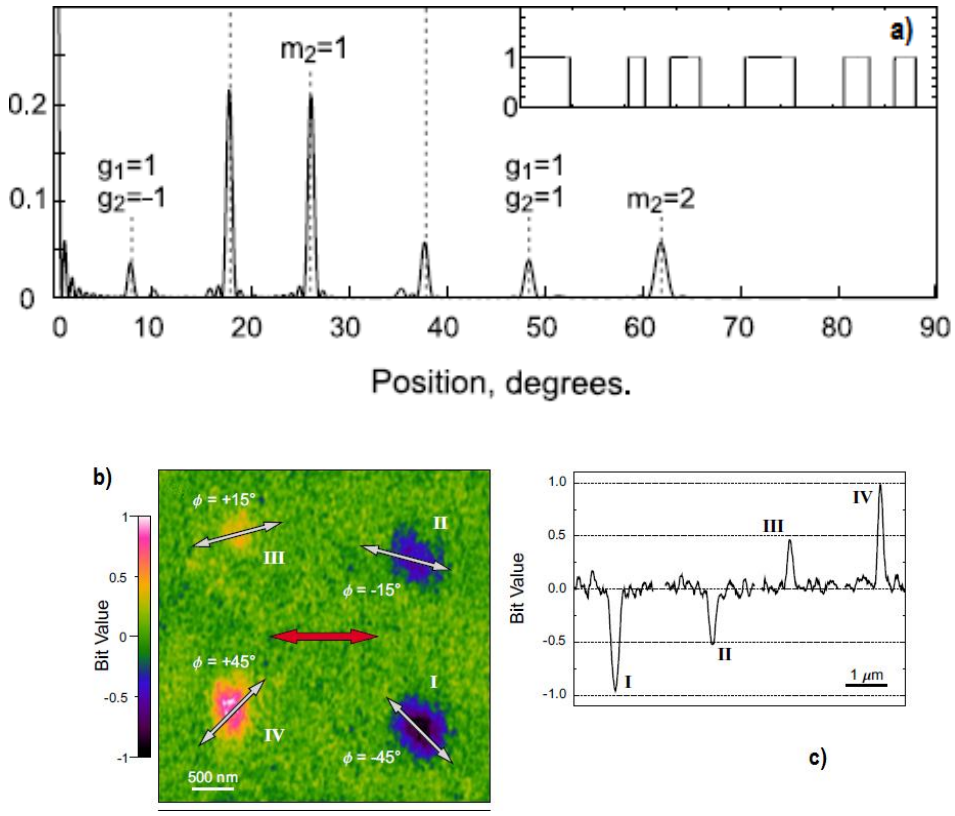

Figure 4. 26. a)-Barcode tags with Nano-line-gratings b)-Polarized birefringence as penta-bit; c)-Readout FWHM for four states and the background as zero-th state

Another trial has employed Nano-scale line gratings in order to create a library of unit tags similar to barcodes [25] (Figure 4. 26-a). These tags can multiply in number as a function of the length of the Nano-scale gratings and the readout signal is the resolved first order of diffraction for each periodicity. This method employs the concept of barcode encoding where a mixture of different grating periodicities allow for different angular positions of the first order diffracted light. The storage density reported for the actual data similar to the trial mentioned prior to this example, is calculated based on nominal values provided by the report. This method has reported to have a storage density of 251.5 Kbits/in^2 .This storage density is been reported to have increased by three orders of magnitude if three layers of Nano-scale diffraction gratings were used. The latter has also (according to the report) is accompanied by the increased probability of error in readout as to the fact the higher orders of the underlying gratings will contribute to ghost signals (unwanted intensity distribution on the CCD sensor screen used for readout). Like the previous example this work also reports on a data encoding capacity with nominally high storage density yet the actual limits of data encoding and possible

production artefacts that may be caused during manufacturing of longer lengths of the proposed Nano-scale line gratings have not been addressed. It is also unclear how would the bit-rot (deterioration of the physical structure of the bit) affect the quality of storage and does not give a clear picture of machine-readability of the features. Table 8 shows a comparison between NOF and two recently reported encoding schemes using Nano-optics and multi-variation state for storing information.

Table 8 Comparison between NOF and recently reported Nano-optical Encoding Systems

	Azo-Polymer-Based Polarisation-Dependent Optical Encoding	Nano-Order Multilayer Diffraction Grating Encoding	Nano-Optical Feature Encoding (NOF)
Max. Reported Storage Density	1.9 Gbits/in^2	251.5 Kbits/in^2	806.5 Kbits/in^2
Reading Optics	High-End	High-End	Affordable
Encoding Algorithm	None	None	Encoder/Decoder
Readout Mechanism	NSOM (Near-Field Scattering Optical Microscopy)	CCD/SEM (Scanning Electron Microscopy)	CCD/Flat-board Scanner (HP 9600 DPI)
Data Encryption	None	None	Three-Layer Compression & encryption
Machine Readability	Weak	Weak	Strong

4.2.5. Overall Comparison of NOF-Encoder with standard Lossy Compressors

The thesis has also focused on designing an algorithm that, before transferring the data into Nano-optical structures, compresses the data to an optimal level hence the amount of fabrication time for the encoded optical medium is reduced. There are several standard methods that are being used in data compression and in this section we give a comparison between what our designed algorithm's output presents compared to two standard compression algorithms. The designed algorithm is using some standard techniques which are common in data processing such as source coding and run-length

encoding along with lossy minimum-variance quantization. Comparing our results to platforms such as Wavelet transform and discrete cosine transform is presented due to the reported efficiency of these two algorithms hence we compare our results with these two algorithms. Figure 4. 27 shows a comparison between a bi-orthogonal wavelet transform-based compression and the changes in the file size as the psycho-visual indicator (quality of the image) progressively enhances in comparison to the output of our encoder. The comparison is made to show the file-size efficiency of the algorithm employed in NOF encoder system and standard lossy wavelet transform which is considered as the most efficient lossy compression scheme at present. The picture chosen for the comparison is the file tagged as “apple” in Table 6.

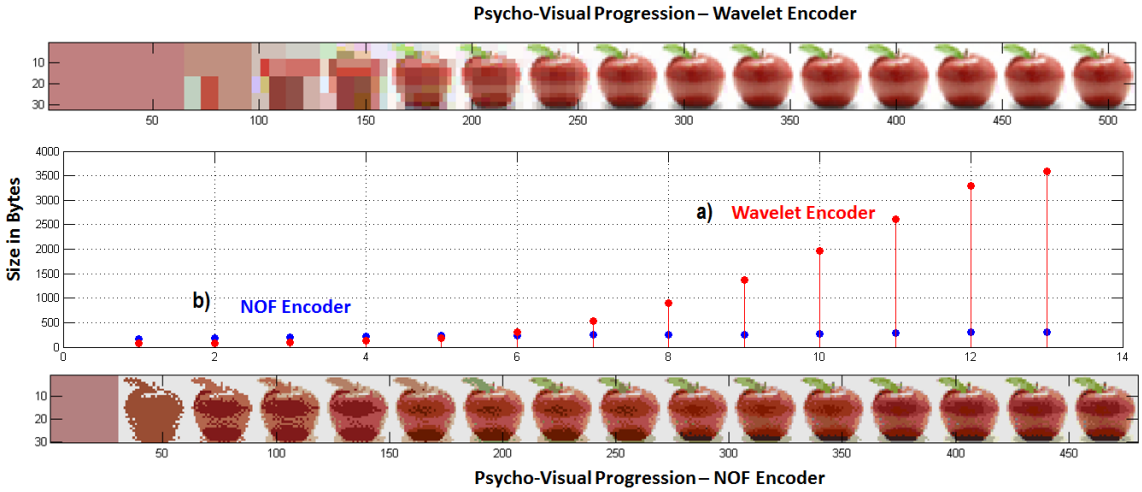

Figure 4. 27. A comparison between a)- wavelet and b)- NOF encoder (bottom/blue) for storage byte size

And the same comparison is been made between a NOF encoder output and a DCT-based compression algorithm (Figure 4. 28):

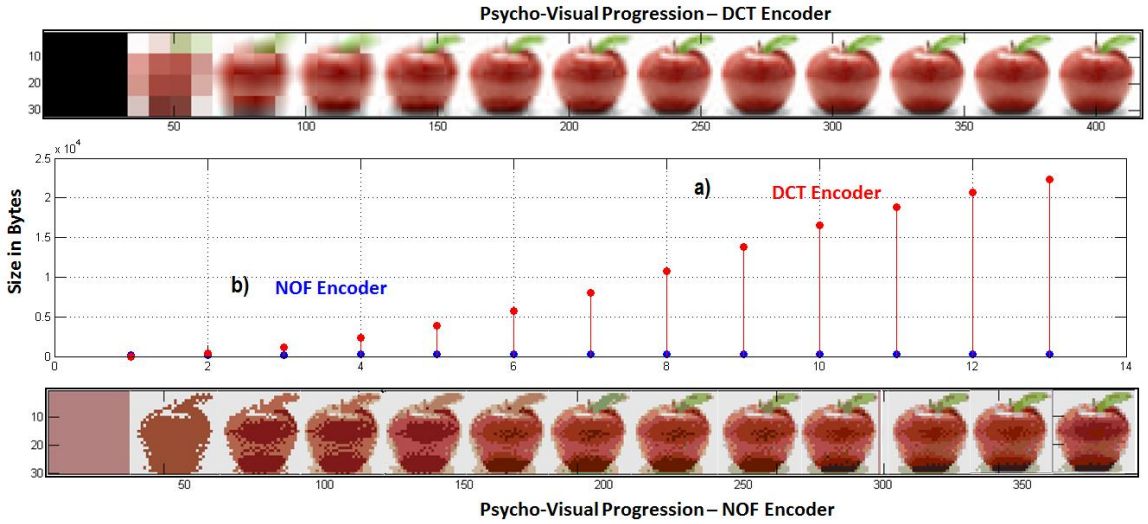

Figure 4. 28. Comparison between a)- DCT encoder and b)- NOF encoder bottom/blue regarding storage size and psycho-visual quality

As indicated by the graphs, the NOF-encoder maintains low-bit size compared to the other two algorithms while outputting a relatively high image quality. The next figure shows the position of the chosen NOF-encoder output's bit depth marked on the bit depth of a bi-orthogonal wavelet-based compressor (Figure 4. 29).

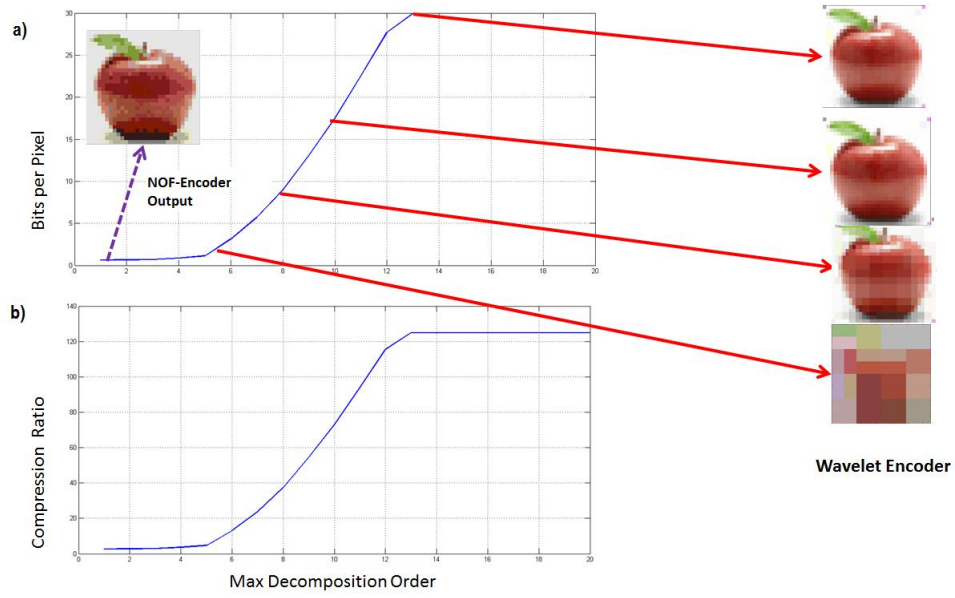

Figure 4. 29. A Comparisons between the applied combinatory Lossy Quantizer/Lossless Huffman encoder and the wavelet encoder for an small image (psycho-visual analysis).

The encoder's bit-depth is defined as the number of bits that can represent one pixel value of an image data. Graph in Figure 4. 29-a shows that if a file is encoded and compressed using a wavelet transform encoder, the number of bits required to represent one pixel of the encoded image increases as the wavelet transform encoder decomposes the image into more blocks of compressed data. 20 levels of decomposition allow the wavelet encoder to restore a compressed image up to an optimal level of visual representation. The purple indicator arrow on the graph shows that our algorithm can restore a compressed image with much less bit per pixel or bit depth than the standard bi-orthogonal wavelet transform and hence at lower decomposition orders, NOF algorithm can represent a better image content compared to a bi-orthogonal wavelet transform.

4.2.6. NOF Readout and Signal to Noise Ratio (SNR)

From reading point of view, NOF requires an image sensor that is economically implementable within a stand-alone reading device. The use of image processing techniques to recover the data from the Nano-optically encoded data removes the need for high-end optical design such as what is used for [24]. The reported system requires a numerical aperture (NA) of circa 1.4 which requires high-end lens design hence increasing the price of the reader device drastically. What was mentioned is in addition to the diffraction-limited system that by definition is an expensive design for an optical reader and is necessary for the recovery of the encoded data. The rest of the chapter is an overview on the readout efficiency of the NOF encoding algorithm as a system-level design. Figure 4. 30 shows a scanned image of NOF encoded data for the image tagged as "CFLG" at 4800 dpi resolution. The use of standard image processing techniques enables efficient segmentation and data recovery.

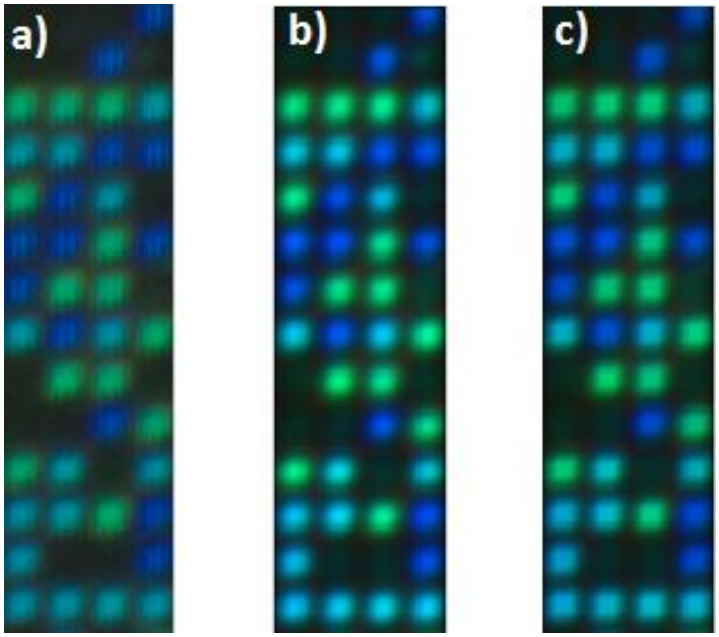

Figure 4. 30. a) NOF image acquired @ 4800 dpi for 50x50 um^{2}features b)-Same Image after averaging filter c)-same image after morphological masking (edges are morphologically preserved)

The Hue-Chroma plane (Figure 4. 31) translates every specific pixel value (corresponding to a specific color) into a coordinate whose magnitude corresponds to the frequency of that color in the image. We describe the Signal to Noise Ratio (SNR) for the acquired image using the Hue-Chroma space through approximation of imaging system (unknown optics) aberration for different degrees of extraction of a specific color.

4.2.6.1. Approximation of imaging system (unknown optics) aberration for different degrees of extraction of a specific color

The Hue-Chroma space (HCS) of an image creates a vector field where each color can be defined as a vector with ambiguous coordinates. The background usually (due to the highest occurrence frequency) gains the maximum intensity in the HCS. By placing the origin of the vector field at its highest value, every color other than background can be viewed as a vector in a particular direction. This multi-dimensional vector-field carries along with it a magnitude of noise parameters such as sensor noise and ambient noise. In order to clarify the signal we use a synthetic map (image) of the encoded data to clarify the directions (colors) we are looking for in the HCS of the acquired image. In general, the color spaces that images are described in are categorized regarding their pixel values (the gray-level intensities that are received by an image sensor) hence

choosing the Hue-Chroma space is based on [26] and the reason for it is the existence of the majority of the color content of an image data within its Hue and Chroma layers once an image is being translated into the Hue-Chroma color space. The Signal to Noise Ratio analysis is performed to show the encoded data using NOF can be extracted and used to decode the encoded data with high levels of confidence even when the SNR values are at levels for which signal extraction can be erroneous for other encoding schemes such as barcodes.

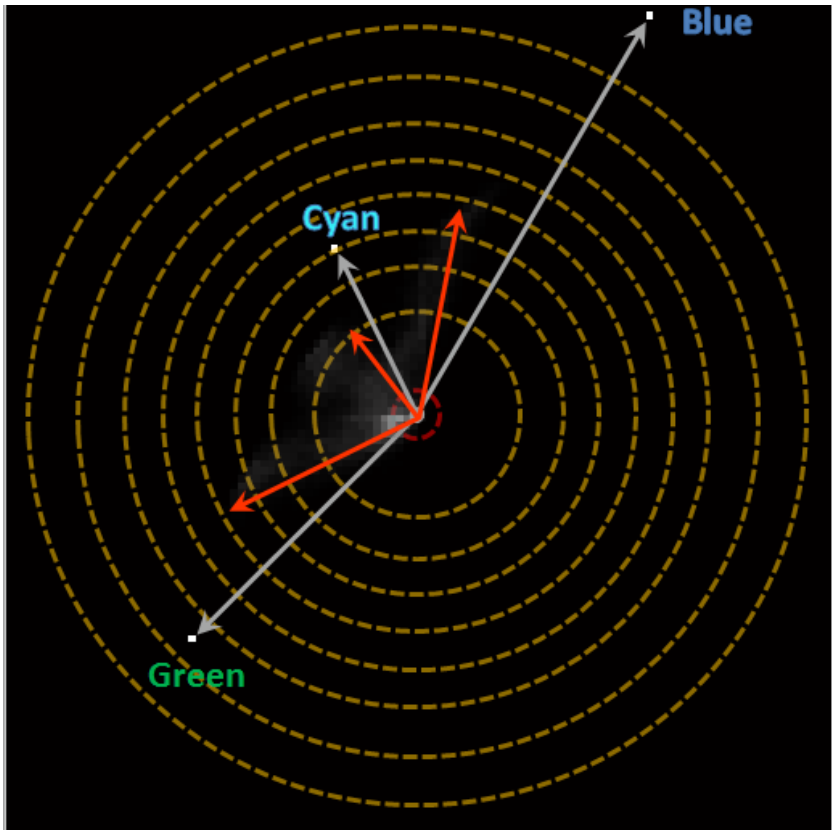

Figure 4. 31. Color vector field for three colors superimposed on an actual HCS for an acquired image

Gray vectors in the above figure show the desired color information direction and the red vectors show the actual color information directions in the 2D histogram (Hue-Chroma Space) of the acquired images.

After choosing the directions in the vector field based on the nearest resemblance to the synthetic map, we can define the readout signal of the encoder in terms of how well each color of the dominant spectrum of the diffracting array can be extracted. With the assumption that the color information of the signal (Hue and Chroma) are being distributed in unique directions with respect to one another while depicted in the 2D histogram, for any spectral (or image sensor) noise introduction this measure separability is distorted. Having chosen the radial distances from the center of the Hue-Chroma plane, we could define the SNR as the radial distance of the designated color content over a radial distance of the color segment lying in that direction for clear extraction. Figure 4. 32 shows that for a scan blurred with white noise (effect of the PSF of the sensor) there is still a solid measure of separability for color blue to be extracted. The SNR of this color can be defined in decibel through (Eq (4-4)):

$$SNR_{Blue}\ (dB) = 10\log\left(\frac{r_{Blue}}{r_{Blue} - r_{res}}\right) \qquad \textbf{4-4}$$

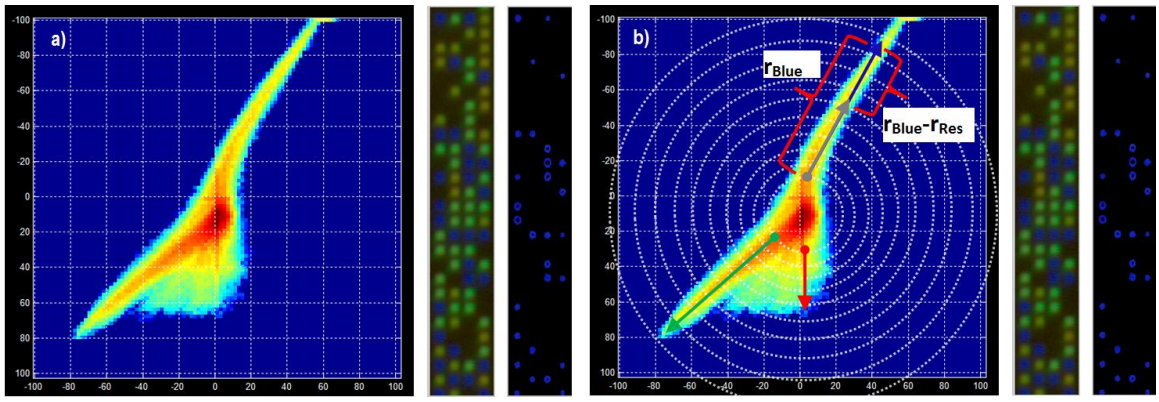

Figure 4. 32. a)-Raw color data for the inset image b)-Vectorized field for the inset image to acquire a measure of SNR for a specific color extraction

Figure 4. 33 shows degree of extracting color blue through choosing two different radial distances from the center of the HCS for an image compared to its synthetic map.

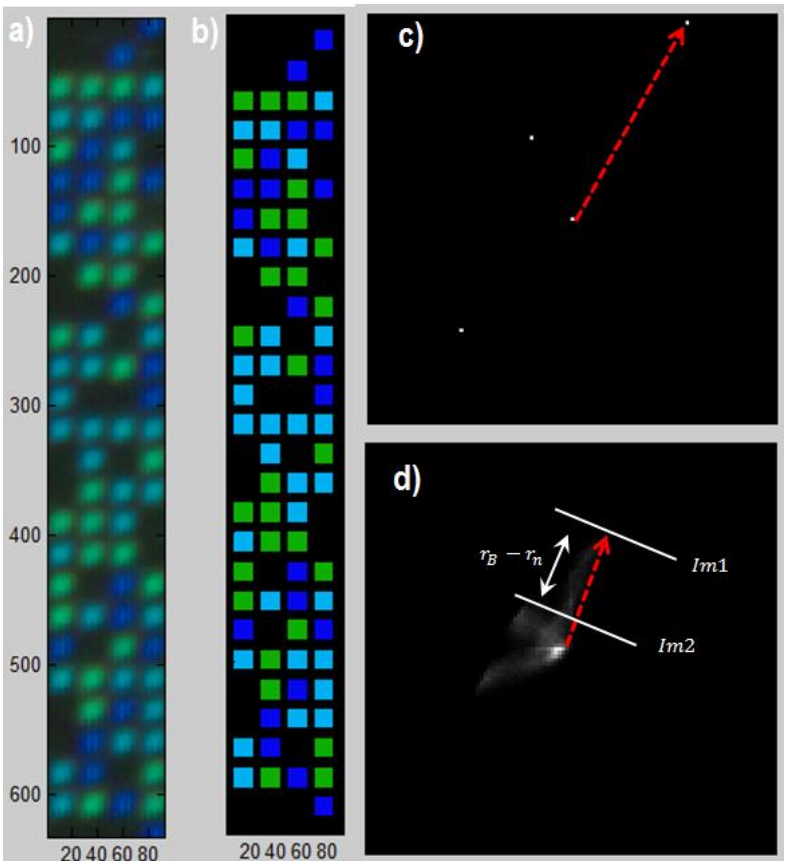

Figure 4. 33. a)-Actual image (50x50 u^2 arrays), b)-Synthetic map,c)-color vector blue for synthetic map d)-Color vector blue for actual image along with the Im1-Im2 segment containing blue information

In Figure 4. 33 the line denoted by Im_1 is the extracted color mask chosen based on the direction of the color vector blue (red dashed arrow) in the synthetic map HCS. The second line is a distance $\mathrm{r_n}$ chosen according to the criterion calculated in Eq(4-4). Figure 4. 34-a shows the trapezoidal surface integral of the blue channel of the synthetic image compared to that of Im_1(red line) and Figure 4. 34-b depicts the trapezoidal surface integral of the actual image compared to that of Im_2(red line). Based on Eq(4-4) the SNR is being calculated as the ratio of the power of the surface integral signals of the synthetic image over that of Im_1 and Im_2 expressed in dB.

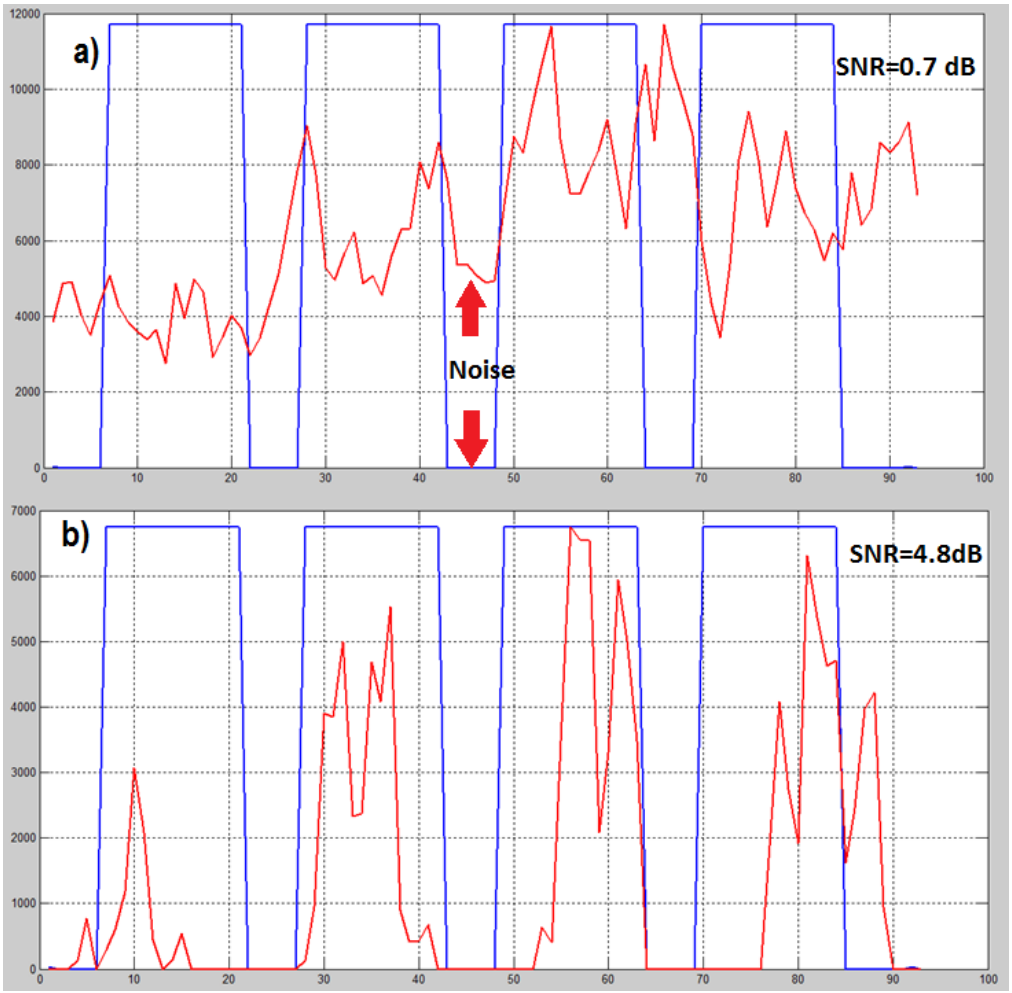

Figure 4. 34. a)-Surface integration of synthetic (blue) and color mask extracted at 0.7dB SNR b)-Surface integration of synthetic map(blue) and color mask extracted at 4.8 dB SNR

The SNR for Im_1 is higher than that of Im_2 due to presence of less noise compared to the extracted color. Amid the low SNR for the acquired sample, the data recovery can still be performed due to color-specific signal extraction (Figure 4. 35).

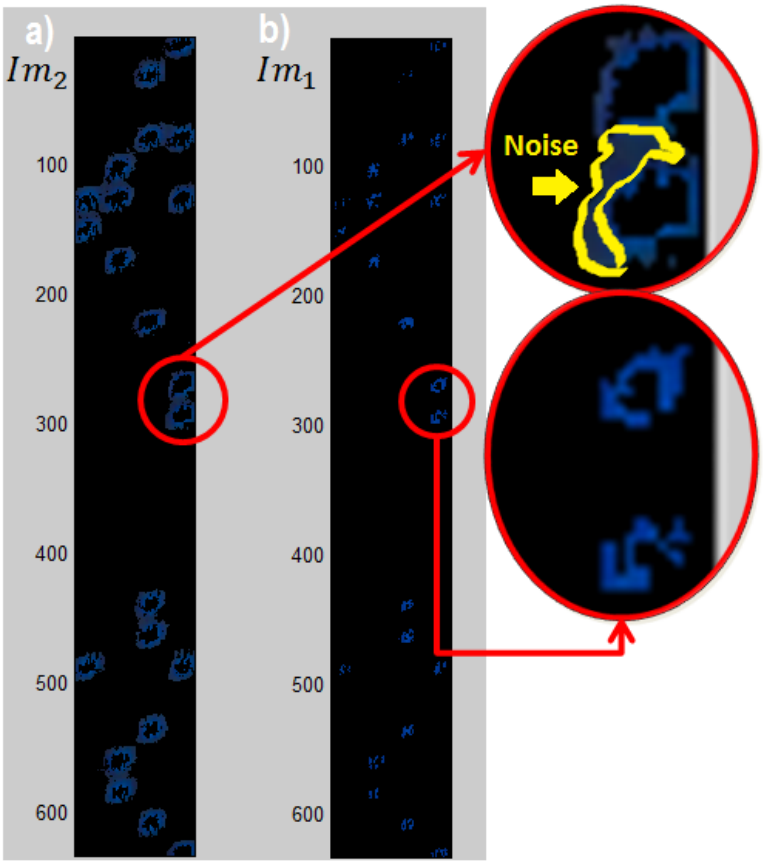

Figure 4. 35. a)-Color mask extracted at 0.7 dB SNR with noise information at the arrays b)-Color mask extracted at 4.8 dB SNR with clear color content

Chapter 5 Conclusion and Future Work

Through the course of this project we have designed, parameterized and fabricated an optical unit information tagged as “NOF” (Nano-Optical-Feature) based on which an encoding system along with a complete system level implementation design have been presented. The actual storage density of NOF as an encoding unit information has been investigated and measured through fabrication of various scales of NOF and analysis of the readout signal in the form of RGB images. The work has focused on demonstrating benefits of NOF-encoding comparing with finite-length storage media used commonly in authentication industry. ID cards and in particular we focused on comparison with commercial barcodes and magnetic stripe cards. The grounds for such comparison with respect to shortcomings of the state of the art solutions have been investigated and NOF has been proposed as a possible new generation of authentication storage media for secure, machine readable data encoding with storage densities 4 to 400 times greater than magnetic stripe standard cards in commercial use, depending on the feature miniaturization (Table 7). The SNR for color-mask extraction has been employed as a measure of signal reconstruction and it has been shown that through use of off-the-shelf flatbed scanners with resolutions as high as 9600 dpi miniaturized encoded data can be extracted in SNR values as low as 4.8 dB (Figure 4. 34). The latter allows for commercial designs specialised for reading and decoding NOF encoded data with higher precision and low costs due to the effective segmentation of the diffracted spectrum of NOF. The conclusion to this work will be 1) a comparison between state of the art Nano-optical-data encoding methods and the current project and future enhancements possible to increase the storage density of the system, 2) Proof of concept for use of plasmonic Nano-structures in data encoding and its advantages over state of the art encoding schemes for authentication media, 3) a brief investigation on the effects of an encoding unit information with more states of variation than binary bit on a transmitting source with constant simple (non-complex) channel parameters.

5.1. Future Design for Security Performance of NOF Encoding System

State of the art Nano-optical encoding schemes regularly used in encoding data for CD or DVD-BRDVD media use encryption algorithms such as DES (Data Encryption Standard) in which the data and the encryption key are both present on the medium (the CD or DVD). This allows for third party enthusiasts to be able to debug the encrypted file into a binary file and rid the execution routine (main routine) from the subroutine(s) that encrypts the file. In comparison to CD or DVD optical encoding, NOF presents an extra level of security for the data. This extra security is the color-based signal extraction that is necessary for the decoder to reconstruct the data. The use of NOF with different grating periodicities makes it extremely difficult for the third party to mimic the encoded data on a NOF secure medium due to the fact that a reader (decoder) reads the data based on certain angle of reading. Having the reading angle and NOF periodicities in an unknown state makes it impossible for an individual or program to merely guess the pattern of the Nano-optical structures either from the colors they reflect or from the way they are read by the detector. This extra security level is accompanied by the encryption that NOF encoding algorithm imposes on the original data. The NOF encoder sets aside a key or portion of the encrypted data that can be saved inside the reader (decoder) hence allows for a key-lock security scheme. Compared to smart cards such as RFID tags and magnetic stripe cards, NOF has a clear advantage regarding both data storage density and security. RFID tags provide a storage density of maximum 165Kbits/in^2 and magnetic stripe cards' storage density is 2.87Kbits/in^2 in its maximum condition. These figures are much smaller than NOF storage density that under experimental conditions and not well-tuned commercial conditions, allows for nearly one megabytes of data per inch square (Table 7). Both magnetic stripe cards and RFID cards can be decrypted using Differential Power Analysis (DPA) which is a side-channel attack that uses the chip power consumption statistical data to decode the information on the cards. NOF data is read and analyzed using image processing techniques (numerical analysis). Such analysis does not leave a trace that can be picked up by a DPA process hence NOF stands out both regarding its storage density and its security compared to the current ID security cards [17] (Figure 5. 1).

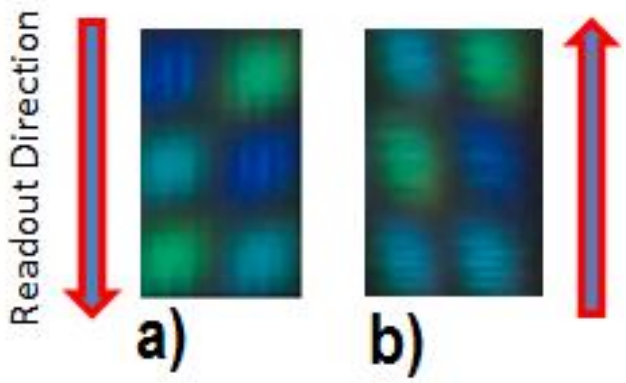

Figure 5. 1. Left)-Readout with pattern one; Right)-Readout with a different pattern producing new image

5.2. Effects of NOF-encoding as a multi-variation encoding unit information on transmission rates

For a simple transmission setup, there would be a channel capacity bounded by Shannon's theorem regarding the source entropy. The ergodicity of the data can be an issue that may enhance the transmission rates over a channel of known parameters (Figure 5. 2). Nano-optical feature encoding can affect the fixed channel parameter transmission in two ways: 1) - by reducing the size of the data transmittable as a non-ergodic sequence. A non-ergodic sequence of data has no means of predictability for long-run observations over time. This only allows for (if not exceeding the channel capacity) an enhancement of transmission when the number of unit information carriers reduces, For example, the more data per / unit read-back storage medium, the higher the transmission rate for that system. This can be viewed through the fact that increased variation states in a Nano-optical feature as unit information carrier outruns the classical binary unit information carrier in both magnetic stripes and barcodes for similar surface area. 2) - Through assumption of infinite-length-run observations over time; if a source is defined with the alphabet of the target data (data to be encoded) and is emitting data infinitely, the measuring of the entropy of the source is strongly affected by the fact that the number of typical sequences for such source will decrease as the states of variation of the unit information carrier is increased. Any source assumed in the aforementioned conditions is an ergodic source and in the case of ergodicity, the boundaries of the

number of typical sets of the source become subject to a significant decrease as the states of variation of the unit information carrier increases (Figure 5. 3).

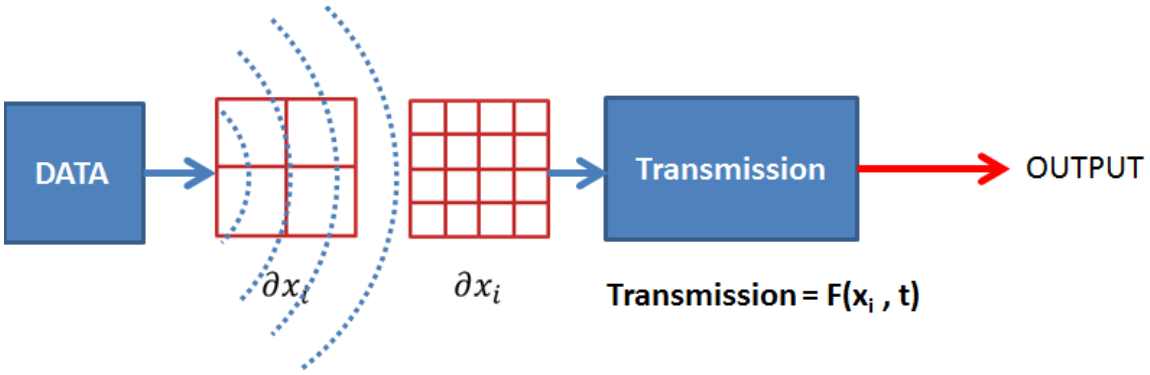

Figure 5. 2. Block diagram of effects of storage density on transmission rates for fixed channel parameters; with higher data density for fixed channel the rate of transmission increases

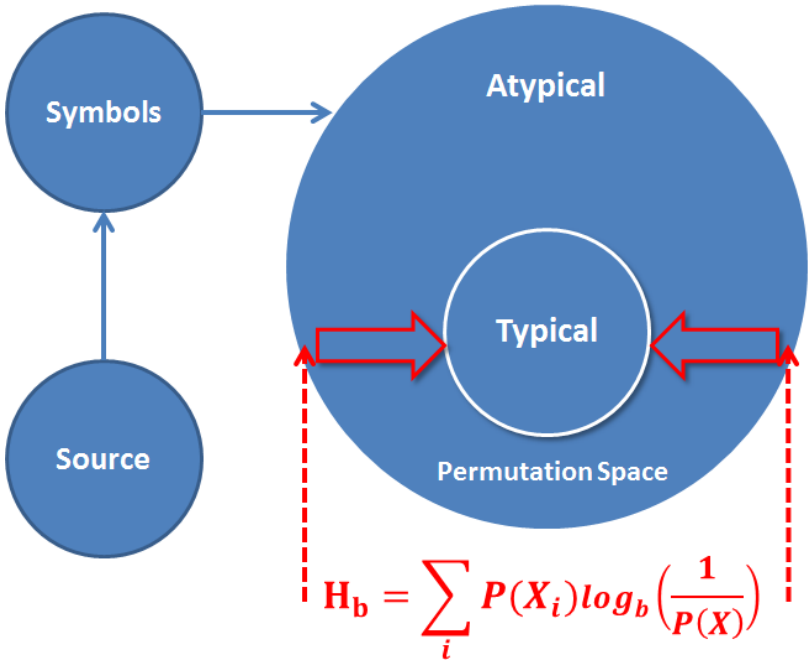

Figure 5. 3. Visualisation of the Shannon's entropy measure on imposing boundaries to the number of typical sequences that emerge in an infinite space of an ergodic source

The ergodic source model pictures a source of information that emits data infinitely yet also has the characteristics to allow its probability density function (PDF) to be revealed to the encoder and decoder that receive the data after a finite amount of data emission. The Typical set of such source is the combination of data strings that are more probable to occur than others. The number of combinations emitted from an ergodic source with

highest probability is the same as the number of observations required for the encoder/decoder setup to figure out the source's PDF. This number has an upper limit which is described via Shannon's measure of entropy [27]:

$$T_{N,\beta} = \left\{ \left| x \in A_X^N : \frac{1}{N} \log_2 \frac{1}{P(x)} - H(x) \right| < \beta \right\} \qquad \textbf{5-1}$$

$T_{N,\beta}$ =Set of most probable strings of the source

x =Data string emitted from the source

A_X^N =Set of all possible combinations of data in the source

$P(x)$ =Probability of data string x

N =Number of random variables constructing a string x

$H(x)$ =Shannon's entropy of data string x

β =Positive number

Eq(5-1) has a direct result drawn from [2] which sets the limit of the most probable outputs of the source as following:

$$\left| T_{N,\beta} \right| \leq 2^{N(H+\beta)} \qquad \textbf{5-2}$$

$H = H(x)$ =Shannon's Entropy

In this term, the Shannon's entropy is measured using the states of variation of a random variable that encodes the data hence the minimum number of variation states (for a binary digit) which is two sets the T_{NB} function at its maximum upper limit. If a random variable has $b>2$ states of variation such as NOF encoding scheme the entropy measure in Eq(5-2) will change into following:

$$H_2(x) = -\sum P(x)\log_2 P(x) \qquad \textbf{5-3}$$

$$H_b(x) = -\sum P(x)\left(\frac{1}{\log_2 b}\right)\log_2 P(x) = -\frac{1}{\log_2 b}\sum P(x)\log_2 P(x)$$

Because b>2 the term $1/\log_2 b < 1$ hence:

$$for\ b = 4\quad |T_{N,\beta}| \le 2^{N\left(\frac{1}{\log_2 4}H_2(x)+\beta\right)} \Rightarrow |T_{N,\beta}| \le 2^{N(0.5H_2(x)+\beta)} \qquad \textbf{5-4}$$

The graphs in Figure 5. 4 show the measure by which the entropy affects the upper limit of the set of most probable outputs of an ergodic source if the encoding variable has 2 more states than a binary encoding variable.

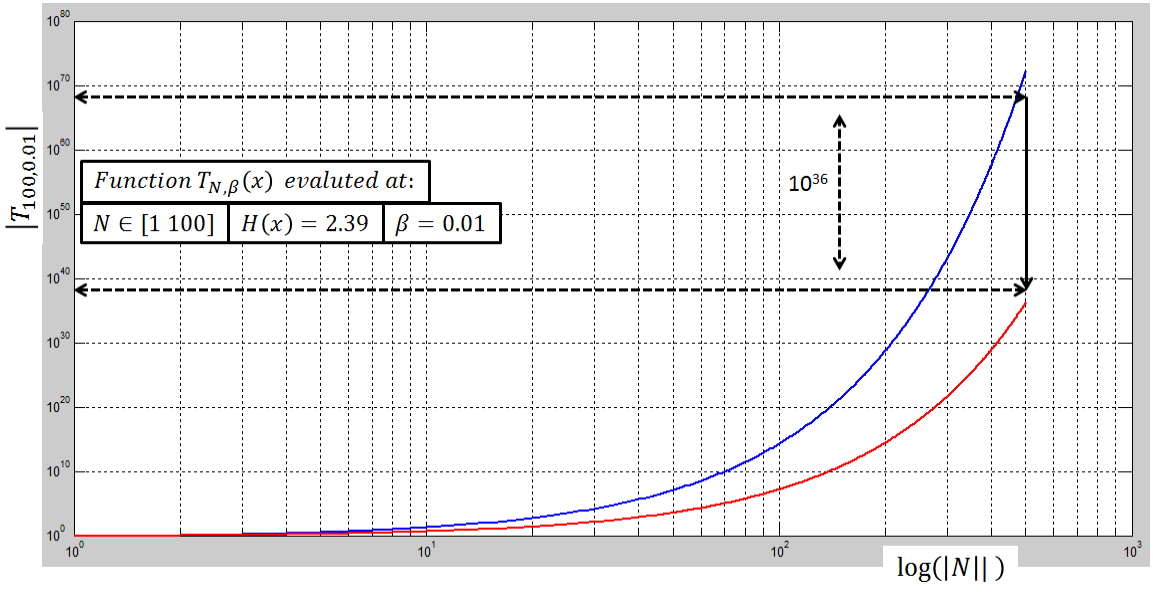

Figure 5. 4. Evaluating eq(5-4) at the given paramters reveals a 36 orders of magnitude decrease in the function T_{NB} which governs the number of most probable outcomes for an ergodic source for binary variable (blue) and NOF variable (red)

5.3. Future Application of Multi-State Optical Encoding

Through the course of this work it has become clear that use of optical signals, as it has been successfully trialed in advanced industries such as fine sensing and telecommunication, and biomedical imaging can also be implemented in fields with less application complexity and more cost-sensitive commercial sectors. The fact that a NOF encoded text data can be stored in physical spaces about 100 times less than that of any efficient barcodes and its ability to be passively yet securely read by specific readers makes it a potential candidate for commercialization in the near future. The future work on this topic will encompass combinatory algorithms that entail Nano-optical technology along with more advanced mathematical models to fully resolve and employ benefits of a multi-variation state optical unit information that can transmit data using angular modulation of the incident wavelengths. Use of optical Nano-structures in order to modulate analog properties of oscillating energy and waveforms can be a new way to achieve multi-stage optical circuits (Figure 5. 5).

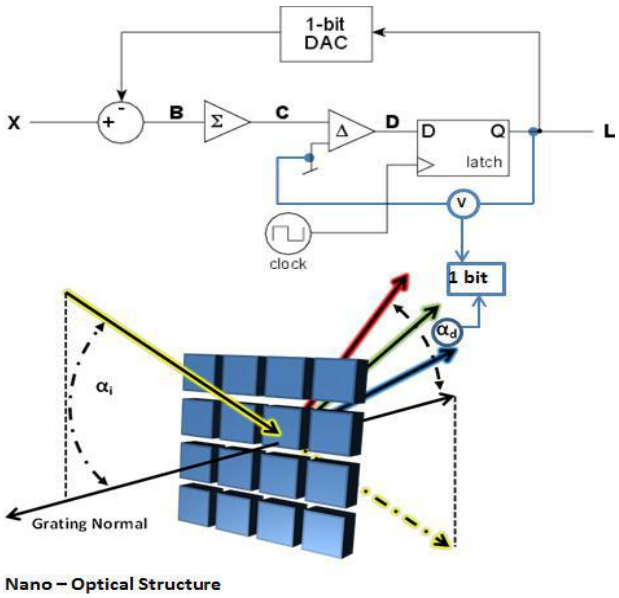

Figure 5. 5. Definition of a bit in a digital to analogue conversion circuit; the NOF or the Nano-optical feature can be viewed as having a variation state as a function of its periodicity

The effect of increasing the permutation space of one bit by having more than two variation states not only affects the storage capacity of the storage device but also has an impact on the arithmetic operators acting in the system. Figure 5. 6-(a) shows a series of logical gates and their overall result in node E whereas Figure 5. 6-(b) shows the same junction when the last gate produces more than two states:

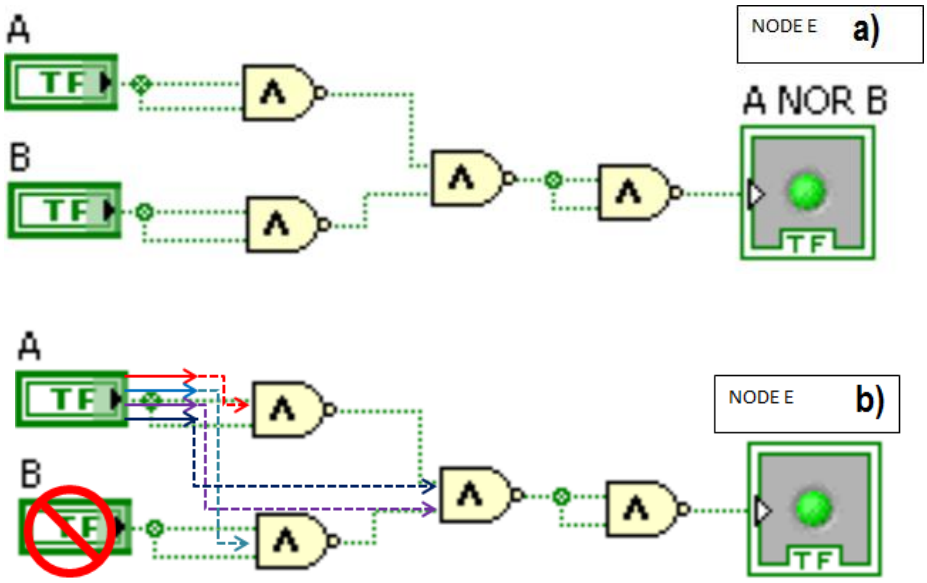

Figure 5. 6. a) - NOR gate using classical Boolean operands b) - NOR gate using a multi-varied state bit in combination with Boolean operands

The second multi-varied bit (bit B) can control a different set of logical gates. The latterly mentioned is in the case of logical gates (acting in a Boolean framework) and not gates that can also generate multiple responses to various sets of inputs. Investigation of combining non-logical gates (gates with more than one response) and multi-state bits is one of the potential scopes of this work yet alongside increase of complexity; the size of such combinations will decrease significantly. The computation speed will also benefit from having non logical gates and multi-state bits since more complex arithmetic operations can take place within smaller sequences of gates and bits. Having described the advantages of multi-state bit it is necessary to mention that in order for the concept to be functional the states of variation must be both distinct and reproducible with high degree of accuracy.

References

[1] S. Vosoogh-Grayli, Diffractive Nano-Structures as Optical Visual and Machine Readable Features, 2012, Master Thesis.

[2] K. Sayood, An Introduction to Data Compression, 2nd ed., K. Sayood, Ed. San Francisco, USA: Morgan Kaufmann, 2006.

[3] V.S.Bagad I.A.Dhotre, Data Communication, 1st ed., I.A.Dhotre, Ed. Pune, India: Technical Publications, 2008.

[4] R. Bangia, Dictionary of Information Technology, 2nd ed., R. Bangia, Ed. New Dehli India: Laxmi Publications, 2010.

[5] A. Godse D.A.Godse, Digital Techniques, 1st ed., D.A.Godse, Ed. Pune, India: Technical Publications, 2008.

[6] R. L. Goodstein, Boolean Algebra, 1st ed., R. L. Goodstein, Ed. New York, USA: Dover Publications, 2007.

[7] S. Bathul, Mathematical Foundations of Computer Science, 1st ed., S. Bathul, Ed. New Delhi, India: PHI Publication, 2010.

[8] J. B. Anderson, Source and Channel Coding: An Algorithmic Approach, 1st ed., J. B. Anderson, Ed. Norwell, USA: Kluwer Academic Publisher Group, 1991.

[9] A. Khurshudov, The Essential Guide to Computer Data Storage, 1st ed., A. Khurshudov, Ed. Saddle River, USA: Prentice Hall, 2001.

[10] E. Meinders, Optical Data Storage: Phase Change Media and Recording, 1st ed., E. Meinders, Ed. Dordrecht, Netherlands: Springer verlag, 2006.

[11] S. K. Singh, Database Systems: Concepts, Design & Applications, 1st ed., S. K. Singh, Ed. New Delhi, India: Pearson Education, 2009.

[12] R. W. Ditchburn, Light, 1st ed., R. W. Ditchburn, Ed. New York, USA: Dover Publications Inc., 1991.

[13] J. A. Stratton, Electromagnetic Theory, 1st ed., J. Audino, Ed. New Jersey, USA: Wiley and Sons, 2007.

[14] (2012, Jan.) Adams Communications. [Online] http://www.adams1.com/39code.html

[15] (1995, September) Adams Communications Introduction to Barcodes. [Online]. http://www.adams1.com/stack.html

[16] (2012, September) Zebra Technologies Online Introduction to RFID Tags. [Online]. http://www.zebra.com/us/en/solutions/getting-started/rfid-printing-encoding/rfid-tag-characteristics.html

[17] W. Rankl, Smart Card Handbook, 4th ed., W. Rankl, Ed. West Sussex, UK: Wiley & Sons, 2010.

[18] H. Lehpamer, RFID Design and Principles, 2nd ed., H. Lehpamer, Ed. Norwood, USA: Artech House, 2012.

[19] E.G. Loewen, Diffraction Gratings and Applications, 1st ed., E.G. Loewen, Ed. New York, USA: Marcel Dekker Inc., 1997.

[20] R. Gordon, "A New Generation of Sensors Based on Extraordinary Optical Transmission," Accounts of Chemical Research, vol. 41, no. 8, pp. 1049-1057, July 2008.

[21] R.V. Baltz, "Surface Plasmons in Bulk Metals and Metalic Clusters and Metalic Heterostructures," Spectroscopy and Dynamics of Collective Excitations in Solids, vol. 356, pp. 1-36, 1997.

[22] R.Gonzales, Digital Image Processing, 2nd ed., R.Gonzales, Ed. Saddle River, USA: Prentice Hall, 2002.

[23] S. Eddins, Freehand Segmentation in a*-b* Plane, 2011, Steve Eddins Blogs on Image Processing using MATLAB.

[24] M. Savoini, "All-optical subdiffraction multilevel data encoding onto azo-polymeric thin films," Optics Letters, vol. 34, no. 6, pp. 761-763, March 2009.

[25] S. W. Birtwell, "Superimposed Nano-scale Diffraction Gratings as High Capacity Barcodes for Biological and Chemical Applications," Optics in Life Science, vol. 281, no. 7, pp. 1789-1795, October 2007.

[26] G. Sharma, Digital Imaging : Handbook, 2nd ed., G. Sharma, Ed. Florida, United States: CRC Press, 2003.

[27] T. M. Cover, Elements of Information Theory, 2nd ed., T. M. Cover, Ed. New Jersey, USA: John Wiley & Sons, 1991.

[28] A. Ghatak, Optics, 4th ed., A. Ghatak, Ed. New Delhi, India: McGraw-Hill, 2009.

[29] T. W. Ebbesen, "Light in Tiny Holes," Nature Physics, vol. 445, pp. 39-46, January 2007.

[30] M. Mrejen, Investigating the Confinement of Light in Nanometric Domain, May 2007,

Master's Thesis from The Hebrew University of Jerusalem.

[31] M. Mansuripour, Classical Optics, 1st ed., M. Mansuripour, Ed. Cambridge, UK: Cambridge University Press, 2002.

[32] A. Zayats, "Nano Optics of Surface Plasmon Plaritons," Physics Reports, vol. 408, no. 3-4, pp. 131-314, March 2005.

[33] S. Dror, Modern Introduction to Surface Plasmons, 1st ed., S. Dror, Ed. Cambridge, UK: Cambrdige University Press, 2010.

[34] S. Kawata, Near-Field Optics and Surface Plasmon Polaritons, 1st ed., M. Ohtsu, Ed. Berlin, Germany: Springer, 2001.

[35] S. Rodrigo, "Influence of Material Properties on Extraordinary Optical Transmission Through Hole Arrays," Physical Review, vol. 77, no. 7, February 2008.

[36] L. Novotny, Principles of Nano Optics, 1st ed., L. Novotny, Ed. Cambridge, UK: Cambridge University Press, 2006.

[37] Z. Cui, Nano Fabrication: Priniciples, Capabilities and Limits, 1st ed., Z. Cui, Ed. New York, USA: Springer Verlag, 2008.

[38] D. MacKay, Information Theory, Inference, and Learning Algorithms, 1st ed., D. MacKay, Ed. Cambridge, UK: Cambridge University Press, 2003.

[39] M. Erickson, Number Theory, 1st ed., M. Erickson, Ed. Boca Raton, USA: CRC Press, 2008.

[40] F. Saadia, "Canalizing Zhegalkin Polynomials as Models for Gene Expression Time Series Data," in Engineering of Intelligent Systems, 2006 IEEE International Conference, Islamabaad, 2006.

Appendices

Appendix I. Physics and Optics used in this Thesis

Characteristics of Light

A complete conceptualization of the nature of light includes light as a particle, as a wave, and as electromagnetic radiation. It is defined as the visible range of the electromagnetic spectrum with wavelengths ranging between 300 nm to 700 nm. The measure for quantifying light is photon. Its wavelike behaviour is using the units of frequency (Hz). The classical propagation of light is explained through Maxwell's equations [13]:

$$\oint \bar{E} d\bar{A} = \frac{q}{\epsilon_0} \qquad \textbf{A- 1}$$

$$\oint \bar{B} d\bar{A} = 0$$

$$\oint \bar{E} d\bar{S} = -\frac{d\Phi_B}{dt}$$

$$\oint \bar{B} d\bar{S} = \mu_0 i + \frac{1}{C^2}\frac{\partial}{\partial t}\int \bar{E} d\bar{A}$$

Basic properties of light used in Engineering applications are Interference, Refraction, Transmission and Diffraction. These properties are briefly reviewed in the following Table (App-Table1).

App-Table. 1. Some Basic Characteristics of Light and their Application in Engineering

Property (of Light)	Corresponding Device(example)
Photoelectric effect	Photodiode/Photodetector
Total internal reflection	Endoscope, Fibre optic
Photon spin polarization	Polarized photographic filter lens
Refraction	Phoropter (Ophthalmology)
Interference	OCT (Ophthalmology)
Dispersion	Elastic Dynamic Light Scattering
Diffraction	Diffraction gratings (Spectrometry)
Surface Plasmon Resonance	Raman Spectroscopy
Interference	Holography
Transmission	Authentication & Security

There are wide varieties of employing the characteristics mentioned in Table 1. Of most importance among these characteristics are optical transmission, reflection and diffraction. One example application of optical transmission is data transfer and data storage in telecommunication. Example for optical reflection is storing and encoding data in a medium such as CDs or DVDs. Optical diffraction is used in spectrometry where the optical intensity of an illuminating field is measured and calculated based on the diffraction theory.

Reflection

Light, having wave-like properties in its propagation, can be reflected from a surface. Formally, reflection is the change in direction of a wave front at an interface between two different media so that the wave front returns into the medium from which it originated. Common examples include the reflection of light from a mirror-like surface. The law of reflection states that for reflection, the angle at which the wave is incident on the surface equals the angle at which it is reflected. Mirrors exhibit specular reflection. (Figure 1)

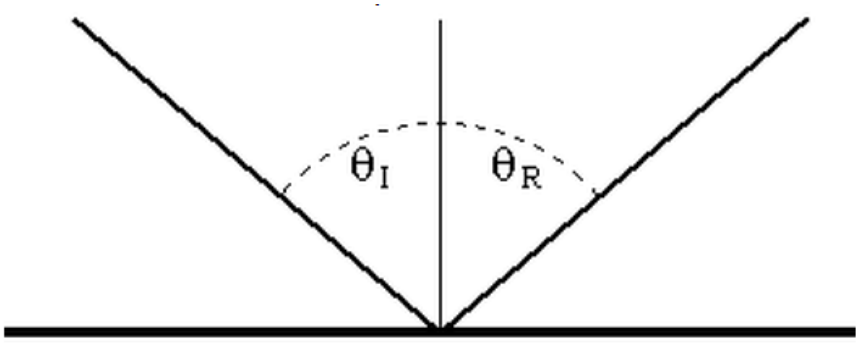

Figure 1. Angle of incidence and reflection are equal when a wave front (light) arrives at a mirror-like surface (θI is the incidence angle and θr is the reflection angle)

Refraction

Refraction is the bending of light as it passes between materials of different density. The index of refraction of a material is the ratio of the speed of light in vacuum to the speed of light in that material [28]. Eq(2-2) quantifies this as follows:

$$n = \frac{C}{V} \qquad \textbf{A- 2}$$

n = Index of Refraction

C = Speed of light in vacuum

V = Speed of light in a medium other than vacuum

The more dense the material is the slower the speed of light in that material thus $n > 1$ for all materials and increases with increasing density. In vacuum n is equal to one. The frequency of light does not change when it passes from one medium to another. According to the formula $v = \lambda f$, the wavelength must change (f is the angular frequency of light). The index of refraction can therefore be written in terms of wavelengths (Figure 2):

$$n = \frac{\lambda}{\lambda_0}$$ ***A- 3***

λ_0= Wavelength of light in the vacuum

λ = Wavelength of light in the medium

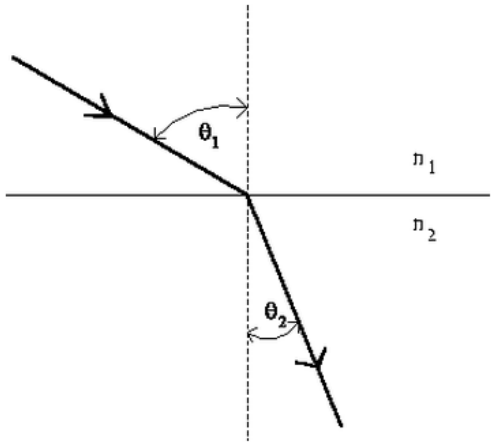

Figure 2. Schematic of optical refraction

The change in speed and wavelength at the boundary between two materials causes light to change direction. If θ_1 is the angle of the ray relative to the normal to the surface in medium 1 , and θ_2 is the angle relative to the normal in medium 2, then:

$$\frac{sin\theta_1}{sin\theta_2} = \frac{\lambda_1}{\lambda_2} = \frac{n_1}{n_2} = \frac{v_1}{v_2}$$ ***A- 4***

θ_1 = Angle of Incidence

θ_2 = Angle of refraction

λ_i =Wavelength of light in medium i

v_i = Speed of light in medium i

Dispersion

The velocity of light in a material, and hence its index of refraction, depends on the wavelength of the light. In general, n varies inversely with wavelength: it is greater for shorter wavelengths. This causes light inside materials to be refracted by different amounts according to the wavelength (or colour). This gives rise to the colours seen through a prism. Rainbows are caused by a combination of dispersion inside the raindrop and total internal reflection of light from the back of raindrops. The following is a chart giving the index of refraction for various wavelengths of light in glass (Figure 3).

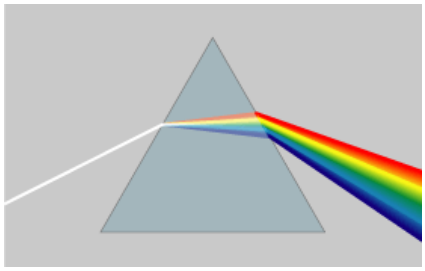

Figure 3. Depiction of polychromatic light refracting through a prism

Transmission

Optical transmission occurs in transparent media and is defined as the transferring of the wave (light) frequency into the medium being illuminated. Transmissions of light waves occur because the frequencies of the light waves do not match the natural frequencies of vibration of the objects. When light waves of these frequencies strike an object, the electrons in the atoms of the object begin vibrating. But instead of vibrating in resonance at a large amplitude, the electrons vibrate for brief periods of time with small amplitudes of vibration; then the energy is reemitted as a light wave. If the object is transparent, then the vibrations of the electrons are passed on to neighbouring atoms through the bulk of the material and reemitted on the opposite side of the object. Such frequencies of light waves are said to be transmitted. If the object is opaque, then the vibrations of the electrons are not passed from atom to atom through the bulk of the material. Rather the electrons of atoms on the material's surface vibrate for short periods of time and then reemit the energy as a reflected light wave. Such frequencies of light are said to be

reflected. The optical transmission was being modeled by Bethe for an infinitely small aperture through [29]:

$$\eta_B = \frac{64(K_0 r)^4}{27\pi^2} \quad \rightarrow \quad \eta_B \propto \left(\frac{r}{\lambda}\right)^4 \qquad \textbf{A- 5}$$

The mathematical derivation in Eq(2-5) gives a transmission efficiency model shown in Figure. 4 :

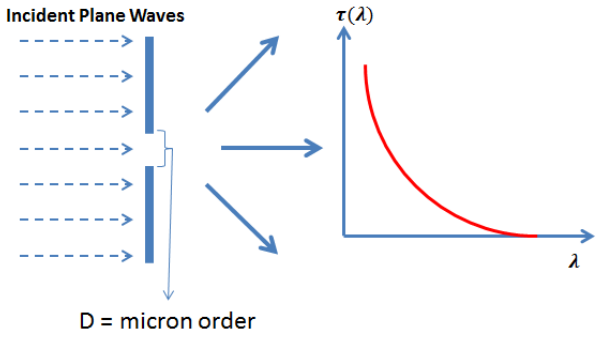

Figure 4. Bethe's approximation for optical transmission efficiency through a small aperture

Extraordinary Transmission and Surface Plasmon Resonance(SPR)

According to experimental results, for optical media composed of metal and dielectric together in a boundary-like contact, there are transmissions within apertures smaller than what Bethe formula (Eq(2-5)) predicted that are enhanced more than what his equation states. The scientists have chosen the title "Extra Ordinary Transmission" (EOT) as a result and this has become the most recent optical anomaly to be explained for the past decades [29][30]. In brief EOT is the result of the coupling of the incident wave and the standing modes of surface charges of an opaque metal which are referred to as surface plasmons (SP). Surface plasmons are the natural result of having a charge separation such as that of large positive ions and free electron sea in metals. According to Ebbesen and his colleagues, the emerging field from a medium with sub-wavelength aperture(s) not only has enhanced field amplitude but also shows abnormality in a number of ways. Of such, one can note the filtering of some wavelengths on the exit side of the interface, changes and shifts in emergent frequency with respect to the surface

parameters (boundary surface), intensity highs and lows proportional to the geometry of the sub-wavelength apertures and etc [29]. These effects can be in brief linked to a hypothesis that has been dedicated to the existence of a fundamental frequency of the bulk plasma that exists within a metallic element. These oscillations are in turn also sources for charge induction as every charged particle is a source of electric field itself. The quantum mechanical definition of this model quantizes the plasma oscillations into quanta called plasmons. Plasmons and their network give rise to the hypothesis of surface charges which are in fact lower in energy compared to those plasmons in the bulk and are limited by a surface boundary between the metal and some other medium (usually a dielectric medium such as air). These surface charges are termed as surface plasmons. Surface plasmon as indicated by [31] is also regarded as a solution (inhomogeneous) to the Maxwell's equation for the boundary conditions imposed on it based on the differences of permittivity in two different media. Of the two usually one has positive and one has negative permittivity. The metals have negative permittivity and a dielectric e.g. air surrounding the metal provides the positive value. Here the analogy is to understand the nature of surface plasmons as an evanescent mode of electric field dependent on the plasma frequency of the bulk material and the charge density at the surface of the metal [32]. The actual interest is when these modes become radiative and/or penetrate the metal. The aforementioned is the explanation of what opposes Bethe's prediction for the emergence of an enhanced field through a sub-wavelength aperture. Because in an isotropic medium such as a metal the permittivity is in fact a function of the wave vector in that medium and the index of refraction, for indices of refraction much smaller than the wave number a large negative permittivity condition for one side of a boundary is automatically satisfied through metals [33]. This in turns allows for the existence of standing surface plasmon modes. It becomes a matter of interest when the surface plasmons couple with an incident photon and turn into surface plasmon polaritons [34]. It is necessary to say that in some texts the term surface plasmon and surface plasmon polariton are being used interchangeably whereas here the work tries to separate the non-propagative modes from the propagative ones through surface plasmon (SP) and surface plasmon polariton (SPP) respectively. The term used in literature for this interaction is "resonant absorption" and the reason for this is that the momentum of the incoming photon must match the wave number of the plasmon in order for allowance of any further modes be it decaying through radiation or through

absorption into the metal [32]. The fact that the wave number of the incident photon must match that of the plasmon (surface plasmon) indicates a resonance. In order to resonate and excite the SP modes, an incident plane wave must be carrying enough amplitude into the space (air) in order to reach the metal with enough energy for excitation. Thereby one must “force” the metal to accept the incoming wave and hence allow for a propagative mode of the surface plasmons known as surface plasmon polaritons.(Figure 5)

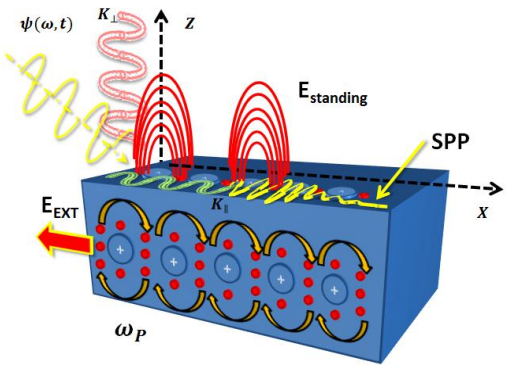

Figure 5. 3D model of plasma oscillation, incidence field and surface plasmon polariton generation. The direction of the SPP is a function of parallel component of the incident field

Surface plasmon resonance (SPR) is the resonant, collective oscillation of valence in the metal stimulated by incident light. The resonance condition is established when the frequency of light photons matches the natural frequency of surface electrons oscillating against the restoring force of positive nuclei. SPR in nanometer-sized structures is called localized surface plasmon resonance. In order to excite surface plasmons in a resonant manner, one can use an electron or light beam (visible and infrared are typical). The incoming beam has to match its momentum to that of the plasmon. In the case of p-polarized light (polarization occurs parallel to the plane of incidence. S-polarized light (polarization occurs perpendicular to the plane of incidence) cannot excite electronic surface plasmons. Surface plasmons obey the following dispersion relation [34][35](Figure 6):

A- 6

$$K_{SP} = \frac{\omega}{C}\sqrt{\frac{\epsilon_d \epsilon_m}{\epsilon_d + \epsilon_m}}$$

K_{SP} =Surface plasmon wave number(Vector)

ω =Wave (light) angular frequency

C =Speed of light

ϵ_m =Metal permittivity

ϵ_d =Dielectric permittivity

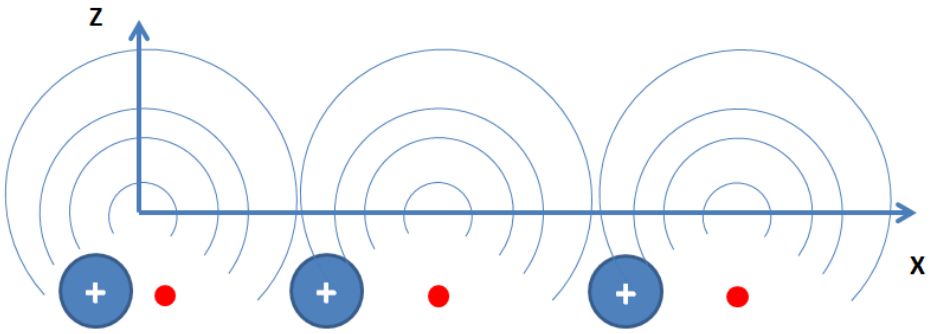

Figure 6. Evanescent or standing modes of the surface plasmon electric field distribution

Diffraction

Diffraction is the apparent "bending" of light waves around obstacles in its path. This bending is due to Huygens's principle, which states that all points along a wave front act as if they were point sources. Thus, when a wave comes against a barrier with a small opening, all but one of the effective point sources are blocked, and the light coming through the opening behaves as a single point source, so that the light emerges in all directions, instead of just passing straight through the slit [28] (Figure 7).

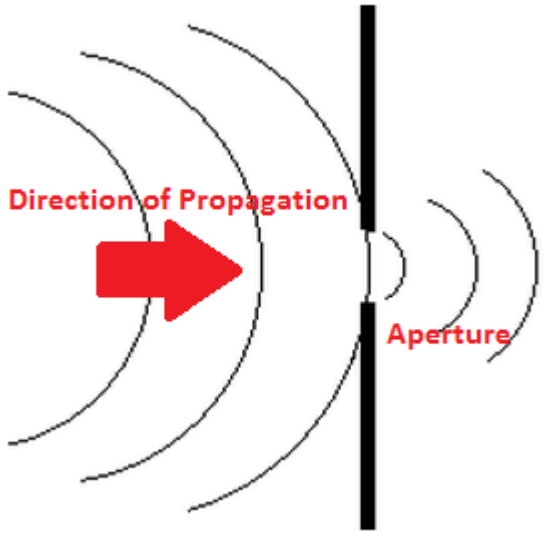

Figure 7. Diffracting light (wavefront) through a small aperture (slit)

The intensity of the diffracted optical field due to the presence of an aperture is calculated through the following equations (Figure 8):

$$E_{tot} = A \sin\frac{(\beta)}{\beta}\cos(\omega t - \beta) \qquad \textbf{A- 7}$$

$$I_{tot,P} = I_0\frac{\sin^2(\beta)}{\beta^2}$$

$E_{tot,P}$ =Total electric field amplitude at point P

$I_{tot,P}$ =Total optical intensity at point P

β =Angle of diffraction

ω =Incident light angular frequency

I_0 = Intensity of the field at the center of its beam axis

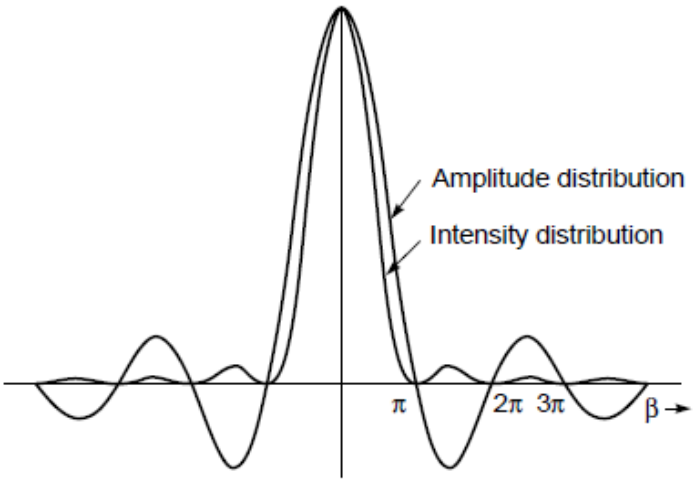

Figure 8. A graph based on the amplitude and intensity distribution of the diffracted field

Types of Diffraction

There are two types of optical diffraction that are related yet the amplitude and optical intensity related to them are different from one another. These types are 1)-Fresnel Diffraction and 2)-Fraunhofer Diffraction (Figure 9). The main factor that determines the type of diffracting system is the distance at which the optical field is being imaged or sensed. Fresnel diffraction can be summarized in an integral form using an arbitrary aperture as shown in Figure 10. The optical intensity describing the Fresnel diffraction is calculated through [28]:

$$\mathrm{U}(x,y,z) = \frac{1}{j\lambda}\exp(jKz)\exp\left\{\frac{jK}{2z}(x^2+y^2)\right\}\int\int A(\hat{x},\hat{y})\exp\left\{\frac{jK}{2z}(\hat{x}^2+\hat{y}^2)\right\}\exp\left(-j(u\hat{x}+v\hat{y})\right) \quad \textbf{A- 8}$$

The Fresnel approximation is used in near field optical analysis. Near field optics is usually implied to those optical systems in which the coupling of diffracted light with a second object occurs in distances smaller than one wavelength of the incident light (Figure 11).

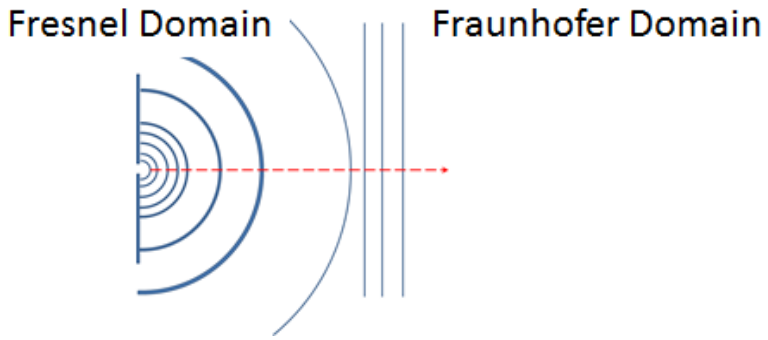

Figure 9. The distance is the key factor of defining which domain the diffracted wave is measured in

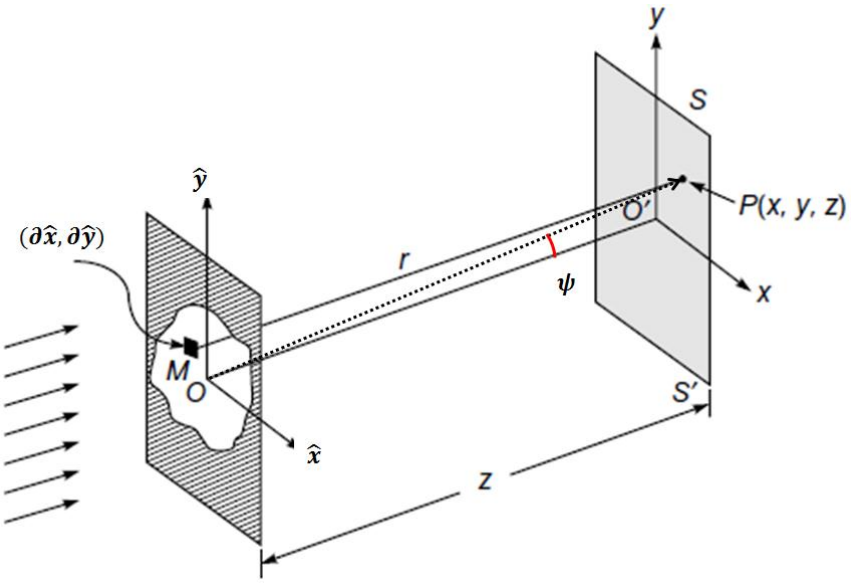

Figure 10. Diagram of Fresnel diffractive spectrum measurement setup

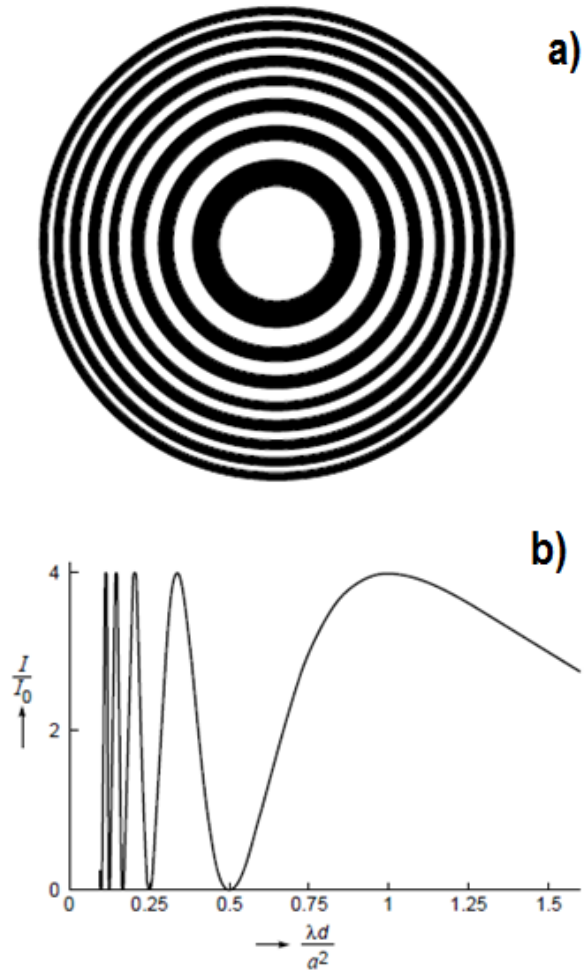

Figure 11. a)-The intensity distribution of a Fresnel diffraction through a zone plate b)- Intensity variation of an axial point corresponding to a plane wave incident on a circular aperture of radius a ;Source: Ajoy Ghatak's Optics

Fraunhofer diffraction is the more practical approximation as to the fact that the distance over which it is defined can be larger than that of Fresnel approximation. The Fraunhofer domain diffraction follows a particular mathematical order for the intensity distribution known as the airy pattern for a circular aperture. This order is shown through (Figure 12) and it can be estimated mathematically through:

A- 9

$$I(P) = I_0\left[\frac{2J_1(v)}{v}\right]^2$$

$I(P)$ =Field luminal intensity at point P

I_0 =Field luminal intensity at the zero diffraction

$J_1[.]$ =Bessel function of the first order

$$v \approx \frac{2\pi}{\lambda}\frac{D}{2}\frac{\sqrt{x^2+y^2}}{f}$$

D =Aperture diameter

f =Imaging lens focal length

x, y =Planar coordinates in the plane of the aperture

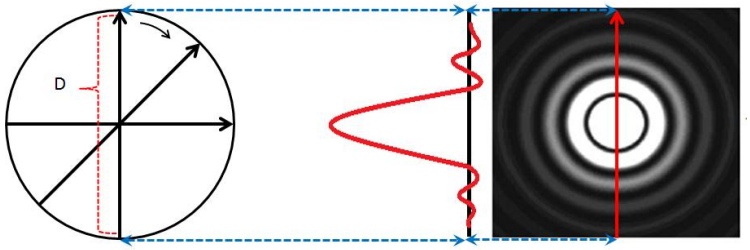

Figure 12. Fraunhofer diffraction pattern for a circular aperture known as the airy disk

Fraunhofer Diffraction for an Array of Identical Apertures

The Fraunhofer diffraction approximation model can be calculated for an array of identical apertures. The diffraction by N identical arrays will be the sum of the fields introduced to the image plane by each individual aperture through [28]:

$$U(P) = C\left[\int\int_{S_1} + \int\int_{S_2} + \cdots + \int\int_{S_N}\right]\exp\left(-j(u\zeta + v\eta)\right)d\zeta\, d\eta \qquad \textbf{A- 10}$$

S_i =Surface area of the aperture number i

u =Spatial frequency in x direction

v =Spatial frequency in y direction

Where P is any arbitrary point for which the field amplitude is being calculated and ζ,η are polar coordinates of P (Figure 13):

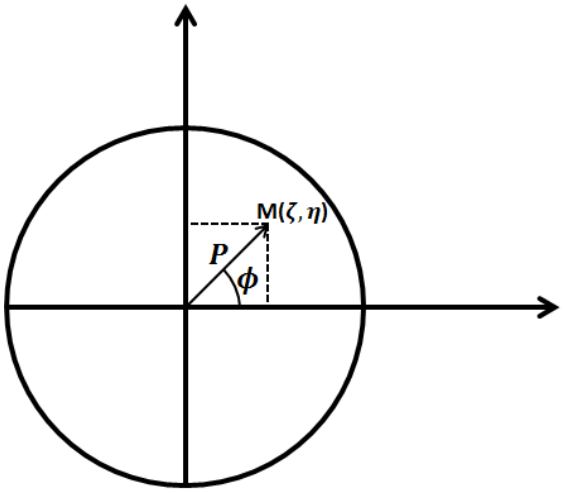

Figure 13. Translation of spatial coordinates into polar coordinates

This approximation holds true for array of sub-wavelength apertures as well. Figure 14 shows an array of sub-wavelength apertures' optical intensity. Comparing the optical intensity of such array with Figure 12 shows that Fraunhofer diffraction for identical apertures follow the mathematical approximation presented in Eq(2-7).

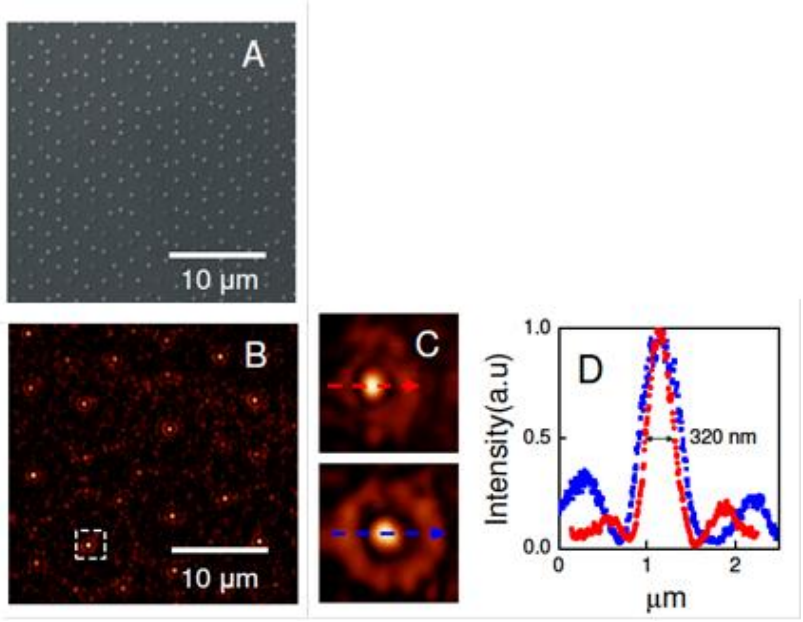

Figure 14. A) SEM B) NSOM images of a Nano-hole array C) The individual field distributions over one aperture D) The intensity profiles for identical apertures in different distances (Focusing of Light by a Nano-Hole Array Fu Min Huang, Yifang Chen, F. Javier Garcia de Abajo and Nikolay Zheludev)

The last two optical properties (SPR optical transmission and diffraction) are being used in combination to enhance data authentication through use of Nano-scale plasmonic optical structures used in development of Nano-optical models.

Nano Optical Design and Plasmonic Structures

Nano optics' is the collection of techniques by means of which optical convergence can be recorded in lengths beyond the diffraction limit. Some of the notable applications that arise from the latterly mentioned extension are super-resolution microscopy and ultra-high-density optical data storage. It also gives rise to the fabrication process of sub-wave length optical structures known as plasmonic structures. These structures due to being below the wavelength of an incident light can guide and manipulate the visible light in sub-wavelength systems. Such manipulation allows for harvesting signals which are capable of travelling longer than expected distances in the Nano-order structures. Definition of Nano-optical design can be interpreted as enhancing the optical space or optical confinement required for a photon through modification of surface parameters such as roughness, thickness, index of refraction etc. Quite simplified, the propagation of light in free space obeys a conservative law as in the following equation [36]:

$$\hbar\omega = \mathcal{C}.\hbar K \qquad K = \sqrt{K_X^2 + K_Y^2 + K_Z^2} \qquad \textbf{A- 11}$$

$\hbar$ =Planck's constant

ω =Wave angular frequency

$\mathcal{C}$ = Wave propagation speed in free space

And the immediate result of Eq(2-11) is a limit for wave solutions to exist through:

$$\Delta_\chi \geq \frac{1}{2\Delta K_\chi} \quad ; \quad \chi = \{X, Y, Z\} \text{ =Orthogonal coordinates} \qquad \textbf{A- 12}$$

Eq(2-12) shows that there will spatial confinement for a propagating quasi particle such as a photon due to the spread of its wave vector in different directions or in brief, under certain angles or beyond certain lengths a particular wave simply, cannot exist. Nano optics and Nano-optical design generally can be said to be dealing with the problem of spatial confinement of photons with respect to different propagation modes and tends to find solutions (analytical and empirical) to enhance and increase the confinement

barriers for better sensing [36]. Figure 15 shows different branching of Nano-optical design.

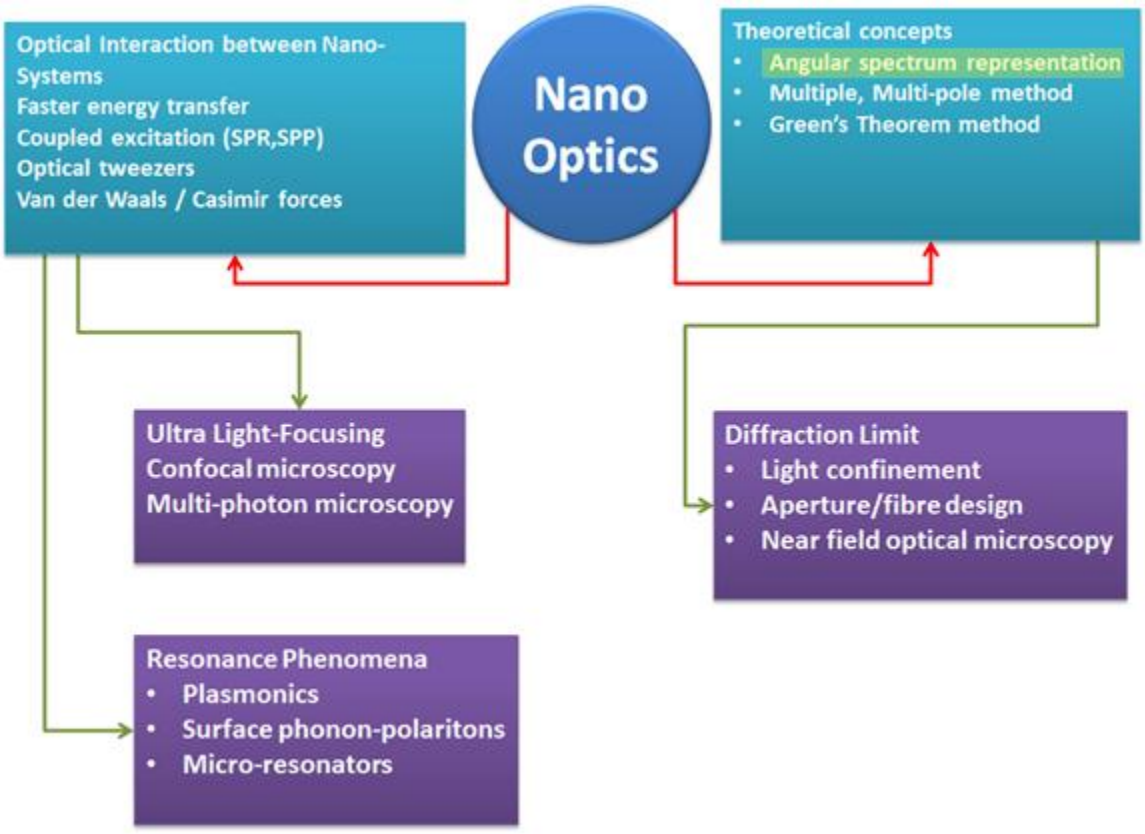

Figure 15. General approaches in Nano-optics. This work's concept is highlighted in yellow

Examples of Plasmonic Nanostructures

Some examples of plasmonic nanostructures are the arrays of Nano-order pillars or holes. These structures have a particular property that allows them to modulate an incident light wave in both transmission and reflection. The arrays of Nano-holes are fabricated using standard methods of nanofabrication. These methods allow for transferring of periodic patterns of both holes and pillars onto the optical medium. Some important properties of these plasmonic nanostructures are the wavelength filtering in transmission and efficient angular dispersion in reflection. Figure 16 shows some SEM images of periodic plasmonic nanostructures in the form pillar arrays and hole-arrays.

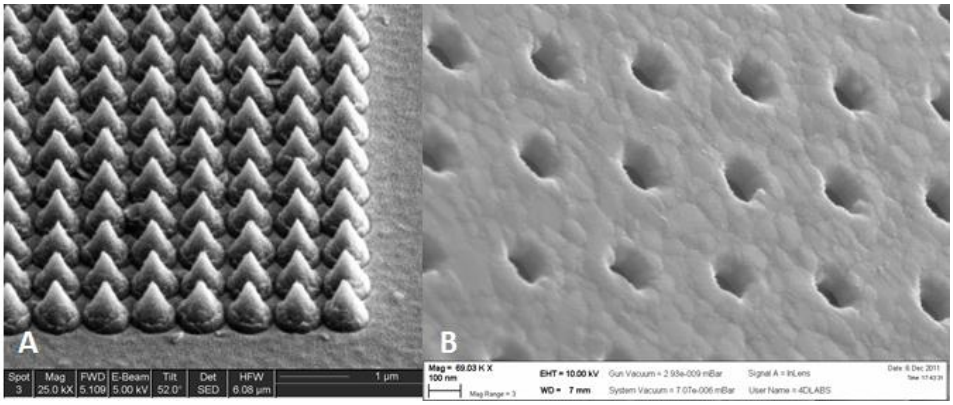

Figure 16. A) Plasmonic nanostructures in the form of Nano-pillars and B)-Nano-hole arrays

Nano-Fabrication Techniques for Fabrication of plasmonic nanostructures

An introduction to what generally encompasses nanofabrication can be as briefly as the following sentence from [37] : “Nano fabrication evolves from micro fabrication, and since the advent of first transistors in 1947, the IC industry has been the main driving force to continuously push fabrication technologies to their new dimensional limits”. The general purpose of a nanofabrication process is being schematically depicted in the following block diagram highlighting the technique used in this work in red outline [37] (Table 9):

Table 9. Fundamentals of Nano fabrication for optics (Nanofabrication: Principles, Capabilities and Limits by Zheng Cui)

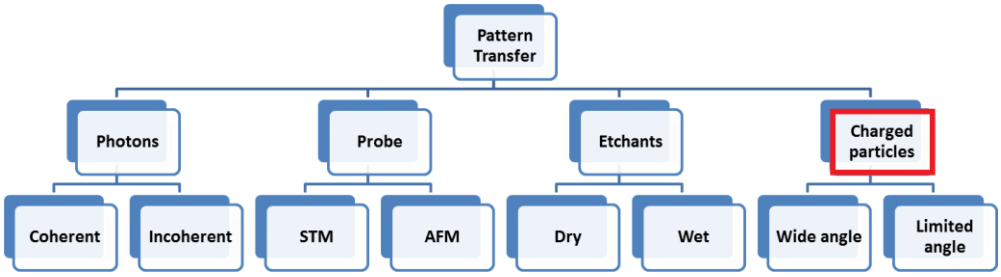

Nanofabrication by Charged Particles (Electron Beam Lithography)

This work from has chosen electron beam lithography as the choice for nanofabrication of the Nano-scale structures (Table 9). What made lithographic processes possible by means of the charged beams (electron beams) was the exploration of electron sensitive polymer “polymethylmethacrylate” or (PMMA). PMMA reacts to electron beams the same way a photoresist acts towards electromagnetic field distribution. Due to the quality of the beam produced by an electron beam emitter, by means of PMMA there was an immediate fabrication of much higher resolution structure than what possible by means of photons, sub-features as small as 10 nm in size. The realization of process was due to focusing of electron beam (e-beam) using e-beam optics. The throughput of an e-beam manufacturing setup is rather slow compared to any lithographic process. The factors contributing to a slow throughput can be named briefly as 1-Energy requirements of an efficient, high resolution e-beam, 2- Exposure time requirements and 3-Highly accurate beam-substrate interfacing [37]. The aforementioned factor by no means is a complete description to why e-beam is not a manufacturing-representable setup for mass production volumes yet it points the reader to the direction of the basic reasons that cause the low throughput. As an example the “highly accurate beam-substrate interfacing” encompasses a large variety of control parameters such as resist sensitivity, beam induced current, pattern density, beam interaction environment, etc. the figure below shows a schematic of an e-beam emitter (Figure 17).

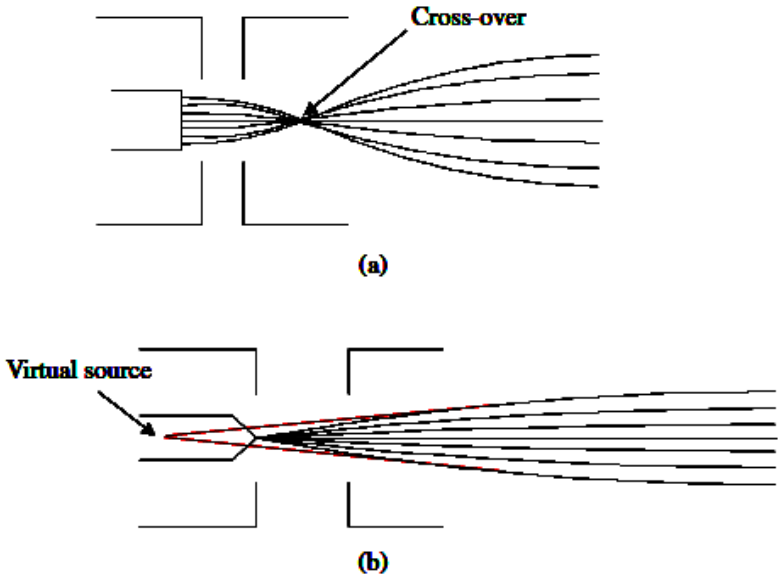

Figure 17. a) Virtual source (the cross-over) in a thermionic cathode. (b) Virtual source in a FE cathode (Nanofabrication: Principles, Capabilities and Limits By Zheng Cui)

An electron has the capacity of occupying a whole of a three dimensional confinement the same way as it can interact and coexist with millions of other electrons in the matter. The propagative nature of electron makes it a point source which has to obey the Maxwell conditions hence act as spherical radiative source when accelerated. For achieving small in diameter electron beams one must resolve the conditions through electron optics [37]. The electron-beam systems employ a rotationally-symmetric electro-static field in which the behaviour of a charged particle obeys the Lorentz force given by (Figure 18):

$$F_E = q(\bar{E} + v\bar{B}) \qquad \textbf{A- 13}$$

F_E = Field effect (force)

q =Charged particle

E =Electric field

B =Magnetic field

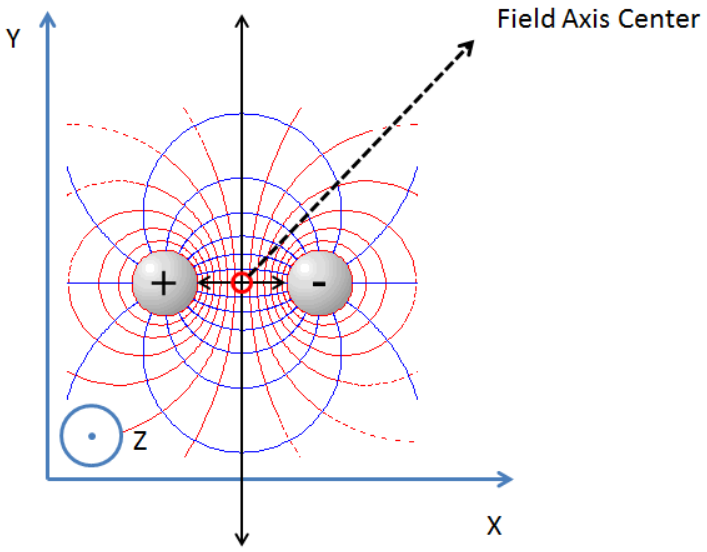

Figure 18. An electrical field of 2nd order symmetry forming a lens for charged particles

Any charged particle in the system will experience a radial pull r that drags it towards the center of the beam and an acceleration that acts in the Z (direction of beam propagation) direction. It is the radial pull that converges the beam into a focus (Figure 19).

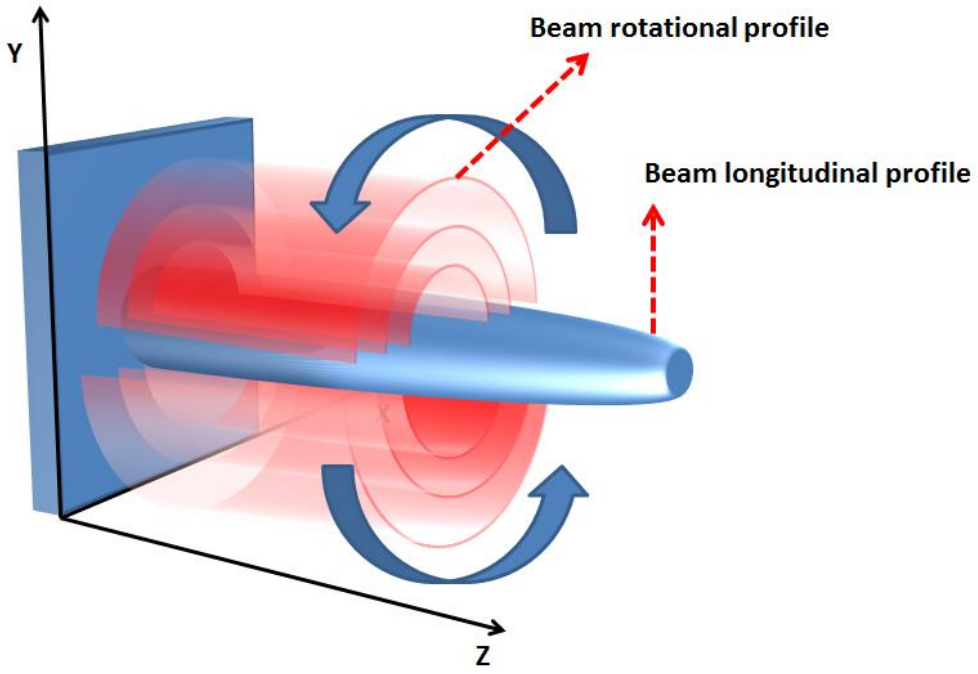

Figure 19. The radial and axial force generate a rotational profile around the axis

In Nano-fabrication technology the pattern transfer is not the final stage of a design. In all of the cases the patterns after being deposited on a sacrificial layer such as the photoresist or electron sensitive PMMA need to be immersed in chemical etchants that dispose of unwanted layers. This post processing includes two major types of chemical etchants and relies on the crystalline structure of the processed materials for correct and ordered disposal of the materials. In general there are two types of etching processes [37]:

1-Wet etching: material is immersed in the etchant solution and reactive layers dissolve

2-Dry etching: material is being exposed to sputtering and reactive gases for sublimation

During a wet etching process the dissolution may tackle the layers in an either isotropic or anisotropic manner. The isotropic dissolution creates so called “craters” or “edge

effects” under the mask in use whereas the anisotropic etching results in geometrically aligned sides (crystalline structure limits the dissolution) and hence can be used to create bridges between structures. Dry etching can be classified into three main classes termed as Reactive Ion Gas (RIE), Sputter etching and vapour phase etching. In RIE in brief the substrate is exposed to a mixture of chemical gases wherein a plasma spark produces ion masses that start reacting with substrate molecules. The mechanism of sputtering is rather similar to that sputter deposition with the difference in the substrate being “bombarded” by non-reactive ions. The etching parameters are quite similar to RIE in principle. Vapour phase etching is another dry etching method, which can be done with simpler equipment than what RIE requires. In this process the wafer to be etched is placed inside a chamber, in which one or more gases are introduced. The material to be etched is dissolved at the surface in a chemical reaction with the gas molecules. The two most common vapour phase etching technologies are silicon dioxide etching using hydrogen fluoride (HF) and silicon etching using xenon di-fluoride (XeF2), both of which are isotropic in nature [37]. Nano fabrication processes described earlier have all one goal in common and that of delivering an accurate enough a profile for the designed Nano-structures. If the design is requiring high accuracy pattern transfer then the process must also become subject to more steps and more phases in order to deliver the required level of accuracy in the pattern transfer. Below is a strip describing one application of a combination of charged particle (E-beam) pattern transfer and wet etching post processing with the aims of delivering arrays of Nano-scale gratings with circular aperture profiles. This work has been the experimental foundation of the current study and the aim as will be discussed in detail in the coming chapters, has been to fabricate small size (few 100 micron) surface area with grating patterns that are excitable by different wavelengths of visible portion of the electromagnetic spectrum. As much said as in this process, the overall excitation of the surface area under grating is more important than aperture design. This means that an overall uniformity of the apertures would be attempted whereas an exact circular pattern (with absolutely no deformity) is not a primary issue [37] (Figure 20).

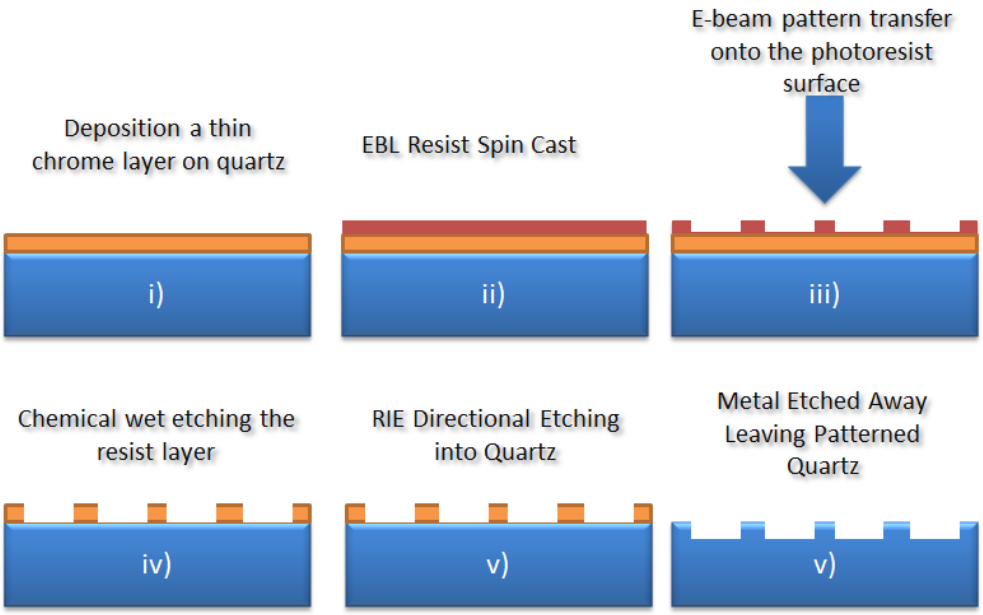

Figure 20. Schematic of fabrication process for arrays of nano grooves (nano holes)

Appendix II. Data field structure analysis for source entropy

Self-information

Each unit of information is considered a random variable with a measure of self-information. The self-information is defined through [38]:

$$i(A) = log_b\left(\frac{1}{P(A)}\right) = -log_b\left(P(A)\right) \qquad \textbf{A- 14}$$

The graphical depiction of self-information is given through:

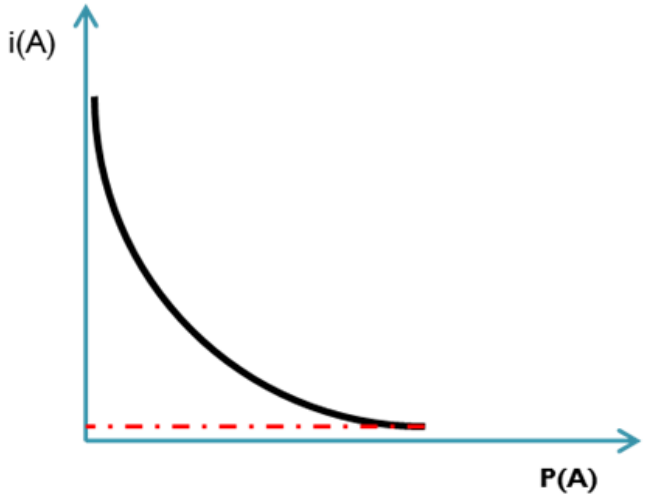

Figure 21 Diagram of self-information as a function of probability

Where P(*) denotes probability of the event * and the base of the logarithm induces a measure of representation that is related to the variation states of the random variable [27].

Source Entropy

Source is/can be depicted as a black box that outputs random variable sequences such as:

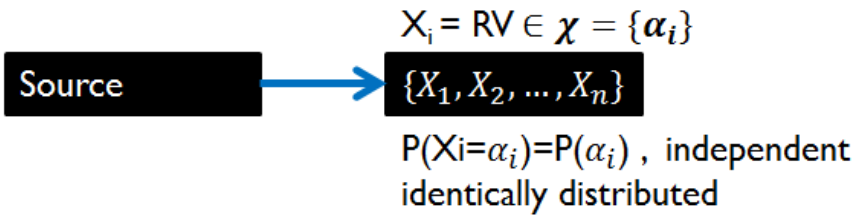

Figure 22 Source of information as a black box outputting sequences of random variables

Entropy is the average self-information of a random variable. In other words, the average self-information is the least amount of representable unit data carrier that we need to encode the given random variable ergo the source. It is given through [38]:

$$\mathbf{H} = \sum_i \boldsymbol{P}(\boldsymbol{X_i})\boldsymbol{i}(\boldsymbol{X_i}) \qquad \textbf{where} \quad \boldsymbol{i}(\boldsymbol{X}) = \boldsymbol{log_b}\left(\frac{\mathbf{1}}{\boldsymbol{P}(\boldsymbol{X})}\right) \qquad \textbf{A- 15}$$

Source encoding

Each source is being defined through its parameters. The source parameters (here in effect) for an ergodic source are:

1-source dimension given through:

$$X^N = \{X_1, \dots, X_N\} \qquad N \in \mathbb{I} \qquad \textbf{A- 16}$$

2- source alphabet defined via:

$$X \in A_x = \{\phi_1, \dots, \phi_n\} \quad n \in \mathbb{I} \qquad \textbf{A- 17}$$
$$\phi_i = unique\ symbols\ in\ A$$

3- source probability mass function which defines how frequently each of the symbols occur [27] [38]:

$$P=\begin{cases} P(\phi_1) = p_1 \\ P(\phi_2) = p_2 \\ \quad : \\ \quad . \\ P(\phi_n) = p_n \end{cases} \qquad \Sigma P_i = 1 \qquad \textbf{A- 18}$$

Source typical set

The typicality of the source relies on an infinite emission of symbols (or sequences of symbols) and the probability of occurrence of certain sequences being significantly higher than the others.

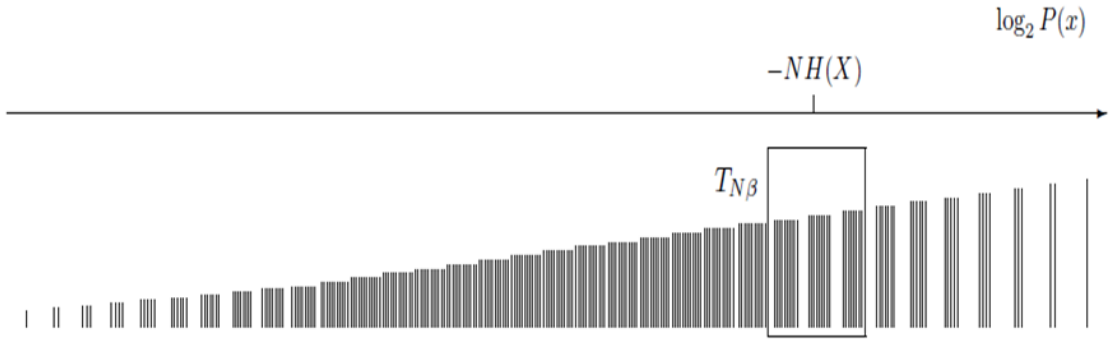

Figure 23 Depiction of the number of elements in a source typical set compared to total number of combinations emitted by the source

The source typical set is those sequences whose probability of occurrence is simply more than the rest of the space. These sequences form a set called the "Typical Set" and can be encoded though series of random variables hence can encode a whole source.

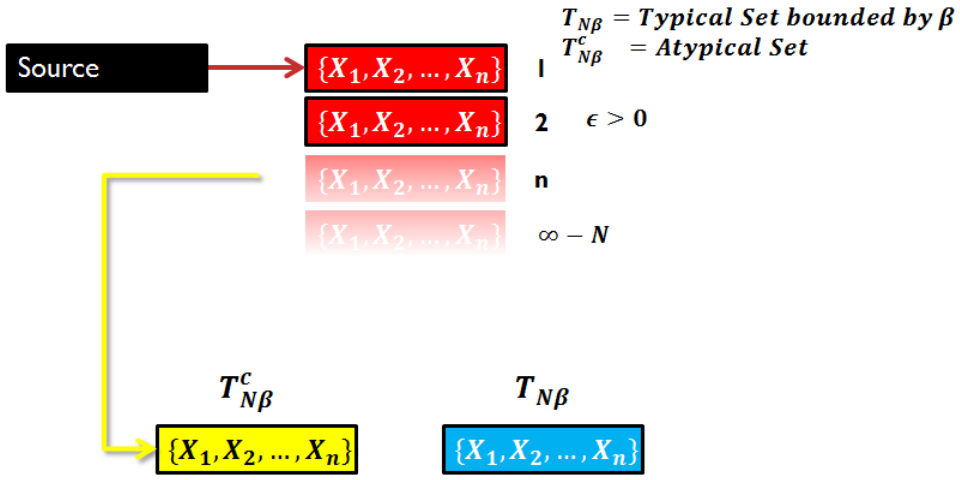

$$Pr\{X^N : X^N \in T_{N\beta}\} \leq 1 - \delta$$
$$\forall \delta \in [0\ 1]$$
$$if\ N \to +\infty\ \delta \to 0$$

Figure 24 The source's output are divided into two complementary set: the typical (blue) set and its complement (yellow); Typicality depends on how large the number of random variables in the emitted sequences get.

When a source begins emitting sequences of length N, as N increases the probability of the emitted sequence falls within a tighter boundary due to the typicality property. Amid the given explanation, a source total outcome will still contain sequences which are not typical and also have lower probability of occurrence yet if a code decides to encode only the typical sequences, if given an indexed order, the code can only encode the indices of the typical set which contains typical sequences and simply rule out other outcome possibilities. In a typical sequence there are n random variables following an iid process over the probability mass function of the source as follows [38] :

$$\mathbf{P(X)_{typ}} = P(X = x_1)P(X = x_2) \dots P(X = x_N) \simeq p_1^{Np_1} \dots p_n^{Np_n} \qquad \textbf{A- 19}$$

Where N is the number of random variables in a sequence and $P(X)_{TYP}$ is the probability of occurrence of a typical sequence. By assuming states of variations required to represent each symbol of the source to be 2, intuitively a log2 is the means to reveal the self-information content of the sequence hence taking a logarithm from either ends results in:

$$log_2\left(\frac{1}{P(\mathbf{X})_{typ}}\right) \simeq N\Sigma_{i=1}^{n} p_i log_2\left(\frac{1}{p_i}\right) \simeq NH(P) \qquad \textbf{A- 20}$$

consequently,

$$\frac{1}{N} log_2\left(\frac{1}{P(X)_{typ}}\right) \simeq H \rightarrow Shannon's\ entropy \qquad \textbf{A- 21}$$

And according to Shannon's theorem (A-20) can be re-written as (A-21) for any number beta>0:

$$\frac{1}{N} log_2\left(\frac{1}{P(X)_{typ}}\right) < H + \beta \qquad \beta > 0 \qquad \textbf{A- 22}$$

As a result, the set containing all of the sequences that satisfy (A-22), may be collectively represented through:

$$\mathbf{T}_{N\beta} = \left\{ x \in \Omega_{\mathbf{X}}^{\mathbf{N}} : \left| \frac{1}{N} log_2\left(\frac{1}{P(x)}\right) - H < \beta \right| \right\} \qquad \textbf{A- 23}$$

Ω_N^X = **set of all N-ary strings defined for random variable X.**

From (A-23) one can draw the following equation:

$$2^{-N(H+\beta)} < P(X)_{typ} < 2^{-N(H-\beta)} \qquad \textbf{A- 24}$$

The above equation can be further expanded to:

A- 25

$$\left|\mathrm{T}_{N\beta}\right| < 2^{(N(H+\beta))} \rightarrow \textit{there are up to } 2^{N(H+\beta)} \textit{ strings in } \mathrm{T}_{N\beta}$$

By assuming a random variable that can take on to more than 2 states of variations such as b states the equation (A-25) falls into the following form for b>2 :

A- 26

$$2^{-N(H+\beta)} < P(X)_{typ} < 2^{-N(H-\beta)}$$

$$\left|\mathrm{T}_{N\beta}\right| < 2^{(N(H+\beta))}$$

$$\mathrm{H_b} = \sum_i P(X_i) log_b\left(\frac{1}{P(X)}\right)$$

$$\mathrm{H_b(x)} = log_b(a)\, H_a(x)$$

Hence equation (A-26) takes the form of:

A- 27

$$\forall b > 2 \rightarrow H_b(x) = \left(\frac{1}{log_2 b}\right) H_2(x), \quad \{0 < \alpha < 1\}$$

$$\therefore$$

$$2^{-N(\alpha H+\beta)} < P(X)_{typ} < 2^{-N(\alpha H-\beta)}$$

$$\left|\mathrm{T}_{N\beta}\right| < 2^{(N(\alpha H+\beta))}$$

And as conclusion, an encoding variable with more than two states of variation can decrease the bitrate required for encoding a source of N unique alphabets.

Appendix II. Grating Angular Dispersion Analysis

For in-plane diffraction, the diffraction grating is described through the grating equation:

A- 28

$$m\lambda = d(\sin(\alpha) + \sin(\beta))$$

where parameters alpha and beta are the angles of incidence and diffraction respectively and m is the order of diffraction along with d being the grating periodicity. For calculation of how well the grating disperses an incident light or to measure the grating's angular dispersion, with considerations for fixed parameters (here the angle of incidence) a derivative of (A-28) with respect to the incident wavelength will result in:

A- 29

$$D = \frac{\partial \beta}{\partial \lambda} = \frac{m}{d\cos\beta} = \frac{m}{d}\sec\beta$$

Where quantity D is dimensionless and deems to show the amount of change of the diffraction angle between a wavelength and a slightly different one. By replacing the diffraction angle in (A-29) with (A-28) solved for β, we come across the following (m=1):

$$1-\ D = \frac{1}{d}\frac{1}{cos\beta} = \frac{G}{cos\beta}\ ; G = \frac{1}{d}$$

$$2-\ = \frac{G}{\cos\left(\sin^{-1}\left(\frac{\lambda}{d} - c\right)\right)}\ ; c = \sin(\alpha)$$

$$3-\ = \frac{G}{\sqrt{1-\left(\frac{\lambda}{d}\right)^2 + \frac{2\lambda}{d}c - c^2}} = \frac{G}{\sqrt{1-(G\lambda)^2 + 2G\lambda c - c^2}}$$

$$4-\ = \frac{1}{\sqrt{\frac{1}{G^2} - \lambda^2 + \frac{2\lambda}{G}c - \left(\frac{c}{G}\right)^2}}$$

$$5-\ = \frac{1}{\sqrt{\frac{1}{G^2} - \left(\lambda - \frac{c}{G}\right)^2}} = \frac{1}{\sqrt{\left(\frac{1}{G} + \lambda - \frac{c}{G}\right)\left(\frac{1}{G} - \lambda + \frac{c}{G}\right)}}$$

$$6-\ = \frac{1}{\sqrt{\left(\frac{1-c}{G} + \lambda\right)\left(\frac{1+c}{G} - \lambda\right)}}$$

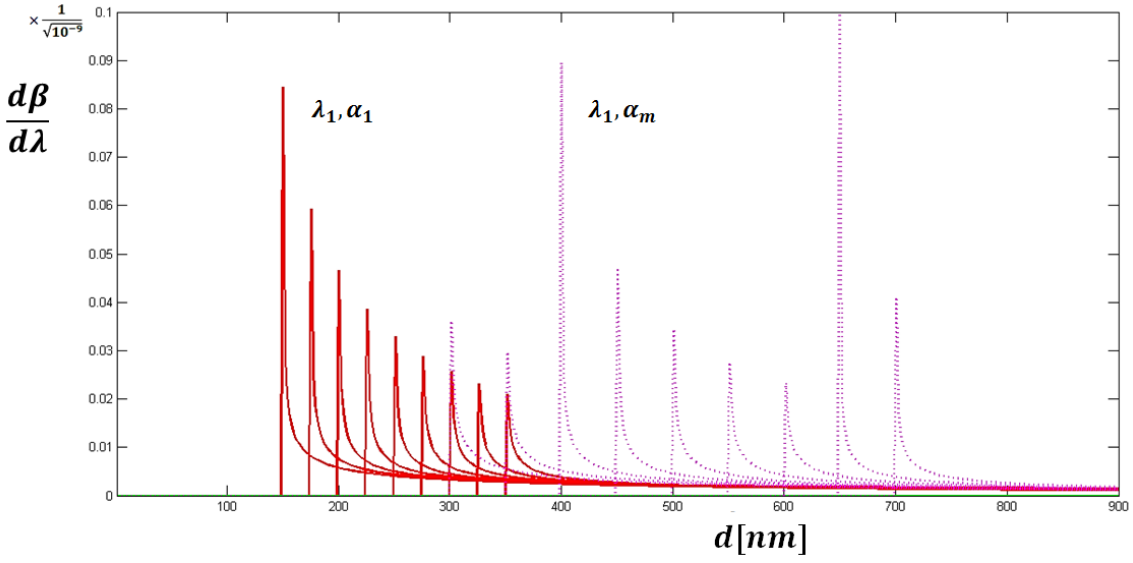

Figure 25 Graphing A-2 3 (6) shows the effect of changes in angle of incidence and wave length as a function of grating periodicity

And further choices for the optimal dispersion (angular dispersion) made clear on the graphs:

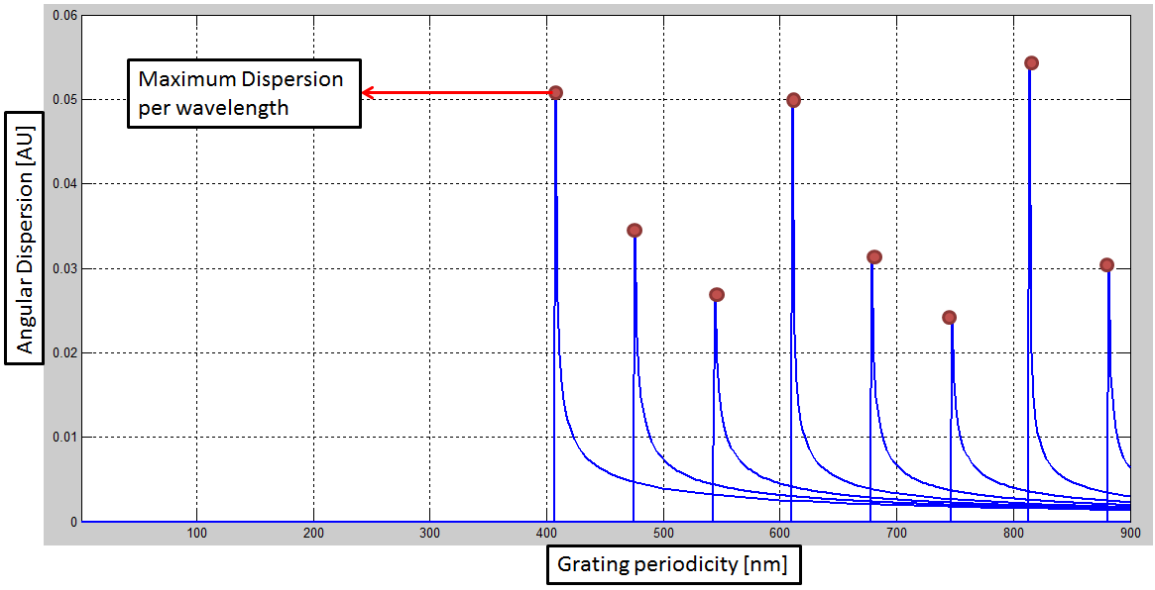

Figure 26 The Grating periodicities chosen based on optimal angular dispersion through equation A-2 3(6)

Appendix III. Nano-Array Design Software

The array design software performs in the following steps as shown in the block diagram.

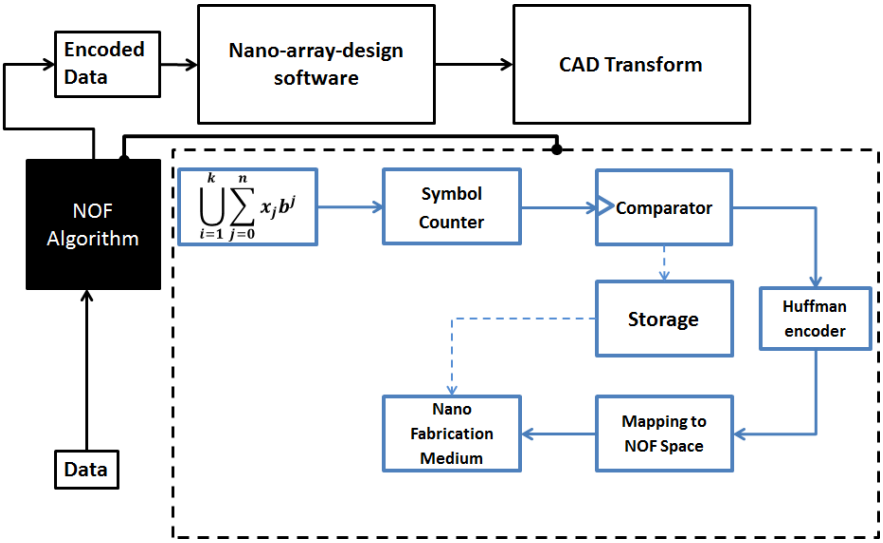

Figure 27 System design block diagram of NOF encoding scheme

Following block diagrams show the general structure of the software algorithm. Due to publication limits the details of the given block diagram cannot be published. The list of variables used in the diagram is as follows:

BL=Block Structure

G=Global Variable

COM=Comparison and decision making

MAIN=Main Function

DIR=File Directory

PTH=Path;FNAME=FileName;FBRW=FileBrowse;PrioX=PriorityX;UGTG=Get(file) Commands

O=Output

HDD=Hard Disk(Storage)

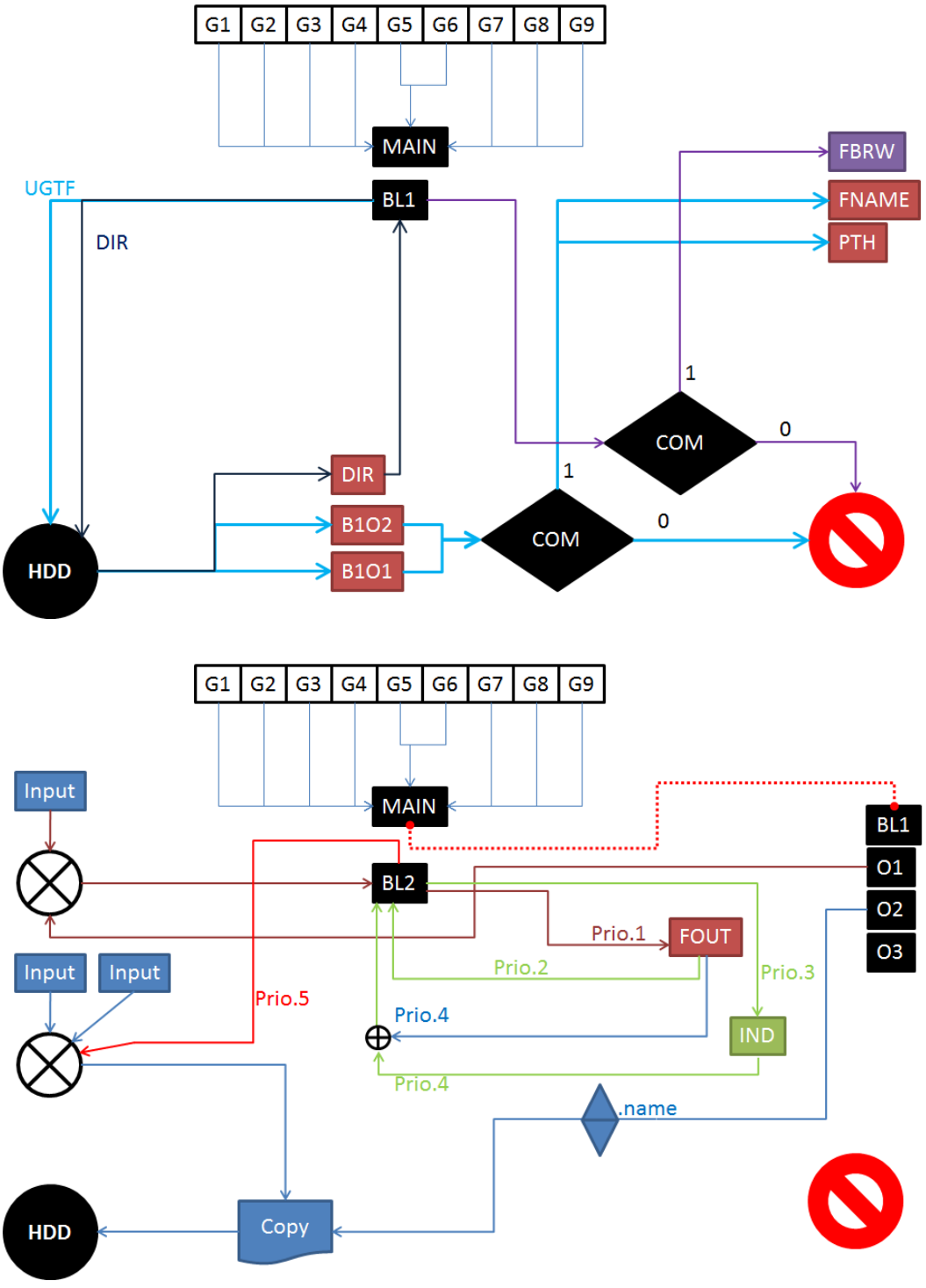

Figure 28 Nano-Array Design Software Schematic Diagram for Top)-GDSII file header generation and Bottom)-GDSII file main structure generation

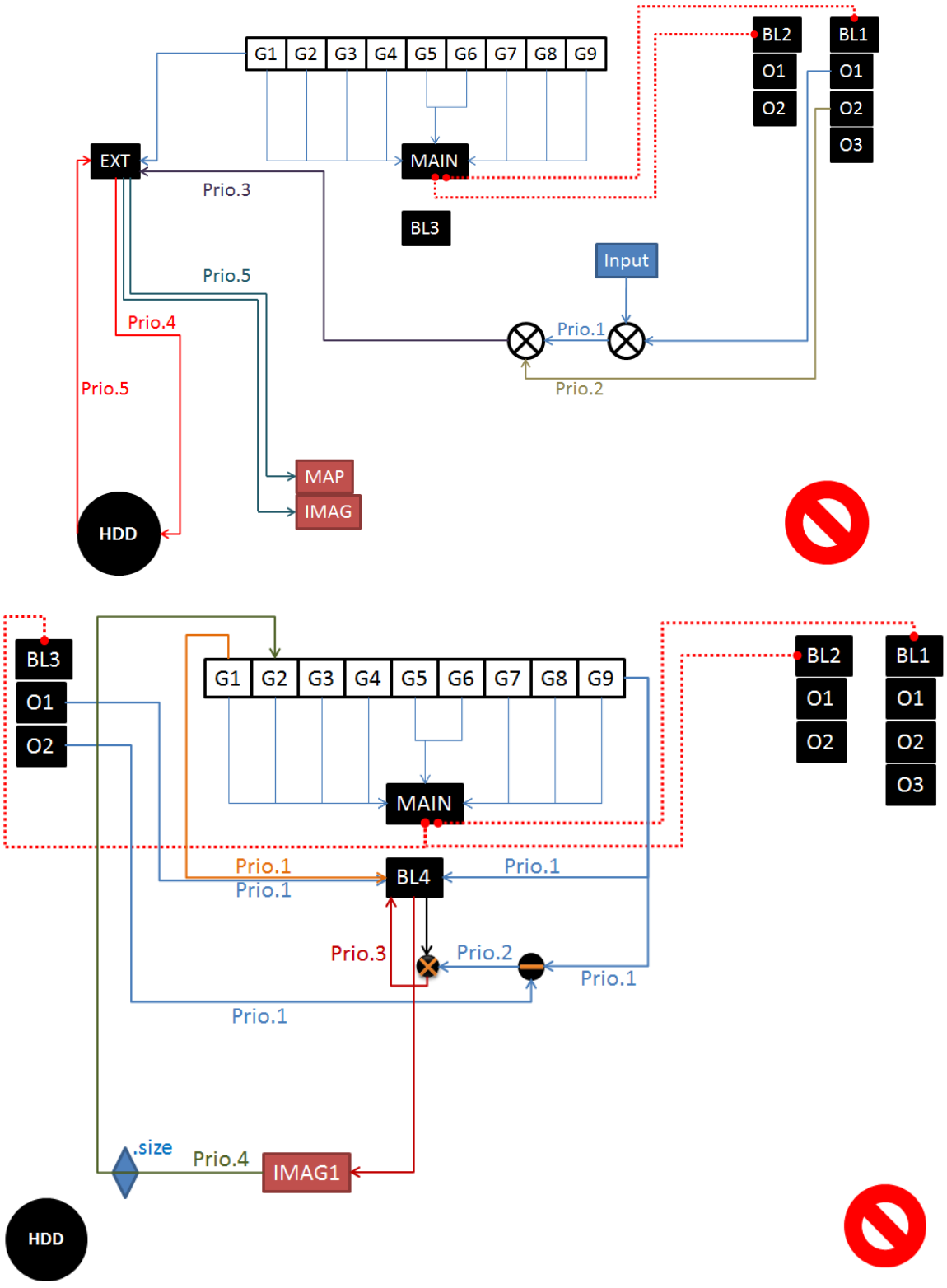

Figure 29 Schematic block diagram of Nano-Array design software for Top)-GDSII file periodicity attribution and Bottom)- CAD-Compatible image writing

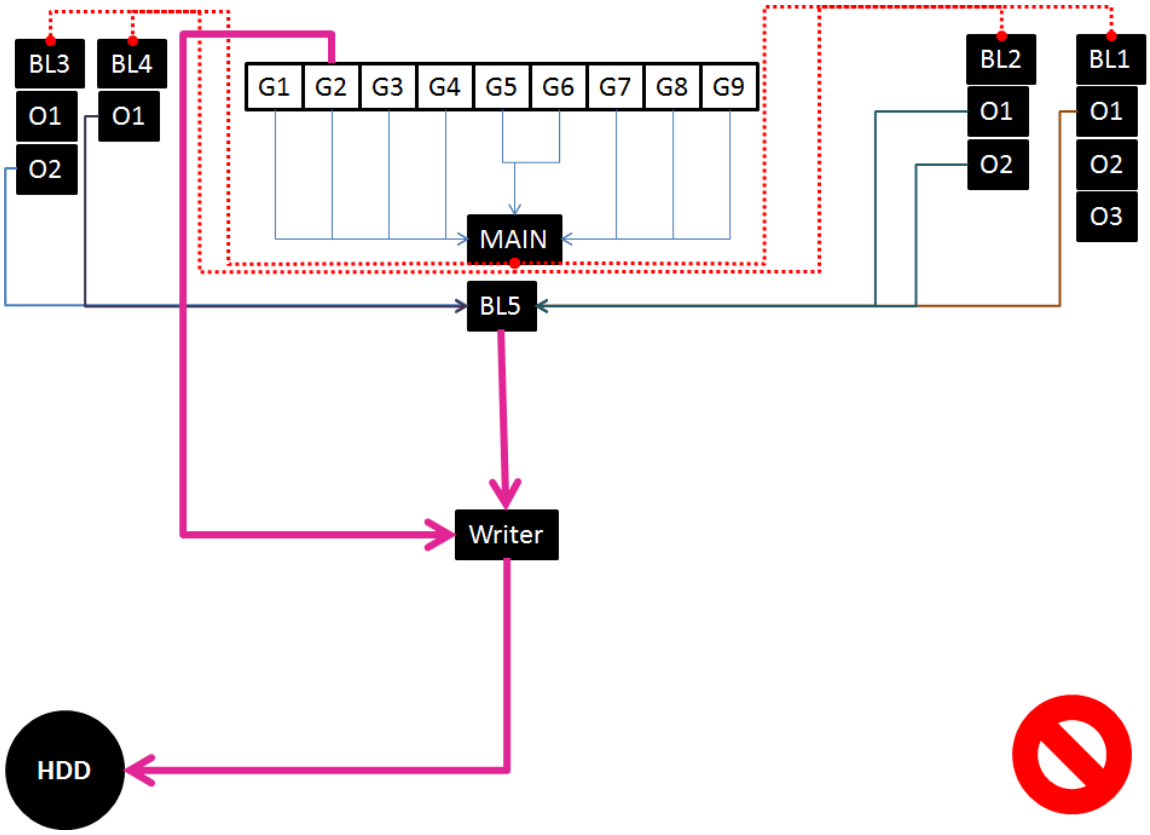

Figure 30 Closed-from schematic block diagram of the Nano-Array design software for generation of CAD-Compatible file formats (GDSII) for EBL Nano-fabrication systems

Appendix IV. Overall Comparison of Applied Lossy Compression Algorithms

- **DCT (Discrete Cosine Transform)**

As to the fact that for every compressor module there is a likelihood of a transmission setup ready to transmit the compressed data, multiple attempts have been made to decrease the bitrate and consequently modulation bit error rate of a data stream, outputted from the algorithm and into the transmitting channel. The Discrete cosine transform has the ability to (similar to wavelet transform) decompose an image into frequency components being uncorrelated. Frequency correlation or autocorrelation is in fact a sign of inter-value data redundancies, which in an image, is the main contributor to the size of the data presented in the output matrix. By applying a DCT to an image matrix with inter-related data values (entries), one can decompose (de-correlate) the pixel values into frequency based cosine wave forms which due to the nature of the transform will get assembled from low to high (base to least). As a known fact in image processing, human brain is more sensitive towards the low-frequency visual data rather than high frequencies and also consequently removal of many high frequency components of the de-correlated image allows for reconstruction of those components which have the least amount of spatial correlation without losing an overall visual integrity of the data. The DCT in two-dimensions is calculated through:

A- 31

$$C(u,v) = \alpha(u)\alpha(v)\sum_{x=0}^{N-1}\sum_{y=0}^{N-1} f(x,y)\cos\left[\frac{\pi(2x+1)u}{2N}\right]\cos\left[\frac{\pi(2y+1)v}{2N}\right]$$

$$\mathrm{f}(x,y) = \sum_{u=0}^{N-1}\sum_{v=0}^{N-1}\alpha(u)\alpha(v)C(u,v)\cos\left[\frac{\pi(2x+1)u}{2N}\right]\cos\left[\frac{\pi(2y+1)v}{2N}\right]$$

$$\alpha(u) = \begin{cases}\sqrt{\frac{1}{N}} & for\ u = 0\\ \sqrt{\frac{2}{N}} & for\ u \neq 0\end{cases} \qquad \alpha(v) = \begin{cases}\sqrt{\frac{1}{N}} & for\ v = 0\\ \sqrt{\frac{2}{N}} & for\ v \neq 0\end{cases}$$

for x,y=0,1,2,…,N-1

Below are the graphs for image compression trials ran through a discrete cosine transform module and being compared regarding psycho-visual quality, Mean Squared Error and Peak signal to noise ratio between the original and the compressed image.

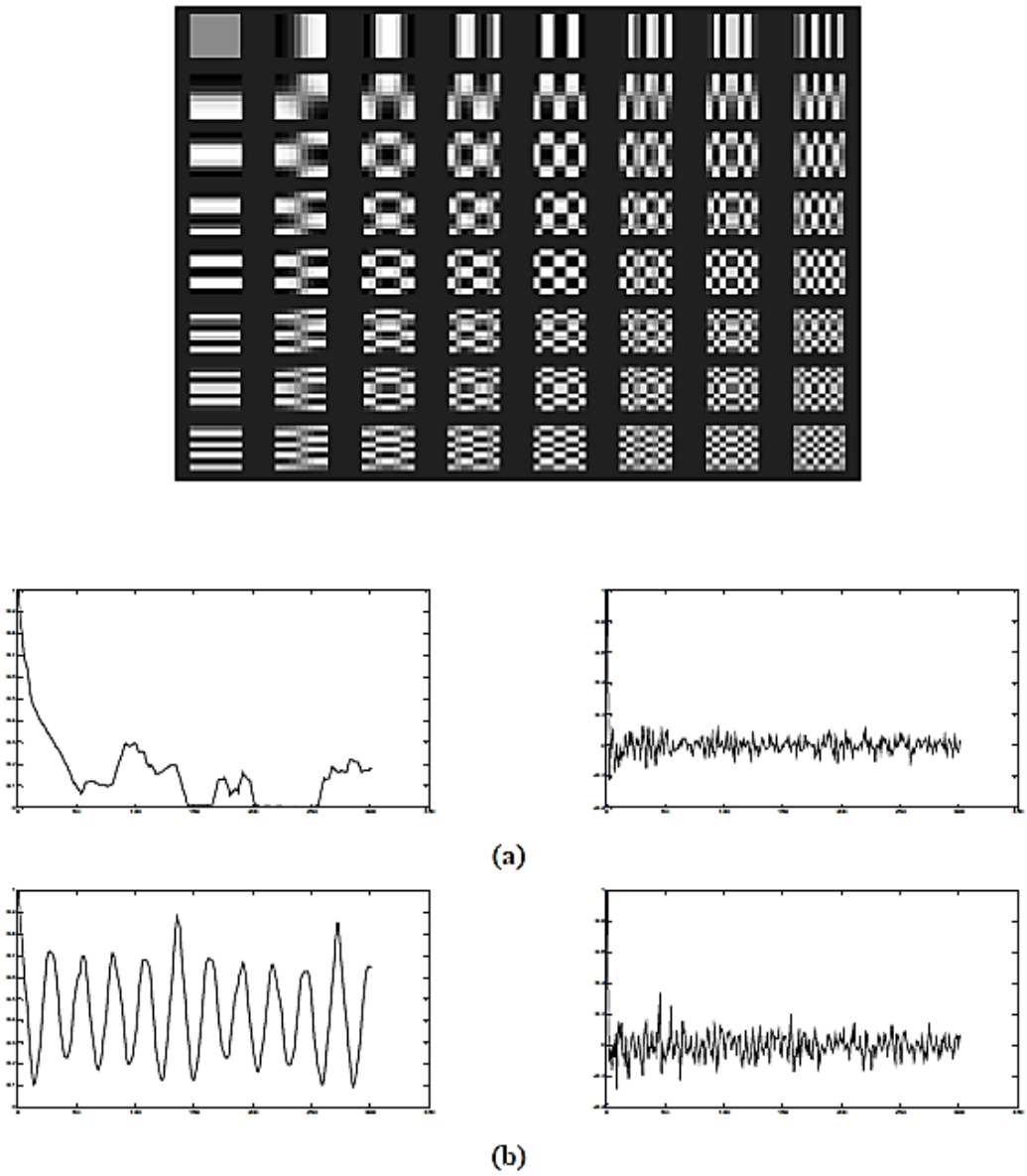

Figure 31 Top)- A 2D DCT coefficient matrix with directional DCT-wavelet distribution bottom)-a) An image scanline before(left) and after dct transform(right) b)Autocorrelation diagram of the image scanline before(left) and after dct transform (right);

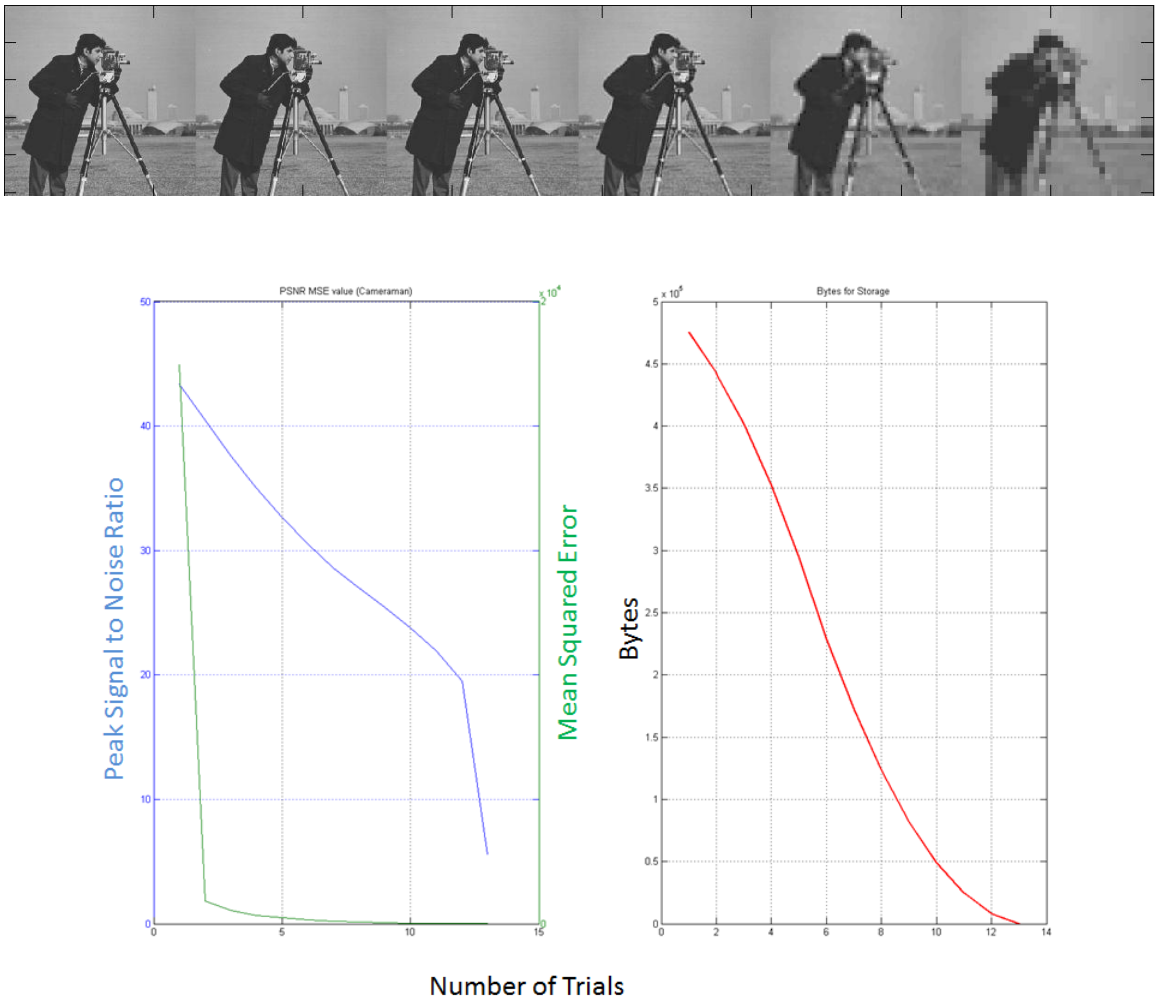

Figure 32 Top)- Psycho-Visual degradation of the image "Camera Man" as a function of decreasing non-zero DCT coefficients; Bottom)- Variation of The Peak Signal to Noise Ration and Mean Squared Error for trials differing in the number of non-zero DCT coefficients (left) Storage size of the DCT coefficients in Bytes (right)

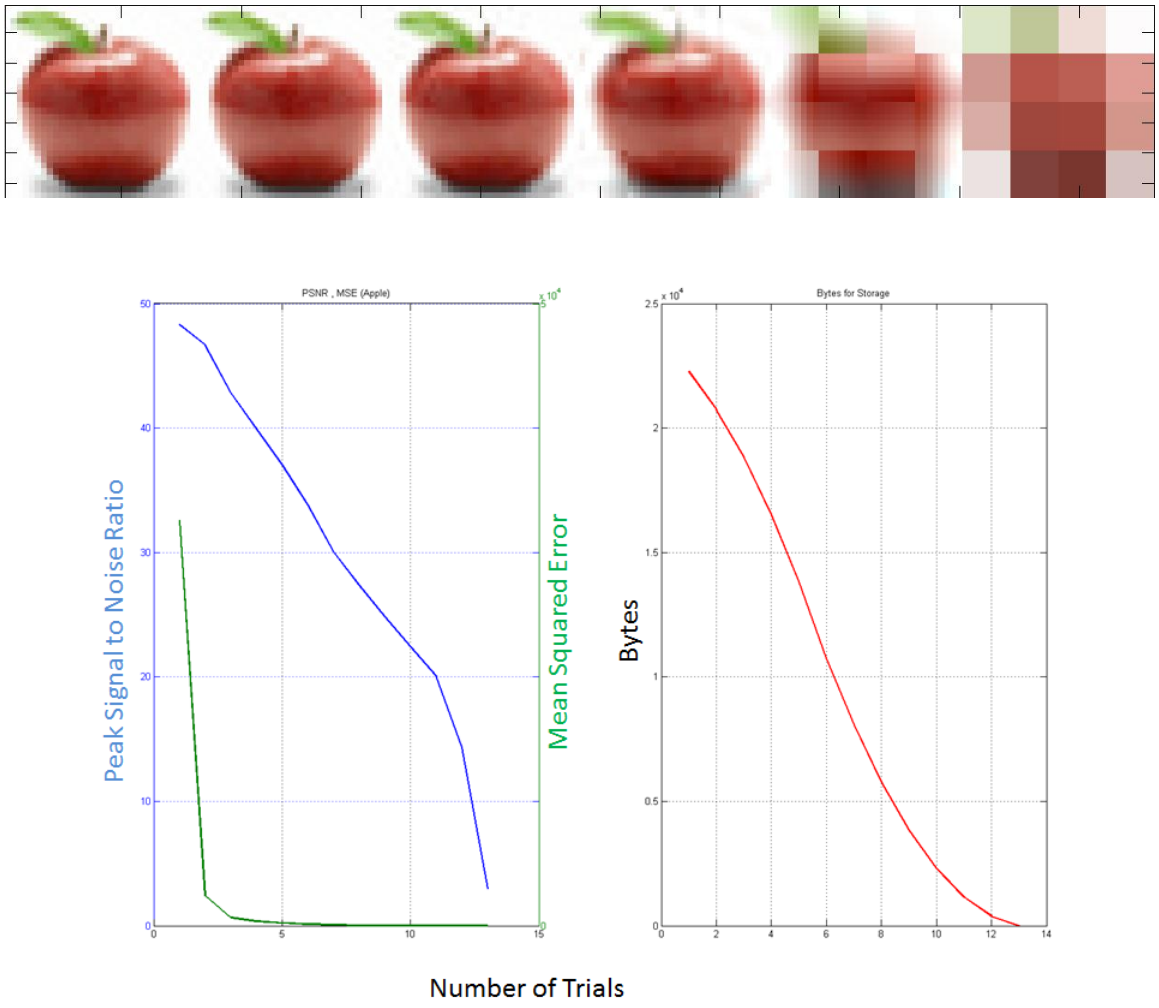

Figure 33 Top)- Psycho-Visual degradation of the image "Apple" as a function of decreasing non-zero DCT coefficients; Bottom)- Variation of The Peak Signal to Noise Ration and Mean Squared Error for trials differing in the number of non-zero DCT coefficients; (left) Storage size of the DCT coefficients in Bytes (right)

- ## Wavelet Transform

The main disadvantage of Fourier Transform is the lack of time lags for a transformed signal. As to the matter that any signal that has been analyzed through an FFT (Fast Fourier Transform) module can mainly remain intact or undergo a total loss if the lowpass of highpass filtering results in loss of visually important yet high energy data in the image. The most recent mathematical solution to this problem has been the wavelet transform. In brief a wavelet transform, similar to a Fourier Transform takes the image (or data) into the frequency domain with the slight difference that what it outputs is localized both in frequency and time due to an scaling factor that is calculated as a result of averaging the entries in a particular window and a translation factor that is calculated due to altering the length of the window that scans the signal. The combination of the two brings about a collection of temporal frequency scattering of a signal in the wavelet space. The resulting small functions that interact with each window (interval) of the signal are called wavelets and they must have certain mathematical characteristics in order to be invertible. These properties in brief are: 1) Admissibility and 2) Regularity. To achieve an invertible wavelet transform coefficient matrix one must perform the admissibility check which imposes that the Fourier transform of the signal must be zero at zero frequency.

A- 32

$$\gamma(S,\tau) = \int f(t)\psi^*_{S,\tau}(t)dt$$

$$f(t) = \int\int \gamma(S,\tau)\psi_{S,\tau}(t)d\tau dS$$

Where γ(S,T) is the wavelet transform of the data, ψ_{ST} is the wavelet notion and S, T are Scaling and Translation of the signal.

A- 33

$$\int \frac{|\psi(\omega)|^2}{|\omega|} d\omega < \infty$$

$$|\psi(\omega)|^2_{\omega=0} = 0$$

Ψ(ω) is the Fourier transform of the wavelet and must be zero at ω=0 for a fast decay of the wavelet approximating moments. The wavelet expansion at t=0 and for zero translation (τ=0) yields:

A- 34

$$\gamma(S,0) = \frac{1}{\sqrt{S}}\left[\sum_{p=0}^{N} f^{(p)}(0)\int \frac{t^p}{p!}\psi\left(\frac{t}{S}\right)dt \; + O(n+1)\right]$$

Where f^p denotes the pth derivative of the scalar function f and O(n+1) denotes the rest of the series (Taylor) expansion of the wavelet transform.

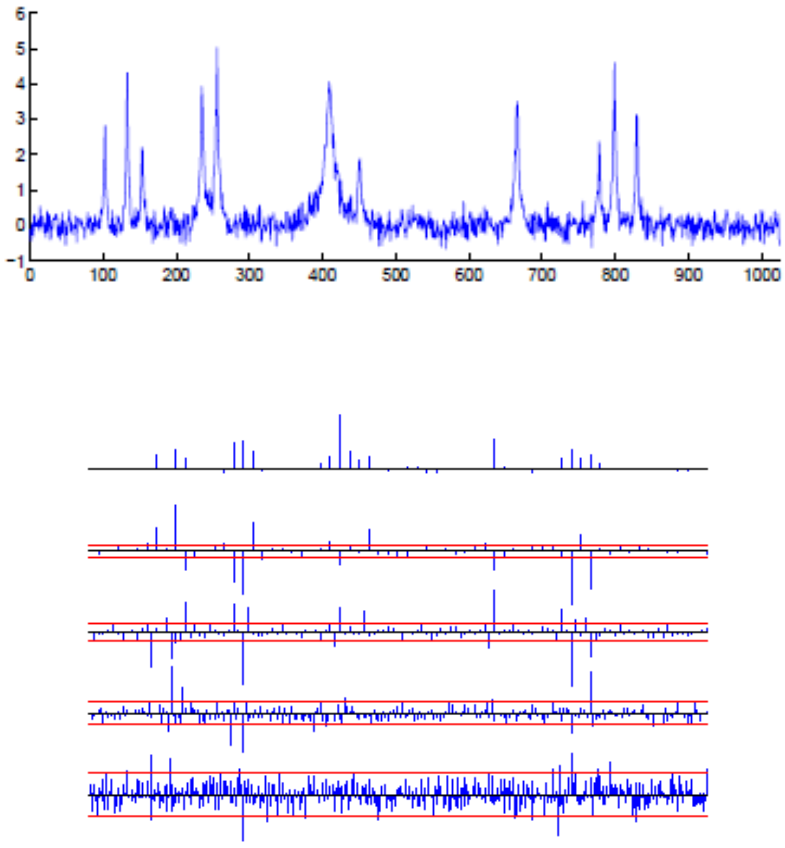

Figure 34 Top)- Noisy sharp impulses embedded in the noise spectrum bottom)- Wavelet decomposition of the signal. The first line is the noisy sub-band of the original signal.

Below are the Means squared error, peak signal to noise ratio and psycho-visual depiction of two images using wavelet transform:

Figure 35 Top)-Psycho-Visual depiction of the reconstructed image using hard-thresholding Bi-orthogonal 1.1 wavelet bases. The arrows show the position of each image on the PSNR (Peak Signal to Noise Ratio) curve for image (Cameraman)

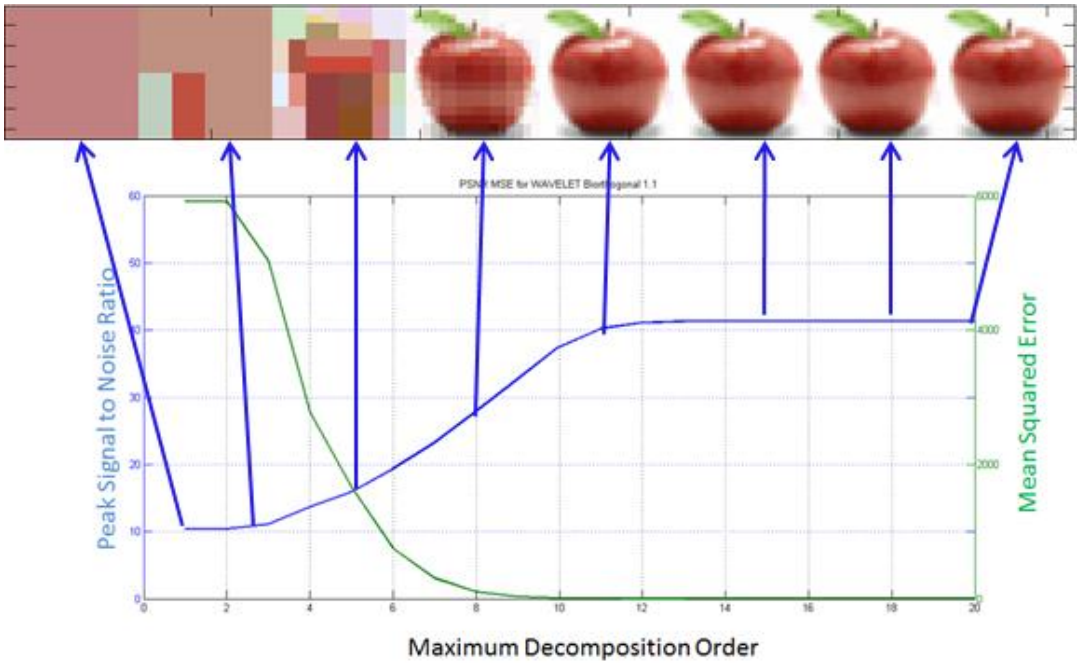

Figure 36 Top)-Psycho-Visual depiction of the reconstructed image using hard-thresholding Bi-orthogonal 1.1 wavelet bases. The arrows show the position of each image on the PSNR (Peak Signal to Noise Ratio) curve for image (Apple)

Appendix V. Deriving A Complex Angle of Incidence for Angular Dispersion

There could be assumed a special case where the changes of dispersion quantity relies only and only on the incident wavelength and the grating periodicity with the angle of diffraction effect being suppressed, this happens under certain conditions for the choice of the incidence angle in which the value chosen becomes complex. The graph in Figure 37 shows an investigation of the aforementioned conditions.

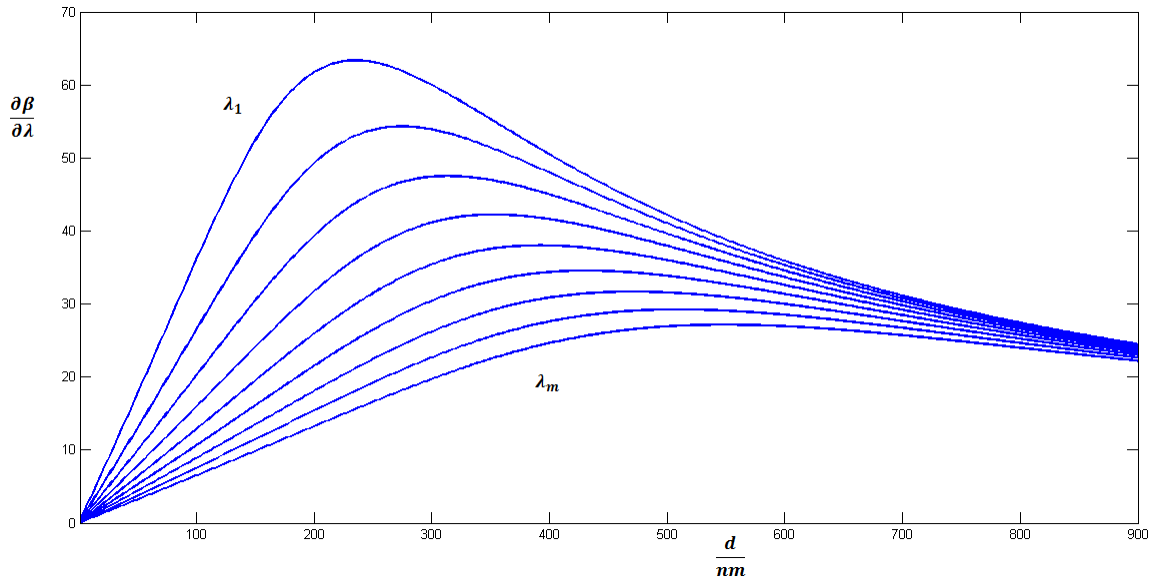

Figure 37 Effect of a complex angle of incidence on the angular resolution (dispersion power) of the grating

This condition is produced through transformation of (A-2 3) into the following equation:

A- 35

$$\frac{1}{\sqrt{\left(\frac{1+j}{G}+\lambda\right)\left(\frac{1-j}{G}-\lambda\right)}}$$

The condition for producing a complex angle of incidence requires complex analysis of the incidence medium and due to presence of a phase (imaginary component) in the equation; one must define physical properties with multiple layer structure and different indices of refraction to achieve a complex angle of incidence. We denote the advantage of using what shown in Figure 37 is a more controllable partial change for the angular

dispersion quantity with respect to the increasing grating periodicity and incident wavelengths. Another approach to understanding complex angles of incidence is through the definition of wave solution through space and at the interfaces. As mentioned in [13] complex angles of incidence can be well associated with inhomogeneous primary waves. It can be shown that in general cylindrical and spherical waves can be represented as a superposition of plane waves with complex directional cosine values, hence complex angles of incidence. Using Euler's formula one can derive a complex value for the term sin(x) in the grating equation:

A- 36

$$e^{jx} = \cos(x) + jsin(x)$$

$$\sin(\alpha) = \frac{1}{j}\left(e^{j\alpha} - \cos(\alpha)\right)$$

Hence:

A- 37

$$1 - \sin(\alpha) = 1 - \frac{1}{j}\left(e^{j\alpha} - \cos(\alpha)\right) \equiv 1 + j\left(e^{j\alpha} - \cos(\alpha)\right)$$

For the sake of simplicity in analysis does one try to rid the equation from the exponential term they would come across a complex angle of incidence as follows:

A- 38

$$e^{j\alpha} - \cos(\alpha) = 1 \;\Rightarrow\; \alpha = \cos^{-1}(e^{j\alpha} - 1)$$

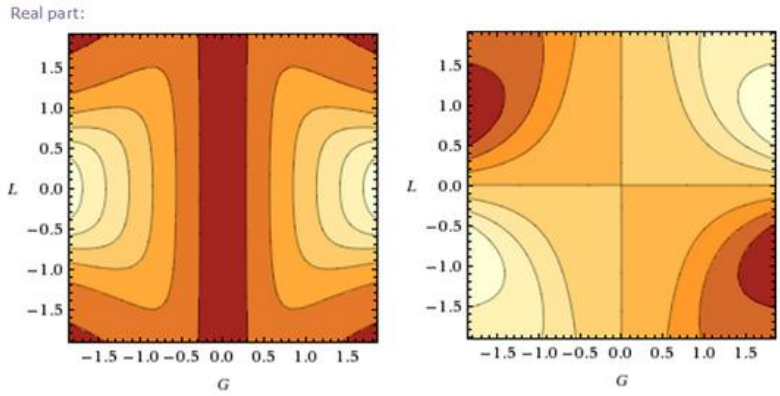

Figure 38. Contour diagrams showing the real and imaginary field distribution of a grating with complex angles of incidence.

In theory such angle of incidence gives rise to a complex field distribution which its physical interpretation and implementation is outside the scope of the current work.

Appendix VI. Encoding Definition via Set Theory and Boolean Logic

The fundamentals of digital data encoding are not that different from the mathematical definition of bijective functions. The mentioned methods in 2.3 transfer the values of the input data from the analog domain into the binary frame of digital domain. Such transform, assigns a binary value to the measured signal sample at the input of the encoder. This transform before being perceived by the machine logic, is usually a voltage or current measurement which is considered to be a continuous real-valued sampling which also stores the quantified continuous value of the real signal within a discrete storage medium. The dimensions of the stored signal (data segment) are (due to Nyquist Sampling Theorem) less than dimension of the real-valued data unless the data itself is in discrete values. The key target of this section is to prove through mathematical derivation that for discrete numerical values it is possible to reduce the number of digital domain unit data carriers through use of higher states of variation for a single digital information unit. We will begin the investigation by having two sets which represent the original and the encoded data respectively. In this example we choose the original set of information to contain quantifications or numerical values which historically tend to be universal among all systems. The set X is the set of all positive integers. This set can be labeled as the upper half of the natural numbers including the quantity for non-existent zero. We argue that if a system tends to encode this original set into a secondary or target set Y, this mapping should allow for existence of equivalent number of encoders hence both the original set and the encoded set have same number of elements or same cardinality. This proof shows that what does it mean to encode a set of data through logical and mathematical approaches with the goal of using the proof to argue benefits of the presented work. Any storage of data is a mathematical concept that can be best described through the set theory. The depiction of the data set to be stored and the stored data set can in general form take the analogy of two sets X and Y respectively where all elements of X are mapped onto the elements of set Y through function f. in order for f to satisfy mapping conditions there are four preconditions to be met:

1. Each element of X must be paired with at least one element of Y,
2. No element of X may be paired with more than one element of Y,
3. Each element of Y must be paired with at least one element of X, and
4. No element of Y may be paired with more than one element of X

In order to have a reversible mapping between the original data field and the stored data field the function that maps elements of X onto Y requires to be bijective meaning it must hold on to all of the given preconditions. When so, the domain of f can be regarded as the original data and its range can be regarded as the stored data.

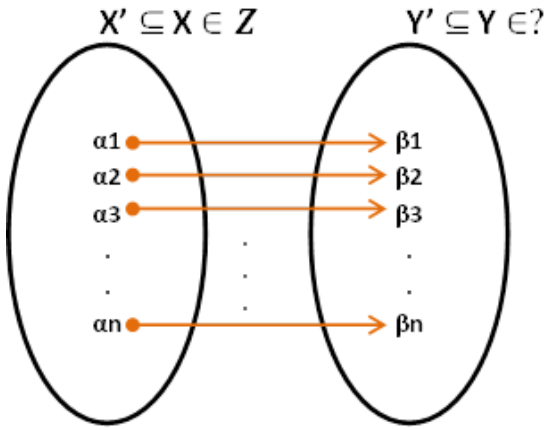

Figure 39 A bijection relationship between an initial set and a target set with ambiguous counting bases

It is important for the two sets to have similar number of elements or cardinality in order to be paired otherwise the two sets will have either an injective or surjective relationship. Having either of the latterly mentioned relationships discards the possibility of reverse mapping the stored data and hence recovering the data from storage set. The nature of the original data field is usually best described with set of natural numbers or upper fraction of the set of integers. Through mathematical reasoning we can see how a system of storing data can be linked with the base counting system [39]. If X is the set of integers hence having a cardinality of N_0 then if X requires being stored, a secondary set such as Y shall be present with cardinality N_α where there exists a relationship between the sets through function f such that f satisfies the following preconditions [39]:

1) f maps every element of X into at least an element of Y hence:

A- 39

$$f: X \to Y$$

2) f maps each element of X to exactly one element of Y and not more

A- 40

$$f: X \to Y \mid X_{i=k} \to Y_{i=k}$$

3) There exists an inverse function f^{-1} such that:

A- 41

$$f^{-1}: Y \to X$$

4) f^{-1} maps each element of Y back to exactly one element of X

A- 42

$$f^{-1}: Y \to X \mid Y_{i=k} \to X_{i=k}$$

Through such system if the chosen data field is a subset of the original set X such that:

A- 43

$$\forall\, X'_i \in X' \text{ then } X'_i \in X$$

and we choose function f with the prescribed attributes to map X' onto the target set Y' where Y' is a subset of the target field Y such that:

A- 44

$$\forall\, Y'_i \in X' \text{ then } Y'_i \in Y$$

$$\aleph_{X'} = \aleph_{Y'}$$

(A-44) clearly indicates that cardinality ***N*** (number of elements of the sets) must be equal and this means that there must be equivalent amount of elements within both sets in order for f to be able to map them back and forth [39]. The computer sciences model the unit information carrier as one bit which is also in a Boolean logic framework. There are quantities of unit information carriers in a machine arithmetic model where each transition between variables follows a true/false state and as a result each function that receives and transmits a single state of true or false also is a Boolean function. The particularity of Boolean algebra is based on having full arithmetic qualities alongside its bi-state initial set. The aforementioned property of Boolean algebra and Boolean functions makes its arithmetic space (set of all bi-element sets and all functions operating on them) a suitable space for storing information using only two elements of a given set. Because a logic set having only two distinct possibilities (e.g. true or false) is easy to replicate in a physical sense (e.g. on/off, current/no current, voltage / no voltage) it seems intuitive for function f mentioned in (A-39) through (A-44) to be a Boolean function [39]. For understanding the significance of Boolean nature of function f it is also necessary to understand the representation of numbers in the set of data to be stored X'. X' is a subset of X which in our analysis is the set of upper fraction of the integers and has an infinite cardinality N_0. The mathematical representation of any element of X' will have the general form [39]:

A- 45

$$K = \iota(d_{n\_1})b^{n-1} + \iota(d_{n\_2})b^{n-2} + \cdots + \iota(d_1)b^1 + \iota(d_0)b^0$$

$$d_i = \{D_0, \ldots, D_{b\_1}\}$$
$$b = \{2,3, \ldots, N\}$$
$$D_i = Unique\ Integer\ Symbol$$
$$\iota = Rank\ of\ digit\ d_i$$

If d_i is considered to expand the numerals to an unknown base b then :

A- 46

$$d_i = [0,1,2,\dots,b-1]$$

And the largest n-digit number to be represented by this system is:

A- 47

$$[b-1][b-1]\dots[b-1] = (b-1)b^{n-1} + \dots + (b-1) = (b-1)^{\frac{b^n-1}{b-1}} = b^n - 1$$

As to the fact that physical representation of elements of the target set Y' are chosen to be of bi-element nature (Belonging to the set {0,1}) and having the constraint of bijection for any function f that maps between the two sets, each element of X' and Y' shall have a relationship where [39] :

A- 48

$$\boldsymbol{\alpha_i = \sum_{i=1}^{n-1} \iota(d_i) b^i \quad : \rightarrow \beta_i = \sum_{i=1}^{m-1} \iota(\hat{d}_i)\hat{b}^i}$$

The relationship between α and β can be found through modular arithmetic [39]:

A- 49

$$\boldsymbol{\alpha_i = \{d_i, b\} \,\&\, \beta_i = \{\hat{d}_i, \hat{b}\} \mid d_i = \bar{A}_i = \{\delta : \delta \equiv A_i (mod\ \hat{b})\} \forall\ \delta, \hat{\delta} \in \mathbb{Z}^+}$$
$$\boldsymbol{\hat{d}_i = \bar{B}_i = \{\hat{\delta} : \hat{\delta} \equiv A_i (mod\ \hat{b})\}}$$

Sets *A_bar* and *B_bar* are the congruent classes of elements α_i and β_i where depending on the divisor b and *b_hat*, the number of unique elements to be represented will be defined. Hence for set X' b=10 and if the goal is to have a logical function to act on α_i then *b_hat*=2. f will have to act on a Boolean domain whereas the set X' is not a Boolean domain. f requires then to be first acting on the Natural domain and next on a logical (Boolean) domain:

A- 50

$$f: \begin{cases} f' & X' \in N \\ f'' & X'' \in \{0,1\}^n \end{cases}$$

In order for f to map from one set to another there has to be a relationship between X' and X'' such as: $X' \Leftrightarrow X''$ hence (A-50) should be rewritten in the form of:

A- 51

$$f: \begin{cases} f' & X' \in N \\ \hookrightarrow \; f'' & X'' \in \{0,1\}^n \end{cases}$$

and $X' \Leftrightarrow X''$ will be described through (A-51). Furthermore there will be a Boolean equivalent of f through the following transformation which will map each element of X' to Y' ∈ {0,1} if and only if [40]:

A- 52

$$\boldsymbol{a} = (\psi^n)^{-1}\, \boldsymbol{Y}$$

$\boldsymbol{a}$ = Zhegalkin Coefficients

$(\psi^n)^{-1}$ = inverse Normal Transform matrix

$Y = f''(x_1,\ldots,x_n)$ = truth variables of Boolean function f''

$$\psi^n = \begin{pmatrix} \psi^{n-1} & 0 \\ \psi^{n-1} & \psi^{n-1} \end{pmatrix}$$

For (A-52) to hold true, the following must hold true as to the fact that Y∈{0,1}:

1) $a^2 \rightarrow a$
2) $a + a = 0$

And the latterly mentioned 1- and 2- will hold true if and only if $\hat{b}$ =2 henceforth f'' is a Boolean function. As for the cardinality of the sets X' and Y' one can deduce the following relationship best described in Figure 40:

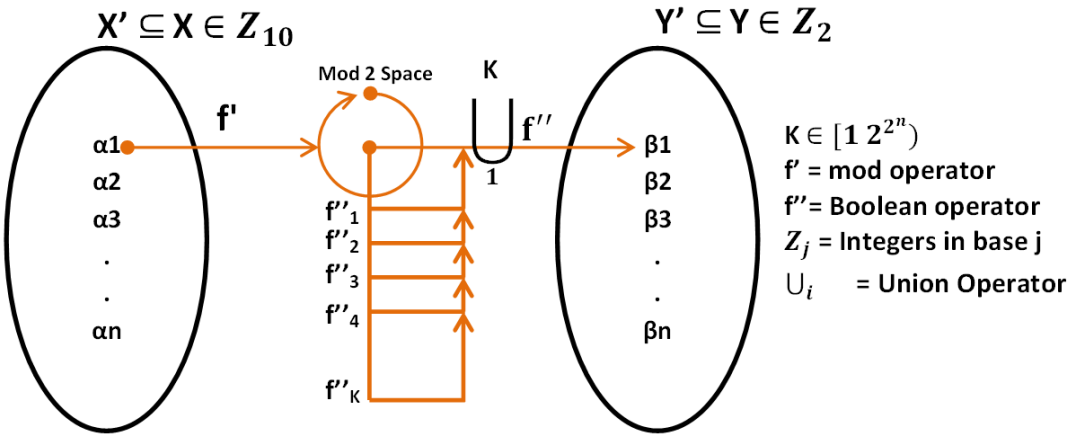

Figure 40 Disambiguated bijection relationship between an initial set of decimal numbers and a target set with binary numbers

Figure 40 is the depiction of the connection between a Boolean Space and the cardinality of the two sets with known bases As its shown in the figure for each element of set X' the first sub-function of function f first maps it into one particular position in the space of mod 2 and from there, there would exist 2^{2n} Boolean functions acting the mod 2 space and transferring the now turned into logical values into the equivalent position in set Y. This way, if the number of elements of set X' (its cardinality) is N_0 for instance (an infinite cardinality smaller than 2^{N0}) then set Y' will have the same cardinality hence the two sets are in bijection and storage is possible. As a result the physical storage capacity of a medium will depend on the available space for Boolean sub-functions f'' and this relates directly to the number of bits assigned to exist in a system of storage.